ACTA FACULTATIS TECHNICAE

TECHNICAL UNIVERSITY IN ZVOLEN

2

ISSUE: XXV
ZVOLEN 2020

Medzinárodný zbor recenzentov / International Reviewers Board

TABLE OF CONTENTS

SCIENTIFIC PAPERS

REVIEW

SCIENTIFIC PAPERS

THE EFFECT OF ADJUSTMENT OF THE CIRCULAR SAW BLADE BODY ON NOISE LEVELS OF THE CIRCULAR SAW

VPLYV ZMENY TELA PÍLOVÉHO KOTÚČA NA HLADINY HLUKU KOTÚČOVEJ PÍLY

Ján Svoreň, Ľubomír Naščák

Department of Manufacturing and Automation Technology, Faculty of Technology, Technical University in Zvolen, T. G. Masaryka 24, 960 01, Zvolen, Slovak Republic, svoren@tuzvo.sk

ABSTRACT: The cutting of wood is proceeded at high feed speed and high cutting speed of the circular saw blades. The cicular saw blades teeth rotate in outer ambient and thus are source of noise with unadvisable effects on working environment. The paper presents the results of the measurement of the noise level of two structuraly different circular saw blades. The types of the circular saw blades were: without slots, with six compensating slots in radial direction and with six compensating slots in tangential direction and in conjunction with RAL 9006 paint. The diameters of the circular saw blades were Ø D = 350 mm. The measurements of the noise level were performed when cutting boards of thickness h = 25 mm (*Picea excelsa* L.) using the standard equipments.. The clamping flanges had an outside diameter Ø d_p = 110 mm. Feed speed of cut material was v_f = 17 m.min^{-1}. The working speed of the circular saw shaft for experimental noise level measurements was n_1 = 4000 rpm; n_2 = 4025 rpm; n_3 = 4050 rpm; n_4 = 4075 rpm and n_5 = 4100 rpm. The circular saw blade with compensating slots emit a higher noise level than the corresponding hygiene regulations, but their noise level was (4 ÷ 6) dB (A) lower than the circular saw blade noise level without slots.

Key words: circular saw blade, compensating slots, circular saw, natural frequency, cutting noise level

ABSTRAKT: Rezanie dreva sa realizuje pri vysokej posuvnej rýchlosti materiálu a vysokej reznej rýchlosti pílových kotúčov. Zuby pílového kotúča rotujú v hmotnom prostredí a preto sú zdrojom hluku s nežiadúcimi vplyvmi na pracovné prostredie. V článku sú prezentované výsledky merania hladiny hluku dvoch konštrukčne rozdielnych pílových kotúčov. Typy pílových kotúčov sú: bez drážok, so šiestimi kompenzačnými drážkami v radiálnom smere a so šiestimi kompenzačnými drážkami v tangenciálnom smere a v spojení s nástrekom farbou RAL 9006. Priemery pílových kotúčov boli Ø D = 350 mm. Merania hladiny hluku boli vykonané pri rezaní dosiek hrúbky h = 25 mm (*Picea excels* L.) s použitím štandardných zariadení. Použité upínacie príruby mali vonkajší priemer Ø d_p = 110 mm. Posuvná rýchlosť rezaného materiálu v_f = 17 m.min^{-1}. Pracovné otáčky hriadeľa kotúčovej píly pre experimentálne merania hladiny hluku boli n_1 = 4000 min^{-1}; n_2 = 4025 min^{-1}; n_3 = 4050 min^{-1}; n_4 = 4075 min^{-1} a n_5 = 4100 min^{-1}. Pílový kotúč s kompenzačnými drážkami emitoval vyššiu hladinu hluku pri rezaní ako povoľuje príslušný hygienický predpis, ale jeho hladina hluku bola o (4 ÷ 6) dB (A) nižšia ako hladina hluku pílového kotúča bez drážok.

Kľúčové slová: pílový kotúč, kompenzačné drážky, kotúčová píla, vlastná frekvencia, hladina hluku pri pílení

INTRODUCTION

Circular saws are the most widely used machinery and equipment for the cutting of wood and wood materials in the wood-working industry. Circular saw blades of different design versions are the cutting tools of such devices. When cutting, as well as for other types of machining it is important to ensure the high quality of the machining surface. The vibration and noise of circular saw blades are basic problems of instability of the tool in the process of cutting. Reduction of the amplitude of the vibrations is essential for improving the quality of surface, accuracy of cutting, increasing the yield of the material, extending the useful life of the tool, but also for the reduction of noise. Especially the noise emission can directly affect the shape of the circular saw blade. In this paper, the idea of passive damping by compensating slots in conjunction with an elastic material layer is presented.

The noise by cutting is generated from the transversal oscillation of the circular saw blade of the excitation cutting forces on the teeth (Leu a Mote, 1979). If the cutting force can not be reduced in terms of the cutting process, there is a possibility to reduce the noise during cutting using the technical results of the modal analyses or using circular saw blade body from materials with higher damping characteristics. In the last years, the axisymmetric circular saw blade is most commonly used as a tool in the wood industry. Some compensating slots are produced in its body. The producers of circular saw blades are used for the reduction of noise emissions of the different passive methods of damping. These methods can be divided into three groups:

a) Sandwich (multilayer) body of the circular saw blade – according to (Westkämper et al. 1990) the reduction of noise levels is 10 dB (A) at idle running and (6 ÷ 8) dB (A) when cutting wood.
b) The body of the saw blade is made of high-damping materials, according to (Hattori et al. 1987; Hattori et al. 1993; Hattori et al. 2001) the reduction of the noise level is about 11 dB (A) when idle running. The disadvantage of this method is the higher price of the material of the circular saw blade body.
c) Laser cutting of compensating slots in the circular saw blade body- according to (Westkämper and Fus, 1994) the reduction of the noise level is (2 ÷ 8) dB (A) when idle running and the cutting of wood and wood-based materials. Laser cutting on CNC machines brings with it a number of advantages as accuracy, speed and the ability to make individual applications on the basis of information supplied by CAD\/CAM.

Influence of the shape, position, length, number of slots, copper rivets, the shape of the teeth and their number on the noise level of circular saw blades have been studied in several research papers (Miklaszewski & Grobelny, 1995; Lučic & Goglia, 2001; Spruit, et al. 2004; Orlowski, 2005; Svoreň & Naščák, 2007; Svoreň &Murin, 2009; Wang et al., 2012; Dimou, 2014; Mandic et al. 2015; Kvietková et al. 2015; Paiva et al. 2017).

The possibilities of reducing acoustic scattering by layers of elastic materials are presented in their work (Dutrion and Simon, 2017). These coatings are shown to enable scattering reduction at a precise frequency or over a larger frequency band.

The authors (Krilek et al. 2016) published the results of measurements of the noise level in the cross-cutting of timber in two different structures of circular saw blades (uncorrected No 1 and corrected No 2). The uncorrected circular saw blade No 1 had a higher noise level L_A eq (dB) for all types of wood, spruce, pine and beech at cutting conditions: $v_f = 12$ m. min^{-1} and the shaft speed n = 3000 rpm.

On the basis of statistics of occupational diseases in the European Union, the noise caused hearing disorders up to 15% (Heisel and Rambacher, 2009). The legislative requirements in individual states are tools for achieving acceptable working conditions in terms of elimination of noise load at the working place. Directive of the European Parliament and Council No. 2003/10/ES regarding to occupational health and safety implemented, three definitions in the Slovak legislation (decree government SR No. 115/2006 amendment according to 555/2006) are:

– occupational exposure limit $L_{AEX,\,8h,\,L}$ = 87 dB,
– upper exposure action value $L_{AEX,\,8h,\,a}$ = 85 dB,
– lower exposure action value $L_{AEX,\,8h,\,a}$ = 80 dB.

Exposure action value is a value of noise in the working environment where after overtaking it is necessary to take appropriate measures to decrease the level of noise (Dado and Hnilica 2015).

MATERIAL AND METHODS

Two circular saw blades manufactured by the company Stelit Ltd in Trenčín, SLOVAKIA have been used in the experimental measurements. The first circular saw blade (CSB1) had the untreated body and uniform spacing of the teeth (Fig. 1a). The second circular saw blade (CSB2) had in the body six compensating slots in the radial direction burned out using a laser, six compensating slots bent at an angle to the radius, copper rivets and nonuniform spacing of multiple teeth repeated the circuit 1/6 – patent number 288483 SR (Fig. 1b). The surface of the circular saw blade CSB2 had coating by color RAL 9006 by producer Tiger LACQUER SLOVAKIA Ltd Pezinok, in the company K-system Ltd Kosorín, Slovak republic. The coating had a thickness of 100 μm from both sides and was burned in an oven at the time of 20 min at the temperature of 192 °C. The material of the body circular saw blades was the steel (DIN 75Cr1, EN 1.2003). Teeth of circular saw blades are fitted with inserts of cemented carbide and are alternately diagonally grinded. The structural differences of the circular saw blades are shown in Fig. 1.

Fig. 1 The structural differences of circular saw blades used for experimental measuring
Obr. 1 Konštrukčné odlišnosti použitých pílových kotúčov

The basic parameters of the used circular saw blades for experimental measuring are given in Table 1.

Table 1 The basic parameters of the used circular saw blades
Tabuľka 1 Základné parametre použitých pílových kotúčov

Parameters	CSB1	**CSB2**
Circular saw blade diameter, mm	350	350
Clamping hole diameter, mm	30	30
Number of teeth, (–)	36	36
Body thickness, mm	2,4	2,4
Length of the cutting edge, mm	4,0	4,0
Tooth height, mm	13	13
Tooth geometry	$\alpha_f = 15°$	
	$\beta_f = 65°$	
	$\gamma_f = 10°$	

Used clamping flange had the outside diameter Ø d_p = 110 mm. Working revolutions of the circular saw blades had been determined on the basis of the calculation of resonant (critical) frequencies of rotation according to the equation (1) (Nishio and Marui 1996):

$$n_{r,k} = \frac{60 . f_{(n=0)}}{\sqrt{(k+Z)^2 - \lambda}} \quad \text{[rpm]} \tag{1}$$

$f_{(n=0)}$ – the natural frequency of oscillations of the non-rotating circular saw blade (Hz)
k – number of nodal diameters (-)
Z – number of harmonics (Z = 0; 1; 2; 3; 4; ...) (-)
λ – coefficient of the centrifugal force (-)

The natural frequencies of oscillations of the non-rotating circular saw blades for k = 1; 2; 3; 4 were experimentally determined by measuring apparatus at the laboratory KVAT of Technical university in Zvolen, which is described in (Svoreň et al. 2015). The coefficients of the centrifugal force for the k = 1; 2; 3; 4 were experimentally determined using the measuring apparatus at the laboratory KVAT of Technical university in Zvolen. Frequency of backward traveling wave f_b was determined on the measuring apparatus.

On the basis of the analysis of the calculated resonant (critical) speeds, the working speeds were chosen for experimental measurements of the noise levels as n_1 = 4000 rpm, n_2 = 4025 rpm, n_3 = 4050 rpm, n_4 = 4075 rpm, n_5 = 4100 rpm.

Boards of spruce (*Picea excelsa* L.) were used as the cut material in experimental measurements of the noise levels. The boards had dimensions of 25 mm x 250 mm x 1500 mm. The moisture content of the boards was w = 12 %. Feed speed of cutting had been v_f = 17 m.min^{-1}. The laths at the width of 15 mm were cut during the experiment. The cutting process had been repeated five times for each of the conditions.

The frequencies that are audible to humans, are in the range of (20 ÷ 20, 000) Hz. This range is referred to as a range of acoustic frequencies. At lower frequencies, vibrations are causing significant shaking of the human body, which is more felt than heard. The upper limit of audibility varies from person to person and decreases with increasing age. Physicists use a logarithmic scale for measuring sound pressure (Sound Pressure Level-SPL), namely the decibel (dB) scale. A decibel is a number that represents the logarithm of the ratio between the given sound pressure and the reference value. In practice, the term sound pressure level SPL is used, which is given by (Dimou, 2014):

$$SPL = 20 \,.\log \frac{p}{p_0} \tag{2}$$

p – sound pressure in pascals in the observed point,
p_0 – the internationally agreed reference value sound pressure, $p_0 = 2.10^{-5}$ Pa.

The machine was located on a concrete floor in a room (length × width × height = 15 × 12 × 4.5 m). Measurement of sound pressure levels in the experimental measurements on the circular saw was realized on the measuring apparatus, which block diagram is shown in Fig. 3. The frequency, which corresponds to the shaft working rotations of the circular saw, was set up by frequency converter. Working rotations were checked using non-contactless speedometer Lutron DT-2236 with measurement accuracy (± 0.05 % + 1 digit). Graded feed speed v_{f1} and at v_{f2} of the conveyer belt has been set up by mechanical wariator. The cut board was pressed to the band conveyer by a top roller driven device MV 102 (TOS Svitavy, Czech Republic). Condenser microphone was placed in the distance of 0,4 m forward the axis of rotation of the circular saw; 0,2 m on the left side of the circular saw blade and at a height of 1,5 m above the floor (STN EN ISO 3744; STN ISO 7960). The measurements were performed at one point, using the method of "sound free field". Hand-held sound Analyzer Brüel & Kjaer 2270 was set to a frequency filter „A" and time – weight filter „F" in range to 140 dB. The entire measuring chain was calibrated before using a calibration device for ½" condenser microphone. The values of the equivalent sound levels L_{eqA}, that the hand-held sound analyzer recorded every 0,1 seconds, were saved in internal memory.

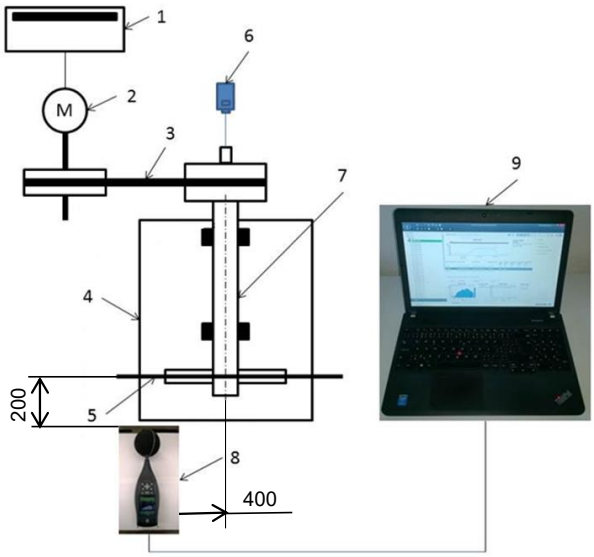

Fig. 3 The bock diagram of the connecting instruments for measurement of the noise pressure level on the circular saw.
1 – frequency converter Micro Master Siemens A.6. MM550/3, 2 – elektric motor Siemens, P = 5,5 kW, 3 – belt drive, 4 – stand circular saw, 5 – circular saw blade mounted with clamping collars, 6 – non-contact speedometer DT-2236, 7 – shaft in the bearings, 8 – hand-held noise analyzer Brüel & Kjaer 2270, 9 – PC
Obr. 3 Bloková schema pripojenia meracej aparatúry ku kotúčovej pile
1 – frekvenčný menič Micro Master Siemens A.6. MM550/3, 2 – asynchrony motor Siemens, P = 5,5 kW, 3 – remeňový pohon, 4 – stend kotúčovej píly, 5 – kotúčová píla s upínaním, 6 – bezkontaktný otáčkomer DT-2236, 7 – hriadeľ s ložiskami, 8 – ručný analyzátor hluku Brüel & Kjaer 2270, 9 – PC

RESULTS AND DISCUSSION

The measured values of the emitted noise by Analyzer Brüel & Kjaer were further processed in program BZ5503 – Measurement Partner Suite. Evaluation of the quantities of emitted noise was divided into two areas. The first area is the measured quantities of emitted noise when idling and turned the exhaust equipment on. From these values, the file of 40 noise levels $L_{ieq100ms}$ was selected for each circular saw blade as is shown in table 2. The second area is the measured quantities of emitted noise during cutting material and turned the exhaust equipment on. From these values, the file of 50 noise levels $L_{ieq100ms}$ was selected for each circular saw blade. The value of the equivalent noise levels L_{eq} have been identified by using the equation (Žiaran 2006):

$$L_{eq} \cong 10.\log\left[\frac{1}{T}\sum_{i=1}^{n}\Delta t_i \,.\, 10^{0.1\,.L_i}\right] \qquad [dB] \tag{3}$$

Table 2 The measured values $L_{eq100ms}$ for CSB1, Δt_i = 100 ms, T = 5 s, n_3 = 4050 rpm
Tabuľka 2 Namerané hodnoty $L_{eq100ms}$ pre CSB1, Δt_i = 100 ms, T = 5 s, n_3 = 4050 min^{-1}

95.49	96.32	96.38	96.64	96.67	99.49	100.33	101.88
102.4	102.46	102.81	102.83	102.96	102.97	103.01	103.15
103.29	103.32	103.57	103.65	103.78	103.78	103.87	104.24
104.39	104.46	105.13	105.27	105.35	105.51	105.72	105.80
105.88	106.1	106.1	106.26	106.28	106.32	106.51	106.57
106.78	106.86	107.07	107.24	107.45	107.6	107.84	107.96
107.98	109.06						

Table 3 Calculated mean values of L_{eq} in dB (A) and standard deviation σ
Tabuľka 3 Vypočítané stredné hodnoty L_{eq} v dB (A) a smerodatná odchýlka σ

Cutting process		
Feed Speed 17 m.min^{-1}		
	Rotation 4000 (rpm)	
	L_{eq}	σ
CSB1	107.5	1.36
CSB2	99.5	1.48
	Rotation 4025 (rpm)	
	L_{eq}	σ
CSB1	106.8	1.32
CSB2	99.1	1.53
	Rotation 4050 (rpm)	
	L_{eq}	σ
CSB1	105.3	1.41
CSB2	99.0	1.42
	Rotation 4075 (rpm)	
	L_{eq}	σ
CSB1	103.8	1.37
CSB2	98.7	1.52
	Rotation 4100 (rpm)	
	L_{eq}	σ
CSB1	102.9	1.29
CSB2	98.5	1.46

The impact of modifications to the body of the circular saw blades to the equivalent noise level L_{eq} circular saws in cutting process at different speeds is shown in Figure 3.

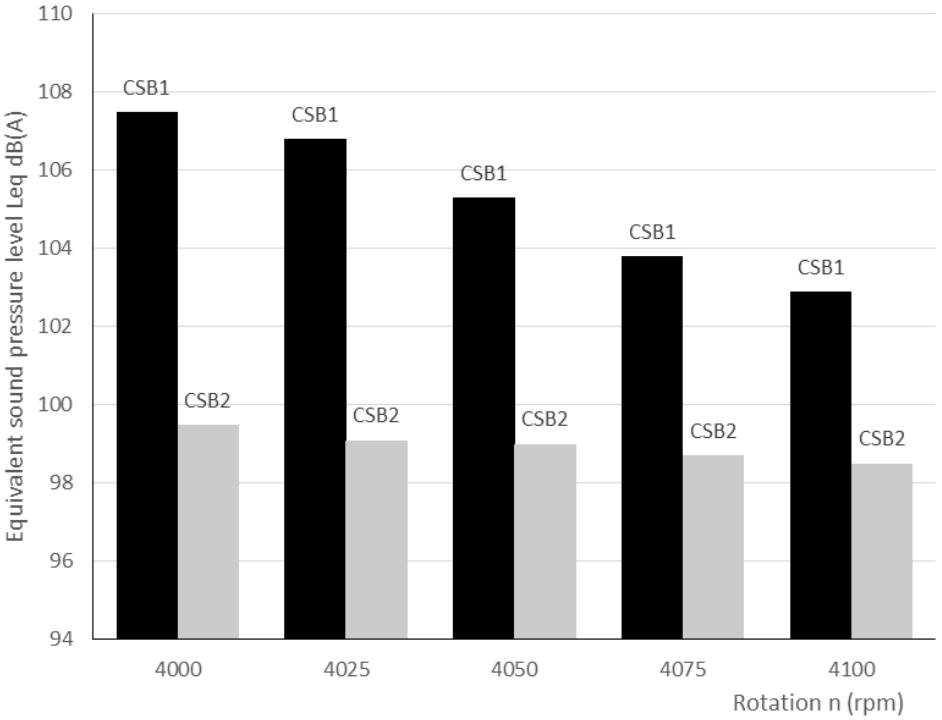

Fig. 3 Equivalent sound pressure levels L_{eq} of the circular saw at cutting process v_f = 17 m.min^{-1}
Obr. 3 Ekvivalentné hladiny akustického tlaku L_{eq} pílového kotúča v procese rezania v_f = 17 m.min^{-1}

In figure 3, we can see that the impact of modification of the body of the circular saw blade on the equivalent noise level L_{eq} of circular saw in cutting process at different speeds is very significant. The maximum difference values $L_{eq} \approx 8.0$ dB (A) is at a speed $n_1 = 4000$ rpm and feed rate $v_f = 17$ m. min^{-1} (CSB1 and CSB2). In figure 3, it is the noticeable effect of the increase in speed on the equivalent noise level L_{eq} in the process of cutting . The decline in the equivalent noise levels L_{eq} can be seen, which is very expressive at circular saw blade CSB 1 in the range $L_{eq} \approx (0.9 \div 4.6)$ dB (A). This dependence is caused due to a decrease in the cutting force, which is confirmed by the basic theory of cutting at circular saw, where the cutting force is by (Koch 1964) defined as $F_c = k_c \cdot A$ (N). The cross-section of the chips $A = s_t \cdot f_z$ (m^2) where s_t is length of the cutting edge and f_z is the feeding per tooth.

One-third octave band spectras of equivalent noise levels L_{eq} of the circular saw during the cutting cycle at the same technological conditions are shown in Fig. 4 for saw blades CSB1 and CSB2

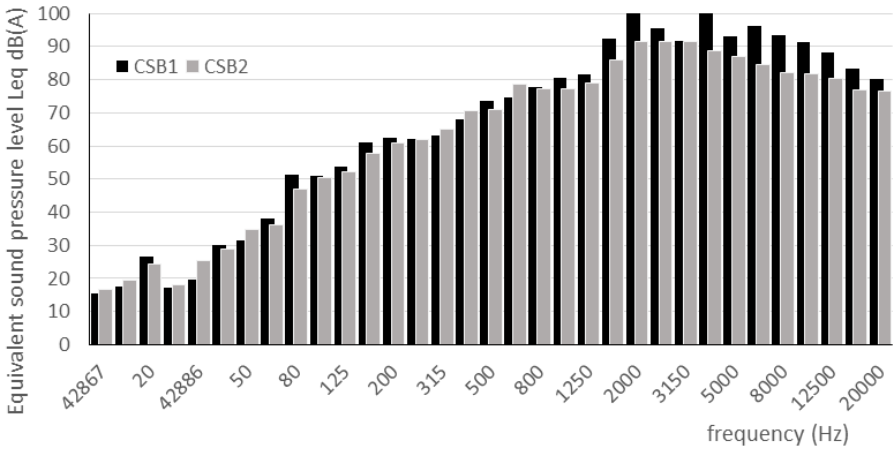

Fig. 4 One-third octave band spectra of CSB1 and CSB2 at cutting cycle v_f = 17 m.min^{-1} and n_3 = 4050 rpm.
Obr. 4 Jednotretikové oktávové spektrá kotúčov CSB1 a CSB2 v procese rezania v_f = 17 m.min^{-1} a n_3 = 4050 min^{-1}.

Based on Fig. 4, we can say that the adjustment of the body of the circular saw blade using the compensating slots, as well as sprayed paint (CSB2) reduces the equivalent noise levels L_{eq} in almost all of the octave bands at the frequency of (63 ÷ 20000) Hz. The equivalent noise levels L_{eq} in octave bands are broadband noise. Fig. 4 confirms the frequency of the maximum noise level, which is part of broadband noise (Reiter and Keltie, 1976):

$$f_k = i.n.z \qquad \text{(Hz)} \tag{4}$$

i – the fundamental harmonic, i = 1, 2, 3,... (-)
n – shaft revolutions (s^{-1})
z – the number of teeth of the circular saw blade (-)

CONCLUSION

By modifying the body of the CSB2 saw blade, a significant reduction in the equivalent noise level L_{eq} of the circular saw in the cutting process has been achieved. The maximum difference of $L_{eq} \approx 8.0$ dB (A) is at n_1 = 4100 rpm and feed rate v_f = 17 m.min^{-1} (CSB1 and CSB2).

Based on the experimental measurements, it can be argued that the adjustment of the saw blade body by compensating grooves as well as paint spraying (CSB2) reduces equivalent noise levels L_{eq} in almost all octave bands with frequency f = (63 ÷ 20000) Hz compared to CSB1.

The compensating grooves and copper rivets in the body, as well as the paint spraying and the uneven spacing of the saw blade teeth, do not provide the same reduction in the

equivalent noise level L_{eq} of the circular saw at the same speed and different cutting conditions as shown in fig. 3.

The production of such modified saw blades should be standard for each manufacturer. In the case of tool users, it is mainly about improving the quality of the working environment in terms of noise and thus protecting people's health at work.

REFERENCES

DADO, M., HNILICA, R. 2015. Impact of cutting circular saw on the level of motor saws vibration. In: Work security in practice: *Technical journal for the management of safety and health within the working environment,* 5(2): pp.12-15, ISSN 1338-2691

DIMOU, V. 2014. Noise Measurements in Timber Industries, *Drvna Industrija,* 65(3), pp. 243-249.

DUTRION, C., SIMON, F. 2017. Acoustic scattering reduction using layers of elastic materials. *Journal of Sound and Vibration,* 388, pp. 53-68. http://dx.doi.org/10.1016/j.jsv.2016.10.034

HATTORI, N., IZUMI, S., NOGUCHI, M. 1987. Suppression of the Whistling Noise in Tungsten Carbide – Tipped Circular Saws Using a High – Damping Alloy. *J.Jap. Wood Res. Soc.*, *33*(4), pp.268 – 273.

HATTORI, N., ANDO, K., KITAYAMA, S., NAKASHIMA, K. 1999. Suppression of the whistling noise in circular saws using a commercially-available damping metal. In. Proceedings of 14th , *International Wood Machining Seminar*. *Volume2*. Paris, Epinal, Cluny – France, September 12 – 19, pp.581 – 587.

HATTORI, N., KONDO, S., ANDO, K., KITAYAMA, S., MOMOSE, K. 2001. Suppression of the whistling noise in circular saws using commercially – available damping metal. *Holz als Roh – und Werkstoff*, *59(5)*, pp. 394 –398.

HEISEL, U., RAMBACHER, M. 2009. New Technologies for the localisation and characterisation of sound sources in woodworking machines. In: Zhou, H (ed.): *Proceedings 19th International Wood Machining Seminar.* Nanjing, China, Oct. 21-23, pp.219-230.

KOCH, P.: 1964. *Wood machining processes*. Ronald Press, New York.

KRILEK, J., KOVAČ, J., BARCIK, Š., SVOREŇ, J., ŠTEFANEK, M., KUVIK, T. 2016. The Influence of Chosen Factors of a Circular Saw Blade on the Noise Level in the Process of Cross Cutting Wood, Wood Research, 61(3), pp.475-486.

KVIETKOVA, M., GAFF, M., GAŠPARIK, M., KMINIAK, R., KRIŠ, A. 2015. Impact of number of saw blade teeth on noise level and wear of blade edges during cutting of wood, *BioResources* 10(1), pp. 1657-1666, (online), ISSN 1930-2126.

LUČIC, R. B., GOGLIA, V. 2001. Some possibilities for reducing circular saw idling noise, Journal of Wood Science, 47(5), pp.389-393.

LEU, M. C., MOTE, C. D. 1979. Noise generation by circular saws. In: Proceedings of 6th *Wood machining seminar*, University of California, Forest Product Laboratory, Richmond, USA, October 15 – 17, pp. 169 – 188.

MANDIC, M., SVRZIC, S., DANON, G. 2015. The comparative analysis of two methods for the power consumption measurement in circular saw cutting of laminated particle board. *Wood Research* 60(1), pp.125-136.

MIKLASZEWSKI, S., GROBELNY, T. 1995. Sound power determination of two circular saws with different constructions of the blades. In: *Zborník I. Medzinárodná konferencia „Stroj – nástroj – obrobok"*, 4. – 6. Október 1995, Nitra pp.83 – 88.

NISHIO, S., MARUI, E. 1996. Effects of slots on the lateral vibration of a circular saw blade. *International Journal of Machine Tools & Manufacture*, 36(7), pp. 771-787.

ORLOWSKI, K. A. 2005. Identification of critical speeds of clamped circular saws. *Drvna Industrija, 56(3)*, pp. 103 – 106.
PAIVA, P., VAZ, M. A., LOPES, H. 2017. Main noise sources of a circular saw blade during operation, In. Zbiec, M. (ed.) *Proceedings of 23rd International Wood Machining Seminar,* 28.05 – 31.05.2017 – WARSAV – POLAND, pp. 299 – 308, ISBN: 978-83-948046-0-2.
REITER, W. F., KELTIE, R. F. 1976. On the Nature of Idling Noise of Circular Saw Blades. *Journal of Sound and Vibration,* 44(4), pp. 531 – 543.
SPRUIT, M., RAO, M., HOLT,J., BOYER,L., BARNARD, A., DAYTON, W. 2004. Table Saw Noise Control. *Sound and Vibration*, June 2004, pp. 20-25.
STN EN ISO 3744:2010, Acoustics – Determination of sound power levels and sound energy levels of noise sources using sound pressure – Engineering methods for an essentially free field over a reflecting plane.
STN ISO 7960:1998, Airborne noise emitted by machine tools – Operating conditions for woodworking machines.
SVOREŇ, J., MURÍN, L. 2009. The Effect of the Shape of the Compensating Slots in the Body of a Circular Saw Blade on Noise Level of a Circular Saws in the Cutting Process, Proceedings of the *ACOUSTICS High Tatras 2009 "34th International AcousticalConference* – EAA Symposium". Starý Smokovec – Tatry. Technická univerzita Zvolen.
SVOREŇ, J., NAŠČÁK, Ľ. 2007. Effect of compensation slots, copper corks in the body of a circular saw blade and unbalanced pitch of several teeth on noise level of circular saws in cutting process. In.: *Proceedings of the 2nd International Scientific Conference ´´Woodworking Technique´´*, *University of Zagreb*, *Technical University in Zvolen*, 11. – 15. 09. Zalesina, Croatia, pp. 311 – 317, ISBN 953-6307-94.
SVOREŇ, J., JAVOREK, Ľ., DROBA, A., KRAJČOVIČOVÁ M. 2015. Determination of Critical Rotational Speed of Saw Blades by Using Varios Methods. In. Procedings of *International Conference ICWSE 2015"Wood Science and Engineering in the Third Millennium",* November 5-7, Transilvania University, Brašov – Romania, pp.495-503, ISSN 1843- 2689.
WANG, T., YOA, T., DUAN., G. 2012. Otimization Design on Vibration and Noise Reduction of Damping Sandwich Circular Saw. *Applied Mechanics and Materials,* Vols.215-216, pp.433-437. ISSN1662-7482.
WESTKÄMPER, E., LICHER, E., PREKWINKEL, F. 1990. Sägen von Holz – und Holzwerkstoffen. *Holzbearbeitung*, N.1/2, pp. 38 –45.
WESTKÄMPER, E., FUS, M. 1994. Stand der Technik beim Kreissägen. *Holzbearbeitung*, N.4, pp. 56 – 64.
ŽIARAN, S. 2006. *Reduction of vibration and noise in the industry.* (Znižovanie kmitania a hluku v priemysle). Bratislava: Slovenská technická univerzita, 339p. ISBN 80-227-2366-5.

Corresponding author:
Ján Svoreň, e-mail: svoren@tuzvo.sk

EFFECT OF THERMAL MODIFICATION ON INSULATING PROPERTIES OF WOOD

VPLYV TERMICKEJ MODIFIKÁCIE NA IZOLAČNÉ VLASTNOSTI DREVA

Áron Hortobágyi, Elena Pivarčiová

Department of manufacturing and automation technology, Faculty of technology, Technical university in Zvolen, T. G. Masaryka 24, 960 01, Zvolen, Slovak republic, xhortobagyi@is.tuzvo.sk, elena.pivarciova@tuzvo.sk

ABSTRACT: The paper is focused on the research of the influence of thermal modification on the insulating properties of wood. The monitored parameter was the heat transfer coefficient between the surface of the heated samples and the ambient air. Spruce wood samples with varying degrees of thermal modification and a control untreated sample were used for the research. The samples were heated from below by a radiant source isolated from the environment. The surface temperatures of the sample and the ambient air were continuously recorded using thermocouples. Temperature fields above the sample were visualized by real-time holographic interferometry. The values of the heat transfer coefficient α were calculated by evaluating the recorded interferograms. Result of the experiment proved that thermal modification had a positive impact on reduction of heat transfer coefficient, thus enhancing insulation property of the studied material. Heat treatment at higher temperatures showed further improvement, although not as notable as a difference between untreated and sample treated at 160 °C.

Key words: thermal modification, holographic interferometry, heat transfer, spruce wood

ABSTRAKT: Príspevok je zameraný na výskum vplyvu termickej modifikácie na izolačné vlastnosti dreva. Sledovaným parametrom bol koeficient prestupu tepla medzi povrchom ohrievaných vzoriek a okolitým vzduchom. Pre výskum boli použité vzorky smrekového dreva s rôznym stupňom termickej modifikácie a kontrolná neupravená vzorka. Vzorky boli zdola zahrievané sálavým zdrojom, izolovaným od okolitého prostredia. Teploty povrchu vzorky a okolitého vzduchu boli priebežne zaznamenávané pomocou termočlánkov. Nad vzorkou boli vizualizované teplotné polia metódou holografickej interferometrie v reálnom čase. Vyhodnotením zaznamenaných interferogramov boli vypočítané hodnoty koeficientu prestupu tepla α. Výsledok experimentu preukázal že termická modifikácia mala pozitívny vplyv na zníženie koeficientu prestupu tepla, čím bola zlepšená izolačná schopnosť skúmaného materiálu. Termická modifikácia pri vyšších teplotách prinášala ďalšie zlepšenie, no nie v takej miere, aká bola pozorovateľná medzi prírodnou a vzorkou a vzorkou modifikovanou pri 160 °C.

Kľúčové slová: termická modifikácia, holografická interferometria, prestup tepla, smrekové drevo

INTRODUCTION

Wood has been used by humans since ancient times, both for the production of tools and as a building material. Due to its availability and properties, it has been used for these purposes up to this day. Some of excavated wooden tools modified by partial charring predate even the Stone Age. With this treatment, the wood acquires a higher resistance to moisture, insects and fungi, which slows down its degradation and prolongs its life. To enable usage of these properties, research of the heat treatment process was raised to a scientific level.

Authors (Stam, Hansen, 1973) have been researching effect of thermal modification on dimensional stability of wood. Researchers (Steborg, Millett, Stamm, 1956) were testing properties of thermally modified wood "staypack", which has been molded in conditions of raised heat and humidity. Scientists (Kollmann, Scheider, 1963) were focused on absorption properties of thermally modified wood. Thermal modification as a method to enhance dimensional stability of wood was studied by (Burmester, 1973). Similar topic was addressed also by (Giebeler, 1983).

Authors (Reinprecht, Vidholdová, 2008) studied mechanical properties of thermally modified wood and its resistance to various molds. Scientists (Kol, Keshin, 2016) compared thermal conductivity of wooden samples, which were thermally modified with various final treatment temperatures. Researcher (Jochim, 2016) was measuring heat transfer coefficient of log cabin walls. Analyst (Zhang et al., 2017) compared experimental values of heat transfer process during thermal modification of wood with an ANSYS analysis. Author (Liu, Sun, Sun, 2018) studied heat transfer properties of wood frame walls. Heat transfer from wooden surface to surrounding air was addressed by (Hrčka, Babiak, 2016).

Effect of thermal modification on color changes on wooden samples was described by (Barcík, Gašparík, Razumov, 2014) and effect of choice of tools and parameters on chip size during machining of thermally modified wood was studied by (Barcík, Gašparík, 2014). Researchers (Koleda et al., 2018) addressed effect of treatment temperature on power consumption of milling machine. Author (Korčok et al., 2018) compared quality of machined surfaces of wooden samples treated with various temperatures.

MATERIAL AND METHODS

As a material for research, spruce wood planks were used. After thermal modification they were cut into samples with parameters 40 × 40 × 10 mm. Treatment levels of wooden planks were 160, 180, 200 °C. Spruce wood with same parameters was used as a control sample. Humidity content of modified samples was lowered to 4–7 %.

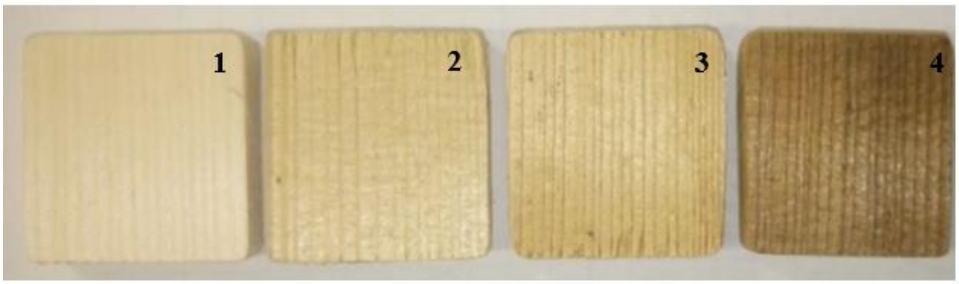

Fig. 1 Used samples. 1 – untreated control sample, 2, 3, 4 – heat treated spruce samples, at temperature levels: 2 – 160 °C, 3 – 80 °C, 4 – 200 °C
Obr. 1 Použité vzorky. 1 – kontrolná vzorka bez úpravy, 2, 3, 4 – tepelne upravené vzorky, po úprave na teplotách: 2 – 160 °C, 3 – 180 °C, 4 – 200 °C

Radiant heat source was used for heating of samples during experiment. The source was cowered by insulation material and it has been placed under the measurement platform.

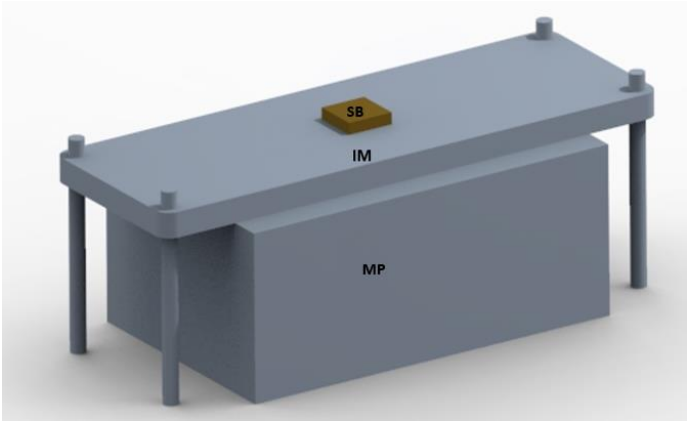

Fig. 2 Measurement platform
SB – sample body, IM – insulation material, MP – measurement platform
Obr. 2 Meracia plošina
SB – skúšobná vzorka, IM – izolačný material, MP – meracia plošina

Air temperature was kept at 23 °C during the experiment. A variant of Mach-Zehnder interferometer was used for the measurement, as shown on Fig. 3. This variant is one of the most frequently used devices for visualization of temperature fields and measurement of two-dimensional transparent objects. It is capable of being adjusted to either finite or infinite fringe width.

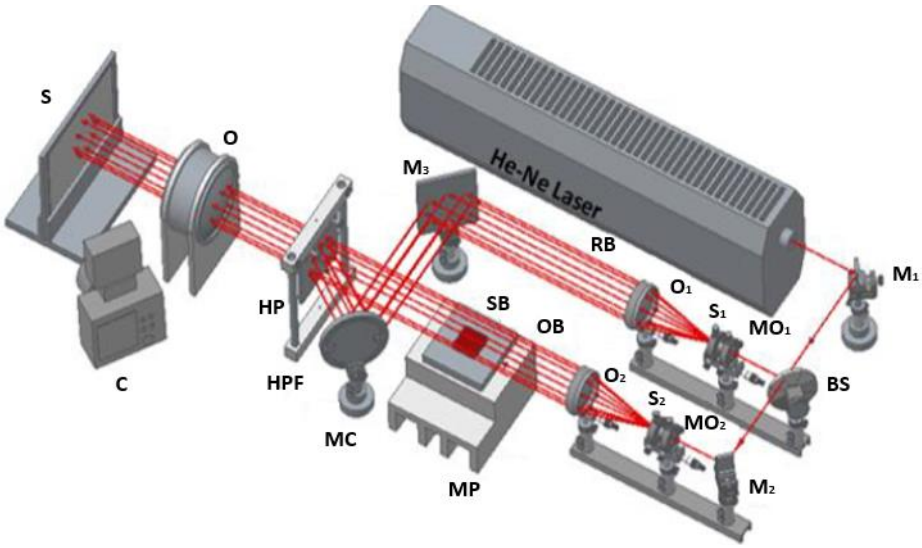

Fig. 3 Scheme of holographic variant of single-wave Mach-Zehnder interferometer
(Pivarčiová et al., 2019)
OB – object branch, RB – reference branch, BS – beam splitter, HP – holographic plate, HPF – holographic plate fixture, MC – mirror in cardan fixture, O1, O2 – objectives, M_1, M_2, M_3 – mirrors, S_1, S_2 – perforated screens, MO_1, MO_2 – microscopic objectives, SB – sample body, MP – measurement platform, C – camera, S – shade, O – system of objectives
Obr. 3 Schéma holografického variantu jednovlnového Mach-Zehnderovho interferometra
(Pivarčiová et al., 2019)
OB – objektová vetva, RB – referenčná vetva, BS – delič, HP – holografická doska, HPF – držiak holografickej dosky, MC – zrkadlo v kardanovom závese, O_1, O_2 – objektívy, M_1, M_2, M_3 – zrkadlá, S_1, S_2 – dierkové clony, MO_1, MO_2 – mikroskopické objektívy, SB – skúšobná vzorka, MP – meracia plošina, C – fotoaparát, S – tienidlo, O – sústava objektívov

He-Ne laser with wavelength $\lambda = 0.6328 \times 10^{-6}$ m was used as a light source. It had continual output and 50 mW performance. Created beam was reflected by mirror Z_1 and when passing through beam splitter D was divided into objective and reference beam. These beams were aimed through optical assemblies of micro objectives (MO_1, MO_2), screens (C_1, C_2) and objectives (O_1, O_2). Function of optical assemblies was to widen laser beams.

When passing through microobjective (MO_1, MO_2), waves gain spherical character. Perforated screens (C_1, C_2) were used to filter bending and interference effects that originated from impurities on prior optical elements.

Objective (O_1, O_2) at the end of the assembly changes wave character from spherical to plane. For system for objective beam, small focal length and small diameter were chosen. For the reference beam, large focal length with large objective diameter was used.

Sample body (ST) was held on measurement platform (SST) after objective for objective beam. The beam passes through medium above the sample body and illuminates holographic plate (H), which was held by holographic plate fixture (DH).

Reference beam is reflected by mirror Z_3 and by mirror in cardan fixture (KZ) and illuminates holographic plate (H). Mirror (KZ) can rotate, and this allows adjustment of fringes to either finite or infinite fringe width. Interference patterns are projected through system of objectives (O) onto shade (T), where they are recorded by camera (F).

HOLOGRAPHIC INTERFEROGRAM ANALYSIS

To make evaluation of interferograms possible, it is essential to know dependency between and division of refractive index in optical inhomogeneity, which appeared due to state values of object, and those values.

Dependency of temperature on state values of surrounding environment, length of the model, light wavelength and number of dark fringes between object and place where is environment homogenous can be calculated using (Černecký et al, 2011):

$$T(x,y) = \frac{T_\infty}{1-0{,}805\cdot\frac{T_\infty}{l\cdot p_\infty}\cdot\left(s-\frac{1}{2}\right)} \tag{1}$$

where $T(x, y)$ – layout of temperatures [°C],
T_∞ – air temperature in reference zone [°C],
p_∞ – air pressure in surrounding area [p],
s – interference grade [-],
λ – chosen wavelength [nm],
l – length of observed object [m].

Change of the interference grade s is visible as a change between dark and light fringes on the interferogram. In locations of bright fringes, it has integer values:

ΔS(x, y) = –n; ...; –3; –2; –1; 0; 1; ...; n

and in locations of dark fringes:

ΔS(x, y) = ...; –3,5; –2,5; –1,5; –0,5; 0,5; 1,5; ...

This is true with interferometer set to infinite width. In such case, object and reference beam are parallel and change in interference grade (ΔS(x, y) = 0) does not occur.

HEAT TRANSFER COEFFICIENT CALCULATION

Heat transfer coefficient α [$Wm^{-2}K^{-1}$] stands for amount of heat, which is transferred from body surface into fluid. It is used when referring phenomena at border between body with rigid arrangement of particles and a fluid, where particles move freely. In our case, the rigid body is the spruce sample and fluid is represented by atmospheric gas. Value of heat transfer coefficient depends on shape and size of surface, properties of fluid and of hydrodynamic condition of the fluid. Local value of heat transfer coefficient can be calculated by equation (Pavelek et al., 2007):

$$\alpha_x = -\lambda_v \cdot \left(\frac{dT}{dy}\right)_x \cdot \frac{1}{T_x - T_\infty} \tag{2}$$

where λ_v – heat conductivity coefficient of surrounding air [W·m^{-1}·K^{-1}] (for dry air at 20 °C, λ_v = 2,524 W·m^{-1}·K^{-1}),
T_x – surface temperature at point x [°C],
T_∞ – temperature of surrounding environment [°C].

For temperature profile $T = f(y)$ in form of second grade polynome and for border conditions

$$y = 0 \rightarrow T = T_w\ , \tag{3}$$

$$y = \delta_x \rightarrow T = T_x,\ \frac{dT}{dy} = 0 \tag{4}$$

derivation of temperature at the surface can be described by equation (Pavelek et al., 2007):

$$\left(\frac{dT}{dy}\right)_x = -2 \cdot \frac{T_w - T_x}{\delta_x} \tag{5}$$

where δ_x – width of border layer.

For temperature profile T = f(y) in form of third grade polynome and for border conditions

$$y = 0 \rightarrow T = T_x,\ \frac{d^2T}{dy^2} = 0\ , \tag{6}$$

$$y = \delta_x \rightarrow T = T_w,\ \frac{dT}{dy} = 0 \tag{7}$$

derivation of temperature at the surface can be described by equation (Pavelek et al., 2007):

$$\left(\frac{dT}{dy}\right)_x = -\frac{3}{2} \cdot \frac{T_w - T_x}{\delta_x} \tag{8}$$

Since the analysis of interferograms makes it possible to determine in detail the temperature distribution in the fluid, the method for calculating the heat transfer coefficient from temperature derivatives is a useful aid in interferometric research of heat transfer research.

RESULTS

During heating of the samples, heat transfer occurred, and a thermal boundary layer formed above the sample. Interference fringes formed in this layer. At low temperatures, there were fewer fringes in the boundary layer, and with growing temperature, their num-

ber increased. This sequence is shown in Fig. 4 and pictures of samples at highest temperatures are shown in Fig. 5.

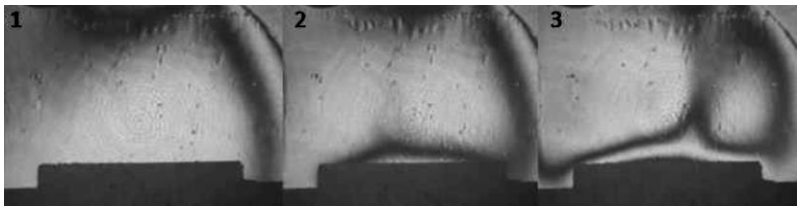

Fig. 4 Sequence of formation of interference fringes during heating of untreated sample. 1 – Sample at the beginning of the experiment, 2 – Occurrence of the fringe 1, after approx. 8 min., 3 – Occurrence of the fringe 2, in approx. 16 min.
Obr. 4 Postupnosť vytvárania interferenčných prúžkov pri ohreve. 1 – Vzorka na začiatku ohrevu, 2 – Vytvorenie prúžku 1, po cca 8 min. ohrevu, 3 – Začiatok vytvárania prúžku 2, po približne 16 min. ohrevu.

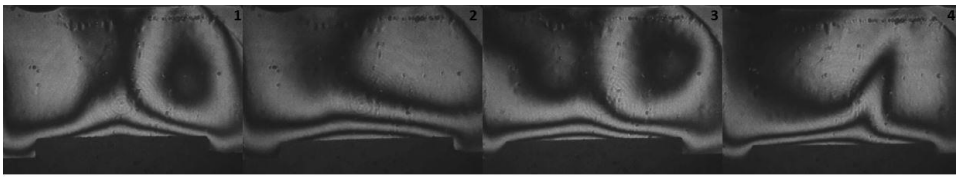

Fig. 5 Samples at their highest surface temperatures. 1 – Untreated wood (338,15 °C), 2 – Wood modified at 160 °C (335,01 °C), 3 – Wood modified at 180 °C (330,48 °C), 4 – Wood modified at 200 °C (338,72 °C)
Obr. 5 Vzorky pri najvyšších teplotách. 1 – Prírodné drevo (338,15 °C), 2 – Drevo upravené pri 160 °C (335,01 °C), 3 – Drevo upravené pri 180 °C (330,48 °C), 4 – Drevo upravené pri 200 °C (338,72 °C)

Obtained images were sampled in approximately two-minute. At least two interference fringes must have been present in the image in order to evaluate the data. Records from the range of heating time 12–25 min met this criterion. By analyzing the interferograms using the Vibra program, we obtained the temperature profile of the thermal boundary layer above the sample.

In Fig. 6. is an example of the evaluation of the temperature profile above the sample.

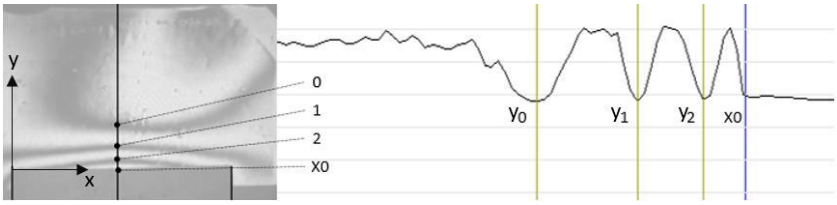

Fig. 6 Evaluation of heat layout above the sample.
Left: interferogram with line drawn in the place of evaluation, right: identification of position of interference fringes (y_0; y_1; y_2) and of sample surface (x_0).
Obr. 6 Vyhodnotenie teplotného profilu nad vzorkou
Vľavo: vyhodnocovaný interferogram s vyznačením línie vyhodnocovania, vpravo: označenie polohy interferenčných prúžkov (y_0; y_1; y_2) a povrchu zohrievanej vzorky (x_0).

Program Vibra used measured surface temperatures as an imput. Second part of imput was a picture of interferogram. Picture was evaluated through its section (right part of Fig 6). Scale of distance was set using edge of sample, which was known to be 0,04 m long. Then, position of interference fringes and sample surface was chosen in the section. From these, local temperatures were calculated using equation (1). Table 1 shows measured distances between fringes and sample surface, from captures taken at highest temperature.

Table 1 Distance of fringes from sample surfaces, measured at highest temperatures
Tab. 1 Vzdialenosti interferenčných prúžkov od povrchu vzoriek, namerané pri najvyšších teplotách

	natural	160 °C	180 °C	200 °C
y_0	0.027	0.029	0.030	0.031
y_1	0.015	0.026	0.027	0.028
y_2		0.019	0.020	0.023

Then, heat profile and heat transfer coefficients were calculated, using equations (2), (5) and (8). Calculated heat transfer coefficients and their dependencies on surface temperatures of samples is shown in Fig. 7.

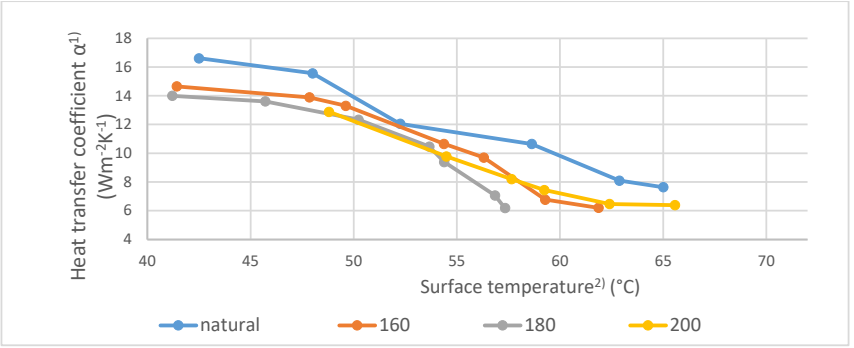

Fig. 7 Dependencies of heat transfer coefficient on surface temperatures of samples.
Obr. 7 Závislosti koeficientu prestupu tepla od nameranej teploty povrchu vzorky
[1)]Koeficient prestupu tepla α, [2)]Teplota

DISCUSSION

In Fig. 7, it can be seen that for all samples of thermally modified wood, the value of the heat transfer coefficient α was lower than the value corresponding to the control sample.

At the beginning of the experiment, heat transfer coefficient of sample modified at 160 °C was 11.8% smaller than coefficient of control sample, while difference of 180 °C sample was 15.7%. At surface temperatures in range (54–56) °C, differences were 11.5 % for 160 °C sample, 22.1 % for 180 °C and 18.8 % for sample treated at 200 °C. At temperatures between (62–66) °C, there is 18.8 % difference for 160 °C sample, and 16.4 % for 200 °C.

According to these values, it could be generalized that heat transfer coefficient of thermally modified wood was 11.8 %–22.1 % lower than coefficient of the control sample. This leads to conclusion that thermal modification does positively affect properties of wood as an insulation material. The biggest difference was noted between control sample and wood modified at 160 °C. Modification at higher temperatures showed better results, although not as notable as a difference between treated and non-treated samples.

The heat transfer coefficient α decreased with increasing sample surface temperature. At temperatures up to 55 °C, the heat transfer coefficient decreased as the level of thermal modification of the sample increased. At higher temperatures, the sample deviation treated at 180 °C reaches the highest deviation. During the experiment, the fastest temperature rise was recorded for this sample.

CONCLUSION

The experiment showed that thermal modification has a positive effect on improving the insulating properties of wood. At the beginning of the experiment, in surface temperature range of (41–43) °C α value of natural wood was 16.61 $Wm^{-2}K^{-1}$, while spruce modified at 160 °C had α = 14.61 $Wm^{-2}K^{-1}$ and sample modified at 180 °C had α = 14 $Wm^{-2}K^{-1}$. When heated to (54–56) °C, coefficient α of natural wood decreased to 12.05 $Wm^{2}K^{-1}$. Heat transfer coefficients of treated samples also declined: spruce modified at 160 °C to α = 10.66 $Wm^{-2}K^{-1}$, sample modified at 180 °C to α = 9.39 $Wm^{-2}K^{-1}$ and wood modified at 200 °C had value α = 9.78 $Wm^{-2}K^{-1}$. By ending of the experiment, in a range of (62–66) °C, heat transfer coefficient of natural wood decreased to α = 7.64 $Wm^{-2}K^{-1}$. For sample treated at 160 °C, it was α = 6.20 $Wm^{2}K^{-1}$ and for 200 °C sample α = 6.39 $Wm^{-2}K^{-1}$. 180 °C sample did not reach surface temperature in this range, its final coefficient was α = 6.18 $Wm^{-2}K^{-1}$, at temperature 57 °C.

A sufficient temperature difference between the sample surface and the ambient air was required to perform the analysis by holographic interferometry. In order to obtain results for a range of surface temperatures corresponding to the conditions in which wood would be used as a building element, it will be necessary to perform an experiment at a constant ambient air temperature maintained at a lower value.

To assess heat transfer coefficients, method of holographic interferometry was used. This method has proven its usability for visualisation of temperature fields and assessment of heat transfer on a boundary between object and a liquid. This could be also useful in research of heat transfer occurring at samples of intricate shape, such as various computer components. It would be also possible to use this method to assess heat losses near inhomogenities of wood, such as small cracks and places with grain direction differing from the surrounding area.

In the following research, ionization impact on the air cleaning efficiency in the wood production halls (Černecký et al. 2015) should be considered. Also, either this method or a method of digital holography could be used for the visualisation of motion of a beam (Černecký, Božek, Pivarčiová, 2015). Drawback of this method is its sensitivity, as the results can be influenced by events in surrounding area. Thus it is yet usable mostly in controlled conditions of a laboratory. Another problem arises from size of optical components of interferometer, as the size of measured objects is restricted by parameters of used objectives.

ACKNOWLEDGEMENT

This research was funded by the project VEGA 1/0086/18: Research of temperature fields in the system of shaped heat exchange surfaces.

REFERENCES

BARCÍK, Š., GAŠPARÍK, M. 2014. Effect of Tool and Milling Parameters on the Size Distribution of Splinters of Planed Native and Thermally Modified Beech Wood. [online] [cit. 2020-10-01]. Available on: <https://www.researchgate.net/publication/260888827_Effect_of_Tool_and_Milling_Parameters_on_the_Size_Distribution_of_Splinters_of_Planed_Native_and_Thermally_Modified_Beech_Wood>.

BARCÍK, Š., GAŠPARÍK, M., RAZUMOV, E., Y. 2015. Effect of thermal modification on the colour changes of oak wood. Wood research, vol. 60, pp. 285–395.

BURMESTER, A. 1973, Investigation on the dimensional stabilization of wood. Bundesanstalt für Materialprüfung. Berlin-Dahlem, pp. 50–56.

ČERNECKÝ, J., PIVARČIOVÁ, E. 2007. Possibilities and Prospects of Holography. Izhevsk, Rossia: State Technical University. [online] ISBN 978-5-7526-0303-7. Available on: <http://www.holografia.wz.cz/holography/index.php>.

GIEBELER, E. 1983. Dimensionsstabilisierung von Holz durch eine Feuchte/Wärme Druck-Behandlung. Holz Roh-Werkst, vol. 41, pp. 87–94.

KOL, S., H., KESHIN, S., A. 2016. The thermal conductivity of solid wood heat-treated using the thermowood method. [online] [cit. 2020-09-25]. Available on: <https://www.researchgate.net/publication/303305151THE_THERMAL_CONDUCTIVITY_OF_HEAT-TREATED_WOOD_MANUFACTURED_BY_THERMOWOOD_METHOD>.

KOLEDA, P., KOČOK, M., BARCÍK, Š., IĽAŠ, Š. 2018. Effect of temperature of heat treatment on energetic intensity of flat milling of picea abies. Sciendo, vol. 26, pp. 151–156.

KOLLMANN, F., SCHNEIDER, A. 1963. Über das Sorptionsverhalten wärmebehandelter Hölzer. Holz Als Roh- Und Werkstoff, vol. 21, pp. 77–85.

KORČOK, M., KOLEDA, P., BARCÍK, Š., VANČO, M. 2018. Effect of technical and technological parameters on the surface quality when milling thermally modified European oak wood. Bioresources, vol. 13, no. 4. pp. 8569-8577.

KOSSACKÝ, E., SUROVÝ, J. 1972. Chemické inžinierstvo. 3. vydanie. Bratislava, Slovenské vydavateľstvo technickej literatúry, pp. 250–252.

PAVELEK, M., JANOTKOVÁ, E., ŠTĚTINA, J. 2007. Vizualizační a optické měřicí metody. Brno: VUT.

PIVARČIOVÁ, E., BOŽEK, P., DOMNINA, K., ŠKULTÉTY, E., FEDOSOV, S. 2019. Interferometric measurement of heat transfer above new generation foam concrete. [online] [cit. 2020-10-02]. Available on: <https://doi.org/10.2478/msr-2019-0021>.

PIVARČIOVÁ, E., ČERNECKÝ, J. 2011. Wood texture influence on temperature fields. In: DAAAM symposium "Intelligent manufacturing and automation: power of knowledge and creativity", Vienna: DAAAM International Vienna, Austria, 2011, pp. 1069–1070. ISBN 978-3-901509-83-4.

REINPRECHT, L., VIDHOLDOVÁ, Z. 2008. Mould resistance, water resistance and mechanical properties of OHT-thermowoods. [online] [cit. 2020-10-05]. Available on: <https://www.researchgate.net/publication/262313914_Mould_resistance_water_resistance_and_mechanical_properties_of_OHT-thermowoods>.

REINPRECHT, L., VIDHOLDOVÁ, Z. 2008. Termodrevo - príprava, vlastnosti a aplikácie: Thermowood - its preparation, properties and application. Zvolen: Technická univerzita vo Zvolene. ISBN 978-80-228-1920-6.
SEBORG, R., M., MILLETT, M., A., STAMM, A., J. 1958. Heat stabilized compressed wood (staypack). [online] [accessed October 2020] Available on: <https://www.fpl.fs.fed.us/documnts/fplr/fplr1580.pdf>.
STAMM, A. J., HANSEN, L. A. 1937. Minimizing Wood Shrinkage and Swelling Effect of Heating in Various Gases. Industrial and Engineering Chemistry, vol. 29, pp. 831–833.
STANISLAV, J. 2016. Determining the heat transfer coefficient of log-cabin walls based on one dimensional thermal transmittance. Acta Facultatis Xylologiae Zvolen, no. 58, vol. 1, pp 75−82. DOI: 10.17423/afx.2016.58.1.09.
ZHANG, J., QU, L., WANG, Z., ZHAO, Z., HE, Z., YI, S. 2017. Simulation and validation of heat transfer during wood heat treatment process. Results in Physics, vol. 7, pp 3806-3812. ISSN 2211-3797. Available on: https://doi.org/10.1016/j.rinp.2017.09.046.
LIU, M., SUN, Y., SUN, CH. 2018. Study on thermal insulation and heat transfer properties of wood frame walls. Wood research, no. 63, vol. 2, pp 249-260.
HRČKA, R., BABIAK, M. 2016. Wood Thermal Properties. [online] [accessed November 2020] Available on: <https://www.intechopen.com/books/wood-in-civil-engineering/wood-thermal--properties>.
ČERNECKÝ, J., BOŽEK, P., PIVARČIOVÁ, E. 2015. A new system for measuring the deflection of the beam support of digital holographic interferometry. Journal of electrical engineering, vol. 66, no. 1, pp 52-55.
ČERNECKÝ, J., VALENTOVÁ, K., PIVARČIOVÁ, E., BOŽEK, P. 2015. Ionization Impact on the Air Cleaning Efficiency in the Interior. Measurement Science Review, vol. 15, no. 4, pp 156-166.

Correspondence author:
Áron Hortobágyi, email: xhortobagyi@is.tuzvo.sk

THE ANALYSIS OF OPERATIONAL RELIABILITY FOR FOREST FORWARDERS

ANALÝZA PREVÁDZKOVEJ SPOĽAHLIVOSTI LESNÝCH ODVOZNÝCH SÚPRAV

Pavel Ťavoda[1], Ján Kováč[1], Pavol Harvánek[1]

[1]Faculty of Technology, Technical University in Zvolen, Slovakia, jan.kovac@tuzvo.sk, tavoda.pavel@gmail.com, pavol.harvanek@gmail.com,

ABSTRACT: Analysis and risk assessment are procedures which help to progress of knowledge and are very important in practice. Risk assessment is possible to create only on the basis of exact true and tested information about the given system, which truly define the given system within the area and time. The High standards of care and treatment are closely linked with the requirements for quality and reliability forestry machinery and technological equipment. The These standards are closely related to the care of the equipment. The paper deals with reliability of forest machines used in Slovak forestry. They are quite modern and helpful in the process of tree felling. This research showed how to decrease costs for maintenance, time for its execution, prepare store of spare parts and finally increase profits of felling companies. The research showed that observation of reliability is very useful regarding to the quality of maintenance and costs of it.

Keywords: risk assessment, reliability management, forest machines, maintenance

ABSTRAKT: Analýza a hodnotenie rizika sú postupy, ktoré napomáhajú rozvoju vedomostí a sú v praxi veľmi dôležité. Posúdenie rizika je možné vytvoriť iba na základe presných pravdivých a otestovaných informácií o danom systéme, ktoré daný systém v danej oblasti a čase skutočne definujú. Vysoký štandard starostlivosti a ošetrovania úzko súvisí s požiadavkami na kvalitu a spoľahlivosť lesných strojov a technologických zariadení. Tieto normy úzko súvisia so starostlivosťou o zariadenie. Príspevok sa zaoberá spoľahlivosťou lesných strojov používaných v slovenskom lesníctve. Sú celkom moderné a užitočné v procese výrubu stromov. Tento výskum ukázal, ako znížiť náklady na údržbu, čas na jej vykonanie, pripraviť sklad náhradných dielov a nakoniec zvýšiť zisky spoločností na ťažbu. Výskum ukázal, že pozorovanie spoľahlivosti je veľmi užitočné z hľadiska kvality údržby a nákladov na ňu.

Kľúčové slová: hodnotenie rizika, riadenie spoľahlivosti, lesné stroje, údržba

INTRODUCTION

The advance of international markets and the consequent increase of global competition have led manufacturers to create more and more customizable products to reach higher customer expectations. Nowadays, manufacturers need to produce high-quality products in less time. In this competitive environment, the manufacturers' interest is to focus

more than ever before on the machines' reliability (Birolini 2007, Shi *et al*. 2016). Then, an appropriate maintenance is essential in manufacturing systems to ensure all operating equipment in healthy condition, reduce failures, and guarantee the quality of the produced items (Lou *et al*. 2015). Several additional factors have motivated this interest growth in reliability, which include the increasing of complexity and sophistication of the systems (Sun *et al*. 2009) and the insistence on product quality, warranty programs, safety laws, and supply chain sustainability (Rodger *et al*. 2017). Some of the latter factors are also influenced by the high cost of failures, their repairs, or their replacement (Ebeling 2010).

The project and reliability of constructional parts have significant influence on reliability of the final product. Reliability is very complicated category and it is not easy to define only on the basis of theoretical analysis of the project. There are often necessary formal tests where the expected operational conditions are simulated and there is evaluated the object from operational time and failure occurrence point of view.

Testing is important from many reasons. The results of tests are often necessary for taking decision (quality point of view), means for reliability evaluation (e.g. maintenance), planning and choice taking process. Adequate testing leads to high reliability results and very good quality (Drožyner *et al*. 2007, Moubray 1997, Moren 1997).

We meet the words like quality and reliability in everyday life. Producers emphasize them in advertisements where they highlight quality of their products and the new owner seldom thinks about the limited reliability and thinks about it only in the case when the product breaks down (Müller 2007, Ormon *et al*. 2002).

According to the data from the first information obtained from observed group of machines, it is possible to define theoretical indicator of reliability for the whole group of machines. Every distribution has its own area for usage, its own parameters, formulas for calculations and tables. In case of observation of forest machines operational reliability there are mostly used Normal distribution and Weibull distribution. Exponential and Rayleigh distributions are special case of Weibull distribution. The advantage of the Weibull distribution is its right side asymmetry of probability density. Due to this asymmetry, the medium, modus and median values of reliability indicator are not equal in comparison with Normal distribution. Quite often Weibull distribution is used theoretical distribution of probability during solve of question in field of reliability of machine objects. This distribution is applied to data modelling, regardless of whether the failure intensity is rising, falling or constant. Weibull's distribution is flexible and adaptable for data of over a wide range (Legát *et al*. 1999, Nassar *et al*. 2017, Teringl *et al*. 2015).

The probability density (differential function) and distribution function (integral function) for Weibull distribution are calculated as follows:

$$f(t) = \frac{b}{a}\left(\frac{t}{a}\right)^{b-1} exp\left[-\left(\frac{t}{a}\right)^{b}\right] \tag{1}$$

$$F(t) = 1 - exp\left[-\left(\frac{t}{a}\right)^{b}\right] \tag{2}$$

a,b – parameters of Weibull distribution (a - parameter of size, b – parameter of shape)
t – total average time between failures.

Distributional function of "malfunction occurrence" f(t) is connected to distributional function of operational working without malfunction occurrence R(t) according to the formula:

$$R(t) = 1 - F(t) \tag{3}$$

After modification of the formulas, we can obtain:

$$R(t) = exp\left[-\left(\frac{t}{a}\right)^b\right] \tag{4}$$

For using Weibull distribution for reliability parameters estimation, it is necessary to define parameters a,b on the basis of empirical information.

Reliability prediction deal with evaluation of a design prior to actual construction of the system. Although the product reliability is not increased by the prediction process, the result of reliability prediction provides an early indication as to whether a design is likely to meet reliability goals, points to potential reliability problem areas in a new design or design modifications, and identifies components needing further testing. It is a tool to determine as early as possible whether the equipment will be reliable enough or whether it needs further improvement to function successfully for the company (Bowles 1992, Dupow *et al*. 1997, Ormon *et al*. 2002).

MATERIALS AND METHODS

The research was held in real working conditions in a company running wood processing business. This is a very important fact because the company follows all service requirements. With the help of observed objects, software and statistical methods there were obtained results. They are going to solve the problem of maintenance costs and make more effective operational conditions.

The object of the research is operational reliability of forest forwarders by John Deere. Their list is shown in Table 1.

Table 1 Observed and assessed forest forwardes machines
Tabuľka 1 Pozorované a hodnotené lesné odvozné stroje

Type of the machine: Forwarder by John Deere	**Production No. of the machine**	**Time of running during observation period (Mh)**
810 D	WJ810D001**829**	6 821
810 D	WJ810D001**136**	4 700
810 D	WJ810D001**001**	2 629
810 D	WJ810D001**002**	2 811
810 D	WJ810D00**1110**	9 680

Main methods of reliability analysis consist of four basic stages (Kováč 2009, Kováč *et al*. 2013).

1. functional and technical analysis where first data about a system are collected (characteristics of a system, functional and technical characteristics),
2. quality analysis goal is to find out all failures, reasons of their creation and description of a system what an individual failure can cause,
3. quantitative analysis creates estimation of numerical value for reliability indicators,
4. synthesis of data and conclusions from quality and quantitative analysis directly show failures and their combinations which system reliability is the most dependent on.

The reliability analysis used conditions shown in Slovak technical standards based on European standards (STN 01 0606). The exact procedure for the research of forwarders according to mentioned methods of reliability analysis is following (Kováčová, 2010):

1. Machine card creation for each device individually. Machine card obtained technical data of a device, resume of working and a drawing of it.
2. Definition constructional groups for each machine. This helped record outputs from service notes.
3. Creation of folders in MS Excel for each device. It helped to classify failures and create analysis of a device.
4. Creation of universal table for each device i.e. each device had the same structure what guaranteed uniformity and repeatability of records and the whole research.
5. Collected data were analysed using mathematical statistics. The results were presented in graphical and table forms.

RESULTS AND DISCUSSION

One factorial table of variance for individual forwarders (f810D-829, f810D-136, f810D-001, f810D-002, f810D-1110) was created in statistical software STATISTICA 7 focused on time between two failures in Mh (Table 2).

Table 2 Basic table of one factorial analysis of variance for individual forwarders (f810D-829, f810D-136, f810D-001, f810D-002, f810D-110) focused on time between two failures in Mh
Tabuľka 2 Základná tabuľka jednej faktoriálnej analýzy odchýlok pre jednotlivé dopravné systémy (f810D-829, f810D-136, f810D-001, f810D-002, f810D-110) zameraná na čas medzi dvoma poruchami v Mh

	Sum of squares	**Degrees of freedom**	**Variance**	**Fisher F test**	**p level of significance**
Total diameter	5 102 590	1	5 102 590	109.5	0.000
No. of the machine	1 001 150	4	250 287	5.4	0.001
Random factors	5 217 923	112	46 589		

The first line of Table 2 speaks about probability if the total average values of times between two failures equals zero. The first row of Table 2 shows the values of the probability that the total average values of the times between two failures are zero. The total average value of times between two failures for individual forwarders (f810D-829, f810D-136, f810D-1001, f810D-1002, f810D-1110) does not equal to zero $H1: t \neq 0$ means

that p=0,000. From the Fig. 1 and the second line of the Table 2 means that the time between two failures for individual forwarders vary statistically significantly. It means that not all forwarders showed the same malfunction.

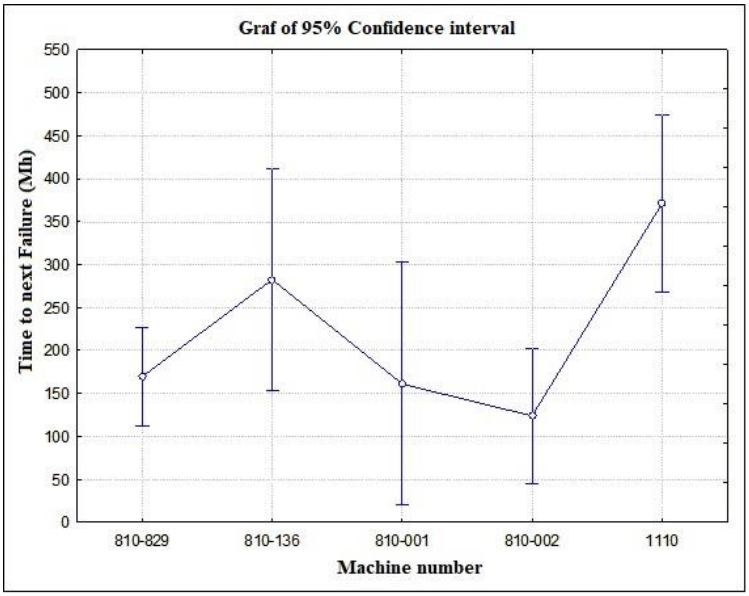

Fig. 1 Graph for 95% intervals of reliability for medium values of times between two failures for individual forwarders (f810D-829, f810D-136, f810D-001, f810D-002, f810D-1110)
Obr. 1 Graf pre 95% intervaly spoľahlivosti pre stredné hodnoty časov medzi dvoma poruchami pre jednotlivé lesné Forvardéry (f810D-829, f810D-136, f810D-001, f810D-002, f810D-1110)

There was created the table of basic statistical characteristics for individual forwarders (Table 3).

Table 3 Basic statistical characteristics for individual forwarders
Tabuľka 3 Základné štatistické charakteristiky jednotlivých forvardérov

No. of the machine	**Average time between two failures**	**Standard mistake**	**95% interval of reliability**		**No. of measurements**	**Standard deviation**	**Coefficient of variation**
			Left border	Right border			
810D-829	169,8	28,5	112,1	227,5	39	178,0	104,9
810D-136	282,6	60,3	154,1	411,1	16	241,1	85,3
810D-001	161,1	65,9	19,8	302,5	15	255,2	158,4
810D-002	124,0	37,6	45,5	202,4	21	172,4	139,1
810D-1110	371,2	50,1	267,9	474,5	26	255,7	68,9

Then, there were calculated failure intensities λ(t) raising from Weibull distribution for forwarders f810D-829 (Figure. 2), f810D-136 (Figure. 3), f810D-001 (Figure.4), f810D-002 (Figure. 5) and f810D-1110 (Figure. 6).

The calculation raised from formula for calculation of failure intensity λ(t) in Weibull two parametric distribution (only for parameter of size a, parameter of shape b, because parameter of position is c = 0), where:

$$\lambda(t) = \frac{b}{a}.\left(\frac{t}{a}\right)^{b-1} \tag{4}$$

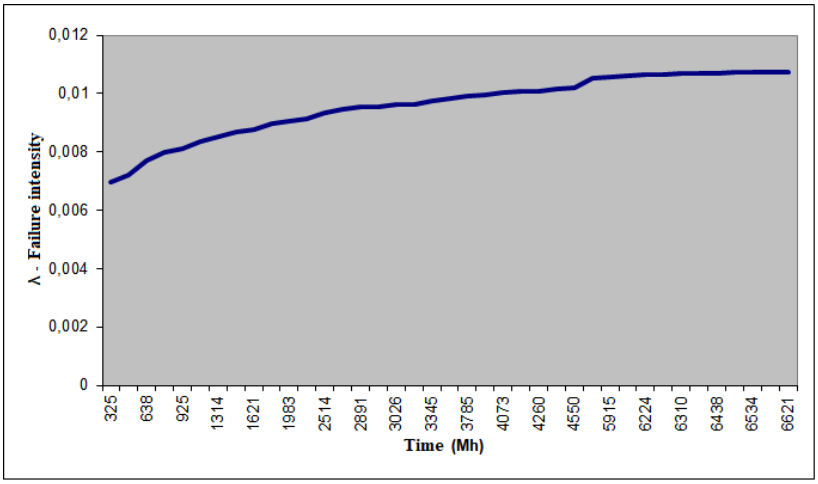

Fig. 2 Failure intensity for forwarder f810D-829
Obr. 2 Intenzita poruchy pre forvardér typ f810D-829

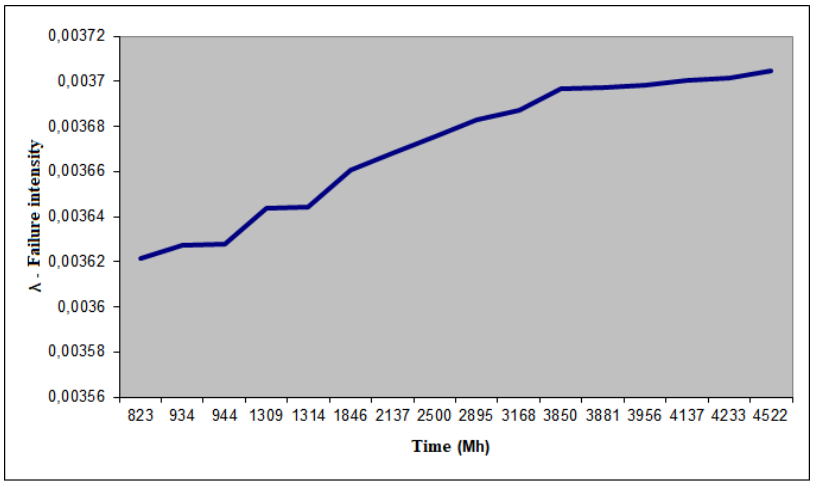

Fig. 3 Failure intensity for forwarder f810D-136
Obr. 3 Intenzita poruchy pre forvardér typ f810D-136

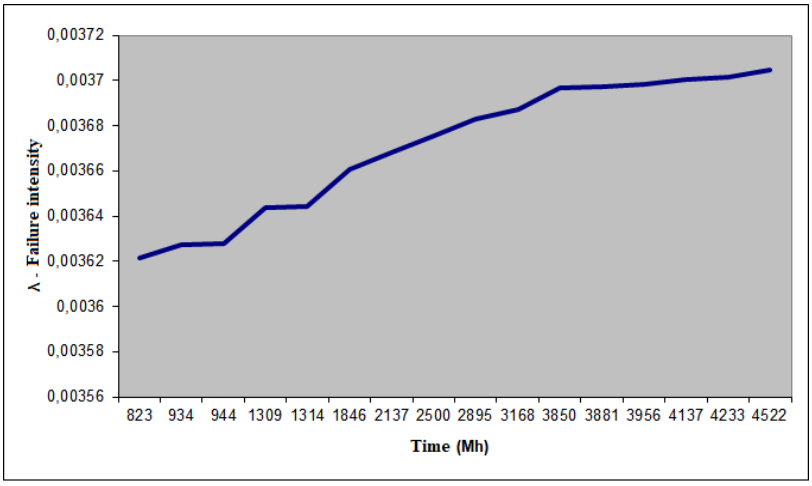

Fig. 4 Failure intensity for forwarder f810D-002
Obr. 4 Intenzita poruchy pre forvardér typ f810D-002

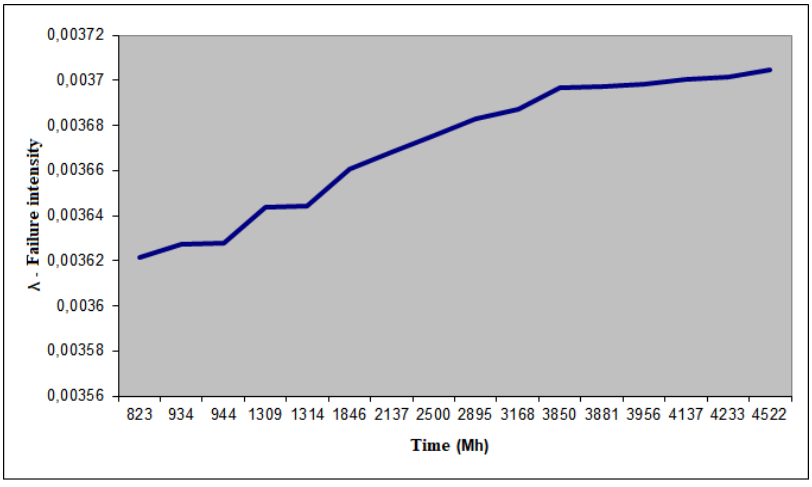

Fig. 5 Failure intensity for forwarder f810D-001
Obr. 5 Intenzita poruchy pre forvardér typ f810D-001

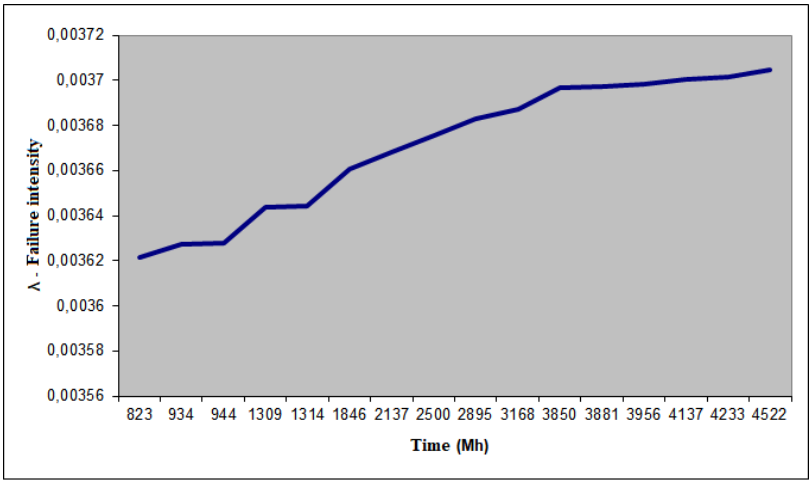

Fig. 6 Failure intensity for forwarder f810D-1110
Obr. 6 Intenzita poruchy pre forvardér typ f810D-1110

As the last indicator of reliability there was defined medium time to failure Ts. For all observed machines there were used Weibull distribution and prediction that:

$$T_S = \bar{t} = a.\varsigma\left(1+\frac{1}{b}\right) \cong a \tag{5}$$

where: a,b are parameters of Weibull distribution,
ς is gamma function (table value).

Medium time to failure Ts for types of machines and individual forwarders are shown in Table 4.

Table 4 Medium time to the failure TS
Tabuľka 4 Stredný čas do poruchy TS

Type / No. of the machine	Medium time to the failure T_S (Mh)
f810D-829	178,543
f810D-136	283,99
f810D-001	134,8187
f810D-002	108,1099
f810D-1110	378,4651
f	210,4088

CONCLUSIONS

The importance of products reliability is a very significant aspect of each device. The outputs of this research can be resumed from many points of view.

This leads to an increase of machinery operating costs – too short maintenance period results in an increase of maintenance costs, too long maintenance intervals lead to increase of costs due to poor technical condition of the production equipment (Legát *et al*. 1999).

The purposeful processing of long-term documented maintenance data can provide plenty of information not only about a machine's history, but also about its maintenance system. The main objective of data analysis is to continually improve the maintenance efficiency, which is closely related to improvements in dependability and overall productivity of the production equipment. Further examples of evaluation of maintenance management data can be found in (Peng *et al*. 2018, Kováč *et al*. 2013, Kováčová 2010).

For these forwarders, the machine had the highest average time between failures number f810D-1110, but not the largest number of failures. On the other hand, he also worked Mh. The closest to the machine was the f810D-136 forwarder, which concerns the average time between failures as well as the mean time to failure. On the contrary, the f810D-002 had the lowest average time between failures. The time differences between failures were statistically significant between machines.

The results bring positive solutions for operational usage of forwarders in organizations using these technologies in practice. This research shown how to decrease costs for maintenance, time for its execution, prepare store of spare parts and finally increase profits of felling companies. The research showed that observation of reliability is very useful regarding to the quality of maintenance and costs of it. The meaning of forwarders in the forest economy increases because it brings profit.

ACKNOWLEDGMENT

Contribution has been prepared within the solving of scientific grant project VEGA project no. 1/0642/18 "Analysis of the impact of structural parts of forestry mechanisms in the forest environment in terms of energy and ecology".

REFERENCES

BIROLINI, A. 2007. Reliability engineering. vol 5. *Springer,* Berlin.
ISBN 978-3-662-54209-5.

BOWLES, J. B. 1992. A survey of reliability-prediction procedures for microelectronic devices. *IEEE Transactions on Reliability*, 1992. 41(1):2-12. ISSN 0018-9529.

EBELING, CE. 2010. An introduction to reliability and maintainability engineering. *Waveland Press, Long Grove.* ISBN: 978-15-776-66257.

DROŻYNER, P., MIKOŁAJCZAK, P. 2007. Maintenance of vehicles, machines and equipment in view of the ISO9001 requirements. *Eksploatacja i Niezawodność - Maintenance and Reliability,* No.4/2007, Polish Maintenance Society, Warsaw. ISSN 1507-2711.

DUPOW, H, BLOUNT, G. A. 1997. Review of Reliability Prediction. *Aircraft Engineering and Areospace Technology,* 1997. 69(4):356-362. ISSN 1929-2020.

GERASIMOV, Y., SOKOLOV, A. 2009. Ergonomic Characterization of Harvesting Work in Karelia. *Croatian Journal of Forest Engineering,* 30(2): 159-170. ISSN 1845-5719.

KOVÁČ, J. 2006. Environmental analysis of working aspects in the harvester technologies. *In: Kolokvium ku grantovej* úlohe *č. 1/3534/06: zborník. – Zvolen,* Technická univerzita vo Zvolene, 2006. S. 28-36. ISBN 80-228-1692-2.

KOVÁČ J., KRILEK J., DVOŘÁK J., NATOV P. 2013. Research on reliability of forest harvester operation used in the company Lesy Slovenskej Republiky. *J. For. Sci.,* 59: 169-175. ISSN 1212-4834.

KOVÁČOVÁ, K. 2010. Research of forest machines.In Problemy inżynierii rolniczej i leśnej. Problems of argo and forestry engineering, *XIX międzynarodowa konferencja naukowa studentów, Warszawa, 26 maja 2010r. Warszawa. Szkoła Główna Gospodarstwa Wiejskiego w Warszawie, 2010*. S. 139-145. ISBN 978-83-928072-8-5.

LUO, M., YAN, HC., HU, B., ZHOU, JH., PANG, CK. 2015. A datadriven two-stage maintenance framework for degradation prediction. *In semiconductor manufacturing industries. Comput Ind Eng,* 85:414–422. ISSN 1976-2020.

LEGÁT, V., JURČA, V. 1999. Management jakosti v údržbě (Quality Management in Maintenance). *Monograph, Czech Society for Quality*. Prague, 1999.

NASSAR, M. A., ALZAATREH, M., & ABO-KASEM, O. 2017. Alpha power Weibull distribution: Properties and applications. Communications. *In Statistics - Theory and Methods,* [online]. 1-17 [cit. 2017-07-29]. ISSN 0361-0926.DOI: 10.1080/03610926.2016.1231816.

MOOREN , R. 1991. Instandhaltungsgerechtes Konstruiren und Projektieren. Grundlagen. *Methoden und Checklisten fuer die Maschinen-und Apparatenbau*. Springer Berlin. 1991. ISBN: 978-3-540-5355-60.

MOUBRAY, J. 1997. Reliability-centetred Maintenance. Butterworth-Heinemann Oxford, 1997. ISBN: 978-0-750-6335-81.

MÜLLER, M. 2007. Maintenance success control (key figures and controlling in maintenance). *Eksploatacja i Niezawodność – Maintenance and Reliability,* No. 4/2007, Polish Maintenance Society, Warsaw. ISSN 1507-2711.

ORMON, S W., CASSADY, C R., GREENWOOD, A G. 2002. Reliability Prediction Models to Support Conceptual Design. *IEEE Transactions on Reliability,* 2002, 51(2):151-157. ISSN 0018-9529.

PENG, W.W., SHEN, LJ., SHEN, Y., SUN, QZ. 2018. Reliability analysis of repairable systems with recurrent misuse-induced failures and normal-operation failures. *Reliability engineering & system safety,* 171(3): 87-98. 2018. DOI: 10.1016/j.ress.2017.11.016. ISSN 0951-8320.

RODGER, JA, GEORGE, JA. 2017. Triple bottom line accounting for optimizing natural gas sustainability: a statistical linear programming fuzzy ILOWA optimized sustainment model approach to reducing supply chain global cybersecurity vulnerability through information and communications technology. *J Clean Prod,* 142:1931–1949. ISSN 0959-6526.

SHI, H, ZENG, J. 2016. Real-time prediction of remaining useful life and preventive opportunistic maintenance strategy for multicomponent systems considering stochastic dependence. *Comput Ind En,.* 93:192–204. ISSN 1976-2020.

SUN, Y, MA, L, MATHEW, J. 2009. Failure analysis of engineering systems with preventive maintenance and failure interactions. *Comput Ind Eng,* 57(2):539–549. ISSN 1976-2020.

TERINGL, A., ALES, Z., & LEGAT, V. 2015. De-pendability characteristics – indicators for maintenance performance measurement of manufacturing technology. *Manufacturing Technology,* vol. 15, no. 3, pp. 456-461. ISSN: 1213-2489.

VÄÄTÄINEN, K., SIKANEN, L., ASIKAINEN, A. 2004. Feasibility of Excavator-Based Harvester in Thinnings of Peatland Forests. International Journal of Forest Engineering, 15(2): 103-111. ISSN 1494-2119.

Correspondence author:
Ján, Kováč, jan.kovac@tuzvo.sk; Tel.: 00421 045 5 206 517

EXPERIMENTAL RESEARCH OF COOLANT THERMAL PARAMETERS IN THE ENGINE COOLING SYSTEM

EXPERIMENTÁLNY VÝSKUM TEPELNÝCH PARAMETROV CHLADIACICH KVAPALÍN V SYSTÉME CHLADENIA MOTORA

Marek Lipnický[1], Zuzana Brodnianská[2]

[1]Department of Environmental and Forestry Machinery, Faculty of Technology, Technical University in Zvolen, Studentska 26, 960 01, Zvolen, Slovak Republic, [1]xlipnicky@is.tuzvo.sk, [2]zuzana.brodnianska@tuzvo.sk

ABSTRACT: The paper is focused on experimental research of thermal parameters of coolants based on ethylene glycol G11, G12+, and G13, used in the engine cooling system of the Škoda Felicia 1.3 MPi. An experimental assembly consisting of the engine, heater and cooling system was designed and constructed for this purpose. The aim of the research is to determine the most suitable coolant for a given type of internal combustion engine and engine cooler. The coolant G12+ achieved faster heating by 4′50′′ and 6′54′′, and cooling by 7′41′′ and 11′30′′ compared to G11 and G13, respectively. The results show that G12+ coolant is most appropriate for examined engine cooling system, which has a positive effect on the car thermal management.

Key words: heating, cooling, engine cooler, coolant, experiment

ABSTRAKT: Príspevok je zameraný na experimentálny výskum tepelných parametrov chladiacich kvapalín na báze etylénglykolu G11, G12+, G13, použitých v chladiacej sústave motora Škoda Felicia 1.3 MPi. Na tento účel bola navrhnutá a skonštruovaná experimentálna zostava pozostávajúca z motorovej časti, ohrevného telesa a chladičovej sústavy. Cieľom výskumu je stanoviť najvhodnejšiu chladiacu kvapalinu pre daný typ spaľovacieho motora a chladiča. Chladiaca kvapalina G12+ dosiahla rýchlejší ohrev o 4′50′′ a 6′54′′ a rýchlejšie ochladenie o 7′41′′ a 11′30′′ v porovnaní s G11 a G13. Z výsledkov vyplýva, že chladiaca kvapalina G12+ má priaznivý vplyv na správny chod motora a jeho životnosť, na nižšiu produkciu emisií a lepšiu ekonomiku prevádzky automobilu. Výsledky ukazujú, že chladiaca kvapalina G12+ je najvhodnejšia pre skúmaný chladiaci systém motora, čo má pozitívny vplyv na tepelný manažment automobilu.

Kľúčové slová: ohrev, chladenie, chladič motora, chladiaca kvapalina, experiment

INTRODUCTION

Car engine cooling system is important for maintaining the proper function and life of the engine part. Approximately one third of the thermal energy produced by internal com-

bustion engines is used as waste heat through the cooling system. Efficient cooling ensures better filling of the cylinders, higher performance with more favorable fuel consumption, higher compression ratio and a more even engine operating temperature. The ideal coolant has a high heat capacity, low viscosity and is chemically non-reactive, does not cause or increase corrosion of the cooling system. Coolant contain components, which increase their boiling point and decrease their freezing point.

Several authors have investigated and analyzed different types of coolants under different operating conditions. Authors (Gollin & Bjork 1996) used five different engine coolers for heat transfer research located in a wind tunnel for the following coolants: 100% propylene glycol, 100% water, ratio of propylene glycol to water 70:30 and 50:50, ratio of ethylene glycol to water 70:30 and 50:50. They came to a conclusion, that the most effective coolant is water, followed by a mixture of ethylene glycol and water 50:50, propylene glycol and water 50:50, ethylene glycol and water 70:30, propylene glycol and water 70:30, and finally 100% propylene glycol. Authors (Juger & Crook 1999) they experimentally tested two coolers with the same flow area, but at the vertical and horizontal position of the tubes. They investigated the effect of tube length on number for glycol-based coolants (ethylene glycol, propylene glycol) mixed with water 50:50, and for the water itself. When using a mixture of propylene glycol and water, there was a more significant decrease in performance at higher flow rates compared to a mixture of ethylene glycol and water or water alone. Authors (Oliet *et al.* 2007) confirmed, that heat transfer and cooler performance are significantly affected by air and coolant flow. As the air and coolant flow increases, the cooling capacity increases, as the inlet air temperature increases, the heat transfer and thus the cooling amount decreases.

Authors (Efeovbokhan & Ohiozua 2013) dealt with the comparison of the cooling properties of water, commercially available coolant and formulated coolant (a mixture of ethylene glycol and water in the ratio 50:50 a 1% corrosion inhibitor). The formulated coolant reached the highest boiling point 110 °C and its mass heat capacity was 4238 $J.kg^{-1}.K^{-1}$. A mixture of ethylene glycol and water with a corrosion inhibitor is much more effective compared to the same mixture without a corrosion inhibitor. Although water itself is effective as a coolant, it also causes significant corrosion. Authors (Turizo-Santos *et al.* 2015) experimentally investigated the heat transfer and pressure losses on the side of the flowing air impinging on the corrugated ribs fitted with soldering on a plate heat exchanger. The cooling water flow was constant 1.82 $m^3.h^{-1}$ and the air flow varied in the range of the Reynolds number 350 to 1270. Heat transfer and pressure drop were evaluated in terms of the Colburn factor *j* and the coefficient of friction *f* at the change *Re*. The experimental results were compared with CFD simulations for the same geometry.

Authors (Channankaiah & Arunpandiyan 2016) focused on the research of the engine cooling system on the air and liquid side using experimental and numerical analysis. On the air cooling side, the cooling capacity can be increased by modifying the fins and the shape of the cooler, on the fluid side, it is possible to modify the tubes, ribs, core, fan and coolant. Cooling on the liquid side transfers heat at the maximum level compared to the air side of the system. In 2017, the authors (Patil *et al.* 2017) dealt with the optimization of heat transfer in smaller car coolers. The compact shape of the cooler leads to a reduction in air resistance, lower fuel consumption and a reduction in the car's weight. Authors (Shariff *et al.* 2018) dealt with a numerical study on the effect of ribs on the performance

of a car cooler at atmospheric temperature in the state of Kano in Nigeria. The 2000 Honda Civic cooler model was modeled in SolidWorks and analyzed in ANSYS Fluent. In order to increase the cooling effects of the cooler, ribs were mounted on the assembly, which increased its heat exchange area. They found that the maximum and minimum temperatures in Kano were 39.5 °C and 30.2 °C in April and August. The results showed that in the case of fitted ribbing, there is a 25% decrease in the outlet temperature from the cooler. The aluminum cooler with a ribbed surface is advantageous for conditions in the Kano due to its greater heat dissipation at a relatively small size.

Authors (Saini *et al.* 2014) deal with the application of carbon foam as the cooler material in the design shows an increased rate of heat transfer Q = 53,414 W, which is much greater than the required value Q_{req} = 35,596 W. Hence, the existing cooler can be made smaller in size by 203 mm (33%) in width. That s means, there is an extra availability of 1630 cm^3 space in engine compartment and decrease in the frontal surface area. Nanofluid, shows an increase rate of heat transfer (Q = 38,078 W) that is also a great way to enhanced the rate of convection between the inner walls of the tubing and the fluid, this rate of heat transfer is greater than the required value (Q_{req} = 35,596 W) and hence the cooler can work efficiently even at higher load and speed requirement in hot climatic conditions.

Authors (Sudhakar & Yasin 2019) performed a computational fluid dynamics (CFD) analysis in the ANSYS program continuously to analyze the heat transfer process. A comparative study was performed between straight and spiral tubes with respect to different coolant mass flow rates. Further analyses were performed by varying coolants from conventional fluids air, water to nanofluids with different volume fractions. CFD analysis was performed on a cooler model with varying mass flow rates, and varying tube designs. In order to enhance the heat transfer, nanofluid SIC (silicon carbide) and MgO_2 were used with two different volume fractions. It is observed that with increase in mass flow rate the heat transfer coefficient increases thereby increasing the coolant efficiency. Further it was found nanofluids have much better tendency to enhance heat transfer than straight and helical tubes standing way a head in terms of heat transfer and nominal in pressure drop.

Authors (Yadav & Singh 2011) deal with, in performance evaluation a cooler is installed into a testing setup and the various parameters including mass flow rate of coolant (5.0 ÷ 8.5 $l.min^{-1}$), inlet coolant temperature (80 °C) etc. are varied. The modeling of cooler has been described by two methods, one is finite difference method and the other isothermal resistance concept. A comparative analysis between different coolants is also shown. One coolant as water and other as mixture of water in propylene glycol in a ratio of 40:60 is used. They found that water is still one of the best coolants, but its limitation is that it causes corrosion and contains dissolved salts that degrade the permeability of the coolant through the pipes. By making a mixture with ethylene glycol its specific heat is decreased but its other properties are enhanced. It also increases the boiling temperature water and decreases freezing temperature also. Authors concluded from the studies that the cooling capacity and the effectiveness are indirect relation with the inlet temperature of hot coolant i.e. with an increase in the value of inlet coolant temperature the cooling capacity and the effectiveness of the cooler increases respectively.

Authors (Hussein *et al.* 2014) deal with heat transfer enhancement using nanofluids in an automotive. The forced convection heat transfer enhancement by TiO_2 and SiO_2 suspended in water as a base fluid inside the flat copper tubes of an automotive cool-

ing system has been measured. Significant heat transfer enhancement was observed and was associated with the concentration of the nanoparticles. Maximum Nusselt number enhancements of up to 11% and 22.5% were obtained for TiO_2 and SiO_2 nanoparticles, respectively, in water. The experimental results showed that the Nusselt number behaviors of the nanofluids highly depended on the volume flow rate, inlet temperature and nanofluid volume concentration. The results showed that the SiO_2 nanofluid produces a higher heat transfer enhancement than the TiO_2 nanofluid; likewise, TiO_2 nanofluid enhanced heat transfer more than pure water. The results also proved that TiO_2 and SiO_2 nanofluid have a high potential for heat transfer enhancement and are highly appropriate for industrial and practical applications.

Authors (Selvam *et al.* 2017) presented an improvement in the overall heat transfer coefficient of the cooler using a nanofluid based on graphene nanoparticles. As a basic coolant, they used a mixture of water-ethylene glycol in a ratio of 70:30 together with a nanofluid which contained nanoparticles of graphene in the range of 0.1% to 0.5%. During the measurements, the nanofluid flow changed from 12.5 $g.s^{-1}$, 25 $g.s^{-1}$, 37.5 $g.s^{-1}$, 50 $g.s^{-1}$ and 62.5 $g.s^{-1}$ at an inlet temperature of 35 °C and 45 °C. The velocity of the thrust air varied in the range of 1 $m.s^{-1}$ to 5 $m.s^{-1}$. Increasing the heat transfer coefficient on the nanofluid side plays an important role in improving the overall heat transfer coefficient. The maximum increase in the total heat transfer coefficient was 104% at 35 °C, 81% at 45 °C at a flow rate of 62.5 $g.s^{-1}$ and an air velocity 5 $m.s^{-1}$. The pressure loss of the nanofluid increases with increasing airflow and the amount of graphene.

In the presented research, we dealt with experimental research of thermal parameters of ethylene glycol-based coolants G11, G12+, G13, in the engine cooling system Škoda Felicia 1.3 MPi (50 kW). The experimental assembly was designed and constructed for research in the laboratory. The aim was to compare the time required for heating and cooling the investigated coolants and to determine the appropriate type of coolant for a particular internal combustion engine and cooler.

MATERIAL AND METHODS

For the research of thermal parameters of coolants, an experimental assembly according to Fig. 1. The individual components come from the Škoda Felicia 1.3 MPi. The engine does not generate heat by combustion, therefore, the coolant is heated in the heater (10). The engine was used for measurements in order to create the most realistic conditions from practice, but in a laboratory. The volume of coolant in the system is approximately 6 liters.

The experimental cooling system assembly has two cooling circuits (short and long). At temperatures up to 80 °C, the coolant flows in a short cooling circuit, which consists of a water pump (14) driving the coolant through the engine cylinder block (19) into the thermostat body (6) and from there into the inlet pipe of the heater (12). In the heater (10), the coolant is heated by a heating spiral (13).

In case of aeration or flooding of the heater, a return pipe is led from its upper part (9) into the expansion tank (8). The outlet pipe of the heater (11) is connected to a water pump (14). The coolant flows through a short circuit, until the temperature rises above 80 °C. Subsequently, the thermostatic valve located in the thermostat body (6) starts to open and

the hot liquid flows to the inlet of the cooler (1). In case the hot liquid does not manage to flow under pressure through the cooler (3), a part of it flows through the return pipe (7) into the expansion vessel (8). Heating spiral (13) with a power of 1500 W is mounted in a body with dimensions of 80 × 80 × 300 mm.

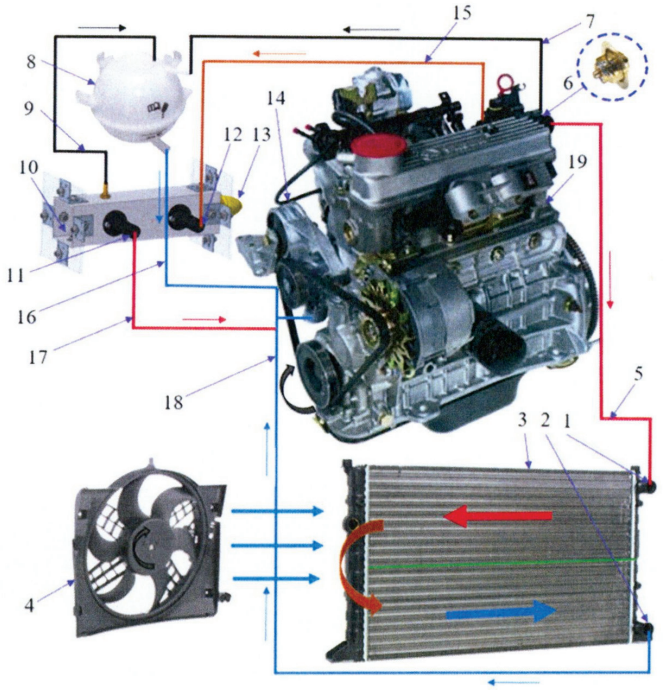

Fig. 1 The scheme of experimental assembly
1 – cooler inlet pipe, 2 – cooler outlet pipe, 3 – engine cooler, 4 – fan, 5 – connecting pipe (thermostat cooler inlet pipe), 6 – thermostat, 7 – reverse pipe, 8 – expansion tank, 9 – vent pipe, 10 – heater, 11 – coolant outlet from the heater, 12 – coolant inlet to the heater, 13 – heating spiral, 14 – water pump, 15 – connecting pipe (thermostat-heater), 16 – filling pipe cooling circuit, 17 – outlet pipe heated fluid, 18 – drainage of the cooled liquid from the cooler, 19 – engine
Obr. 1 Schéma experimentálnej zostavy
1 – vstupné potrubie chladiča, 2 – výstupné potrubie chladiča, 3 – chladič motora, 4 – ventilátor, 5 – spojovacie potrubie (termostat-chladič), 6 – termostat, 7 – spätné potrubie termostatu, 8 – vyrovnávacia nádržka, 9 – odvzdušňovacie potrubie, 10 – ohrevné teleso, 11 – výstup chladiacej kvapaliny z ohrevného telesa, 12 – vstup chladiacej kvapaliny do ohrevného telesa, 13 – ohrevná špirála, 14 – vodné čerpadlo, 15 – spojovacie potrubie (termostat-ohrevné teleso), 16 – plniace potrubie chladiaceho okruhu, 17 – výstupné potrubie ohriatej kvapaliny, 18 – odvod ochladenej kvapaliny z chladiča, 19 – motor

An important part of the assembly is the engine cooler (3), in which the coolant flows in the sense of the arrows shown in Fig. 1. Through the cooler outlet pipe (2), the cooled medium flows back to the water pump (14) and from there back to a short circuit until the coolant temperature drops below 80 °C. In case the coolant cannot be cooled by the

engine cooler itself (3), the fan (4) is started, which more intensively dissipates heat from the cooler tubes and ribs.

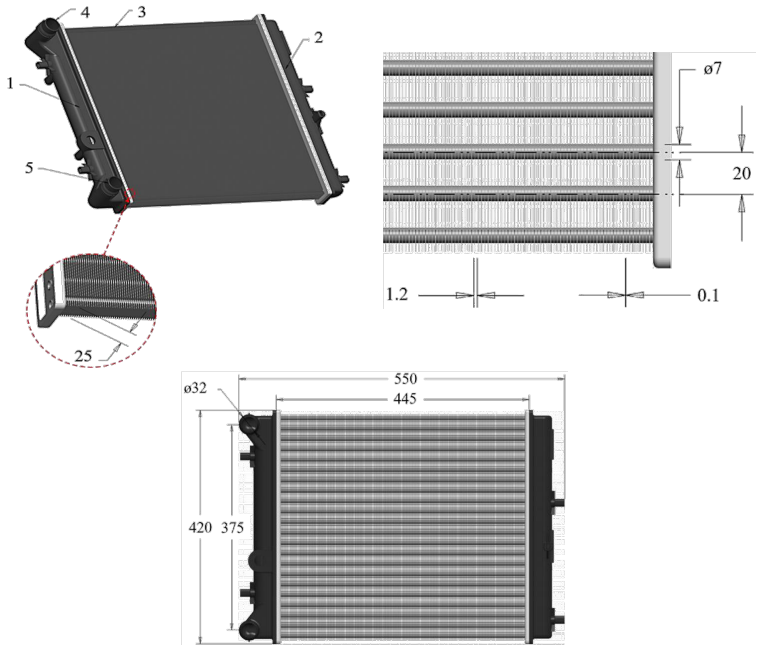

Fig. 2 Engine cooler
1 – plastic cover with holes for liquid inlet and outlet, 2 – connecting plastic cover, 3 – heat exchange surface with ribs, 4 – fluid input pipe, 5 – fluid output pipe
Obr. 2 Chladič motora
1 – plastový kryt s otvormi pre vstup a výstup kvapaliny, 2 – spojovací plastový kryt, 3 – teplovýmenná plocha s rebrami, , 4 – potrubie pre vstup kvapaliny, 5 – potrubie pre výstup kvapaliny

Material of tubes and fins is aluminum. The outer diameter of the fan blades is 350 mm. The engine cooler (Fig. 2) consists of 44 tubes with an inner diameter of 6.5 mm arranged in two rows of 22 tubes. The vertical spacing between the tubes is 20 mm and the spacing between the first and second rows of tubes is 10 mm. Through the entire height of the cooler (420 mm) there are lamellas (ribs) mounted on the pipes in the number of 400 for more intensive heat dissipation. Each of the ribs is 0.1 mm thick and 25 mm wide. Space between the cooler fins is 1.2 mm.

The experimental setup includes sensors for measuring the temperature of the flowing coolant in the inlet and outlet pipes of the cooler (Fig. 3a). These are NTC thermistors ZA 9040-FS (Negative Temperature Coefficient), whose heating resistance decreases (Koleda *et al.* 2016). Their measuring range is –50 °C to 125 °C, with an accuracy of ± 0.01 °C. A flowmeter, with a measuring range of 2 $l.min^{-1}$ to 40 $l.min^{-1}$ and an accuracy of ± 1% of the measured value, is inserted in the pipe between the thermostat body and the cooler inlet pipe (Fig. 3b). The coolant temperature and flow values are recorded in the ALMEMO

2590-4S data logger. For non-contact surface temperature measurement, a Flir i7 thermal imaging camera with a resolution of 120 × 120 pixels, the accuracy of ±2% of the measured value and a temperature range of –20 °C to +250 °C is used.

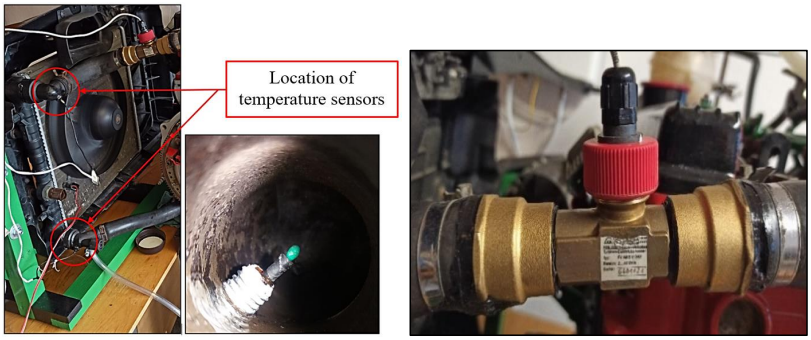

Fig. 3 Built-in sensors of physical quantities into the experimental assembly
a) coolant temperature sensors NTC ZA 9040-FS, b) flowmeter FVA 915 VTH
Obr. 3 Zabudované snímače fyzikálnych veličín do experimentálnej zostavy
a) snímače teploty chladiacej kvapaliny NTC ZA 9040-FS, b) prietokomer FVA 915 VTH

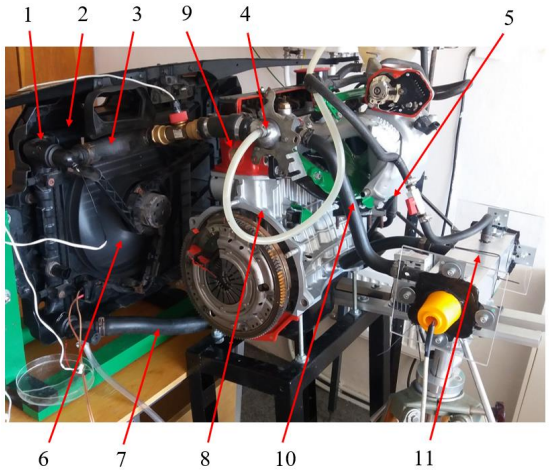

Fig. 4 Experimental assembly of the engine cooling system in the laboratory
1 – cooler, 2 – cooler wall, 3 – upper cooler hose, 4 – thermostat, 5 – water pump, 6 – fan, 7 – lower cooler hose, 8 – engine block, 9 – cylinder head, 10 – heating hose, 11 – heater
Obr. 4 Experimentálna zostava v laboratóriu
1 – chladič, 2 – stena chladiča, 3 – horná hadica chladiča, 4 – termostat, 5 – vodné čerpadlo, 6 – ventilátor, 7 – dolná hadica chladiča, 8 – blok motora, 9 – hlava valcov, 10 – hadica kúrenia, 11 – ohrevné teleso

In Fig. 4 shows an experimental assembly of the engine cooling system in the laboratory. Assembly is put into operation after starting the electric motor controlled by the frequency converter on which we set the required speed. By means of a circulation pump,

the coolant flows into the engine block and around the individual engine cylinders and enters the cylinder head (9). It is led through the collecting channel to the thermostatic valve (4). Until the coolant temperature reaches operating temperature, the thermostatic valve closes and the liquid returns to the pump suction in a short circuit. When the operating temperature is reached, the thermostat opens the inlet to the pipe connecting the engine to the cooler (3). At this point, the temperature is recorded using a data logger at the inlet and outlet of the cooler, as well as the liquid flow (Tab. 4). After heating the assembly to the operating temperature, we recorded the temperatures of the individual surfaces of the components with a thermal imaging camera. The cooler was sensed at several points from the inlet pipe to the outlet pipe. The coolant is thus cooled before entering to the pump suction; it circulated in a long circuit. The required air flow through the cooler ensures a surge of air while driving, possibly a fan located on the cooler (6). The fan turns on depending on the cooler temperature.

RESULTS AND DISCUSSION

Gradual heating of individual parts of the experimental assembly was recorded by a thermal-imaging camera Flir i7 (Fig. 5). Using the coil power regulator, the temperature at the outlet of the cooler was set to 88 °C (Fig. 5a). The coolant then flowed through the engine (Fig. 5b) at 84.1 °C, through a thermostat opening above 80 °C, and entered the cooler at 80.3 °C (Fig. 5c).

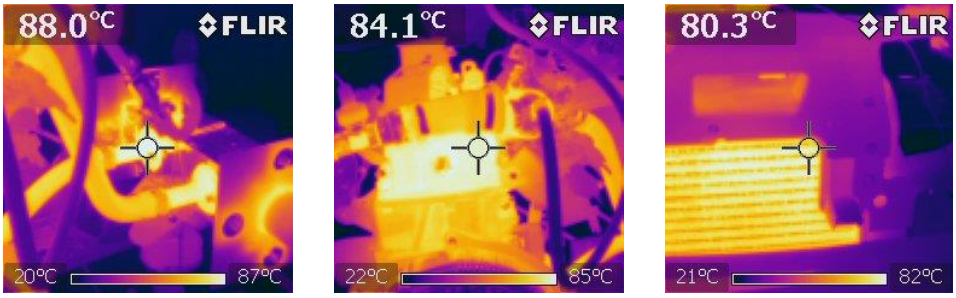

Fig. 5 Thermal images of gradual heating of parts of the experimental set-up
a) heater, b) engine, c) cooler
Obr. 5 Termovízne snímky postupného ohrevu častí experimentálnej zostavy
a) ohrevné teleso, b) motor, c) chladič

The manufacturer‘s tested coolants protect the engine cooling system from freezing, corrosion, deposits all year round and are gentle on engine sealing elements. Concentrated coolant type G11 based on ethylene glycol containing organic corrosion inhibitors is suitable for cooling systems of internal combustion engines, especially with aluminum components. Complies with ASTM D 1177 – freezing point determination, ASTM D 1384 – corrosion protection and meets the requirements of VW TL 774 C.

Concentrated coolant type G12+ based on ethylene glycol containing organic corrosion inhibitors without silicates is suitable for cooling systems of internal combustion engines, especially with aluminum components. Complies with ATM D 1177 – freezing

point determination, ASTM D 3306 – ethylene glycol specification for coolants, ASTM D 1384 – corrosion protection, ASTM D 4656, ASTM D 4985. Meets the requirements of VW TL 774 D / F, PSA B 715110, BMW N 600 69.0, BS 6580: 2010, Daimler, Chrysler 325.0, MAN 324 – SNF, ANFOR NF R15 – 601, JIS K 2234, SAE J 1034.

Concentrated coolant type G13 based on ethylene glycol containing organic corrosion inhibitors and silicates is suitable for cooling systems of modern internal combustion engines. Conforms to ASTM D 1177 – Freezing Point Determination, ASTM D 3306 – Ethylene Glycol Specification for Coolants, ASTM D 1384 Corrosion Protection. Meets the requirements of VW TL 774 J, BS 6580: 2010, MB 325.5, SAE J 1034. The physical parameters of the investigated coolants (water, ethylene glycol) and their mixture for the temperature 22 °C and 80 °C are shown in Table 1, 2. Mixing ratio of the coolants and their freezing points are shown in Table 3.

Table 1 Physical parameters of the investigated coolants
Tabuľka 1 Fyzikálne parametre skúmaných chladiacich kvapalín

Fluid		**Water**		**Ethylene Glycol**	
		22 °C	80 °C	22 °C	80 °C
Fluid properties	Density [kg.m^{-3}]	9.9733×10^{2}	9.7121×10^{2}	1.1142×10^{3}	1.0748×10^{3}
	Dynamic Viscosity [kg.m^{-1}.s^{-1}]	9.3130×10^{-4}	3.4599×10^{-4}	0.019520	3.5153×10^{-3}
	Kinematic Viscosity [m^{2}.s^{-1}]	9.3379×10^{-7}	3.5625×10^{-7}	1.7519×10^{-5}	3.2708×10^{-6}
	Specific Heat [J.kg^{-1}.K^{-1}]	4.0748×10^{3}	4.0696×10^{3}	2.3953×10^{3}	2.6528×10^{3}
	Thermal Conductivity [W.m^{-1}.K^{-1}]	0.60781	0.67002	0.25066	0.26189
	Prandtl number [-]	6.2434	2.1015	1.8653×10^{2}	35.608
	Thermal diffusivity [m^{2}.s^{-1}]	1.4956×10^{-7}	1.6952×10^{-7}	9.3919×10^{-8}	9.1855×10^{-8}
	Thermal Expansion Coefficient [K^{-1}]	3.3881×10^{-3}	2.8317×10^{-3}	3.3881×10^{-3}	2.8317×10^{-3}

Table 2 Physical parameters of the mixture water/ethylene glycol
Tabuľka 2 Fyzikálne parametre zmesi voda/etylénglykol

Mixture 66,67% water + 33,33% ethylene glycol G12+		22 °C	80 °C
Fluid properties	Density [kg.m^{-3}]	1055	1022
	Dynamic Viscosity [kg.m^{-1}.s^{-1}]	2.0375×10^{-3}	6.0729×10^{-4}
	Kinematic Viscosity [m^{2}.s^{-1}]	2.0375×10^{-6}	0.6065×10^{-7}
	Specific Heat [J.kg^{-1}.K^{-1}]	3.6284×10^{3}	3.7886×10^{3}
	Thermal Conductivity [W.m^{-1}.K^{-1}]	0.4854	0.4785
	Prandtl number [-]	15.614	4.6673
	Thermal diffusivity [m^{2}.s^{-1}]	1.2588×10^{-7}	1.2995×10^{-7}
	Thermal Expansion Coefficient [K^{-1}]	3.3881×10^{-3}	2.8317×10^{-3}

Table 3 Dilution of the antifreeze fluids
Tabuľka 3 Riedenie mrazuvzdorných kvapalín

Coolant	Mixing ratio Coolant:distilled water	Freezing point
G11	1:1 / 1:2	–36 °C/ –17 °C
G12+	1:1 / 1:2	–37 °C/ –18 °C
G13	1:1 / 1:2	–38 °C/ –17 °C

In Fig. 6 shows the heating and cooling processes of the coolants G11, G12+, and G13 at the inlet to the cooler t_{in} and at the outlet from the cooler t_{out}. The investigated coolants achieved different heating and cooling times due to their different composition and physical properties.

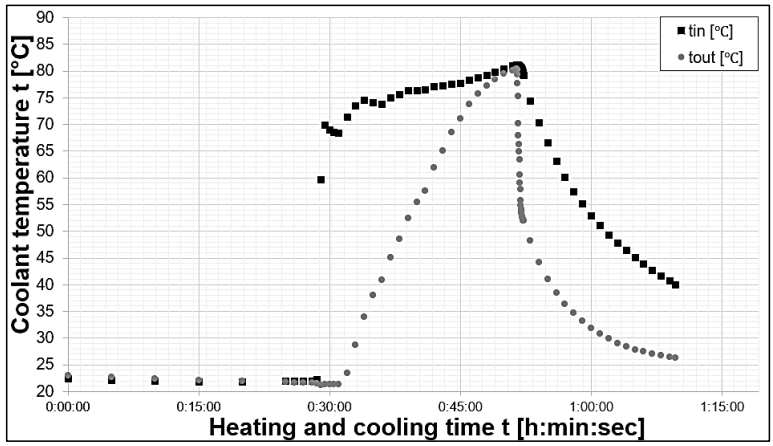

a)

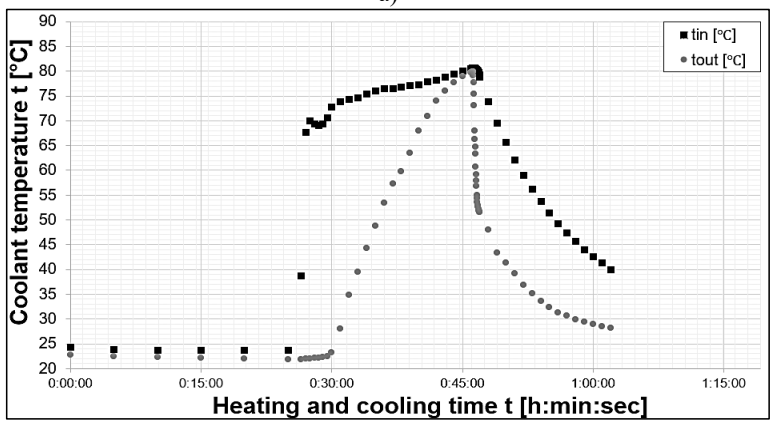

b)

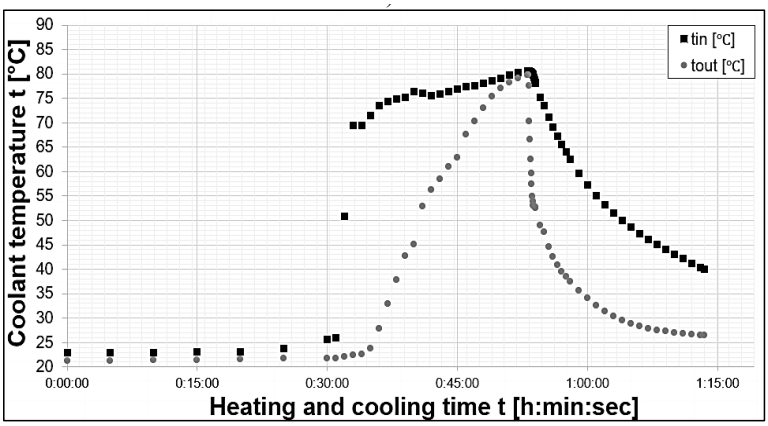

c)

Fig. 6 The course of coolant temperatures during heating and cooling
a) G11, b) G12+, c) G13
Obr. 6 Priebeh teplôt chladiacich kvapalín počas ohrevu a ochladzovania
a) G11, b) G12+, c) G13

The investigated coolants contain components that increase their boiling point and decrease their freezing point. The higher boiling point of the coolant allows more heat to be removed from the engine, thus preventing engine damage due to overheating. G12+ coolant achieved the shortest heating and cooling time compared to G11 and G13 coolants.

Although G12+ coolant can be mixed with G11 blue-green and G12+ red liquids, however, for long-term operation and service life, it is advisable to use only one species concentrated with water. Coolant type G11 and G13 had to be heated for the longest, also their cooling required a significantly longer time compared to G12+ liquid. These types of fluids are prescribed for newer and brand new automobile, but can also replace any fluid in the cooling system of older automobile. G11 fluid is primarily intended for engines whose cylinder heads are made of aluminum alloys. The G13 coolant standard allows a certain silicate content, which provides continuous protection for metal particles.

In Fig. 7 shows the course of the temperature difference at the inlet to the cooler and the outlet from the cooler Δt of the coolants G11, G12+, and G13. The most suitable coolant for the used type of engine and cooler is G12+ (a mixture of water and antifreeze). Other measured types of coolants are especially suitable for engines with higher performance parameters, other design and materials of individual components.

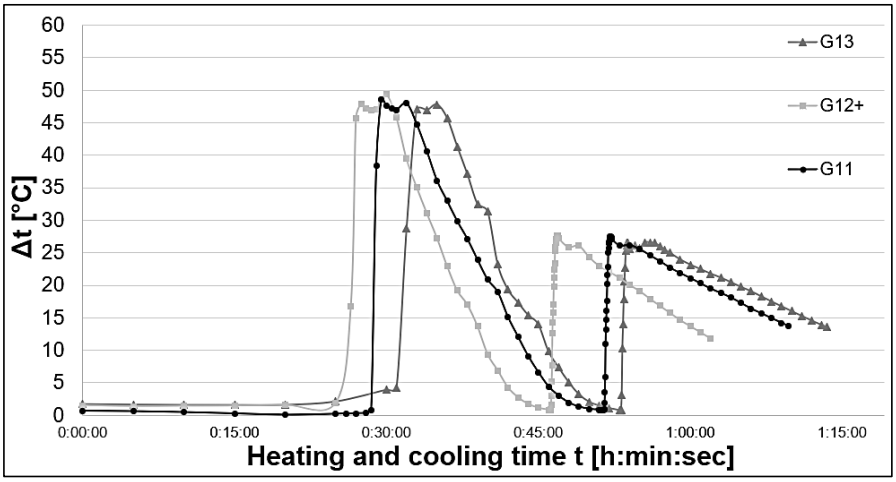

Fig. 7 Comparison of heating and cooling of coolants
Obr. 7 Porovnanie ohrevu a ochladzovania chladiacich kvapalín

The thermal parameters of heating and cooling of the coolants are show in Tab. 2. The initial opening of the thermostat occurred when the liquid was heated [h:min:sec]: G11 (0:33:00), G12+ (0:27:00), G13 (0:33:00), when the temperature and flow fluid at the inlet to the cooler have reached the values G11, G12+, G13. The thermostat was fully opened when the liquid was heated: G11 in time 0:51:00; G12+ in time 0:46:10; G13 in time 0:53:04. The coolant G12+ achieved faster heating by 4´50´´ and 6´54´´ compared to G11 and G13, respectively. When using the G12 + the thermostat opened and closed in the shortest time (0´36´´) compared to G13 (0´38´´), G11 (1´06´´).

Table 4 The thermal parameters of the heating and cooling coolants
Tabuľka 4 Tepelné parametre chladiacich kvapalín počas ohrevu a chladenia

Coolant	Thermostat	Heating				Cooling			
		τ [h:min:sec]	t_{in} [°C]	t_{out} [°C]	Q [m^3.h^{-1}]	τ [h:min:sec]	t_{in} [°C]	t_{out} [°C]	Q [m^3.h^{-1}]
G11	1st open	0:33:00	73.44	28.68	0.1	0:52:06	80.08	52.57	2.5
	fully open	0:51:00	80.93	80.11	2.5	1:09:41	40.01	26.29	0
G12+	1st open	0:27:00	67.69	21.95	0.6	0:46:46	80.08	53.01	2.5
	fully open	0:46:10	80.72	79.95	2.5	1:02:00	40.01	28.20	0
G13	1st open	0:33:00	69.44	22.41	0.2	0:53:42	80.00	53.84	2.6
	fully open	0:53:04	80.62	79.85	2.5	1:13:30	40.01	26.43	0

The liquid was cooled to temperature t_{in} = 40.01 °C for Q = 0 m^3.h^{-1} at different times (Tab. 2). The coolant G12+ achieved faster cooling by 7´41´´ and 11´30´´ compared to G11 and G13, respectively.

Comparison of coolants solved by the authors (Yadav & Singh, 2011) they used water as the first cooling medium and 40% water and 60% propylene glycol as the second medium. They have found that water is one of the best coolants, but its limitation is that it causes corrosion, it contains soluble salts which degrade the permeability of the coolant through pipes. In experiment, the authors used, as in our case, a cooler made of aluminum due to its low weight and high thermal conductivity. During their measurement, the fan ran continuously behind the cooler, in our case it was only after reaching the temperature of the thermostat opening and reaching the maximum flow in the inlet pipe to get closer to the real conditions of car operation. The temperature was fixed at 80 °C in both cases. A comparison of temperatures is shown in Table 5. The flow rate has changed with increasing temperature. In their experiment, the authors found flow values ranging from 5.0 to 8.5 $l.min^{-1}$ using a smaller and smaller diameter pipes, in our measurement we recorded a maximum flow value of 41 $l.min^{-1}$ using a larger with horizontally placed tubes in two rows and using larger pipe diameters.

Table 5 Outlet temperature versus inlet temperature of cooler without fan/with fan
Tabuľka 5 Výstupná teplota verzus vstupná teplota chladiča bez ventilátora/s ventilátorom

Cooler temperature [°C]		Water (Yavad & Singh 2011)	40% Water + 60% P.G. (Yavad & Singh 2011)	Water (present study)	40% E.G. + 60% Water (present study)
Outlet	without Fan	70	72	78.27	77.71
Inlet		80	80	80	80
Outlet	with Fan	54	56	50.93	50.84
Inlet		80	80	80	80

Authors (Roslan *et al.* 2017) investigate the effects of ethylene glycol on its specific heat capacity and freezing point. The data shows that the freezing point temperature decreases when the volume of the ethylene glycol that were used in the experiment increases. In this experiment, it is found that 40% of ethylene glycol and 60% of ultrapure water are the best properties for a coolant to be used because the freezing point that were obtained is –45.97 °C. This ratio is also recommended by the engine manufacturer Škoda Felicia 1.3. The same ratio of ethylene glycol to water was used in our experiment and also proved to be the most optimal. It is because only a moderate amount of ethylene glycol is needed in a car coolant, so that the coolant will not crystallized easily.

CONCLUSION

The use of a suitable coolant in a particular engine's cooling system is essential to maintaining its proper function and service life. Rapid heating and cooling of the coolant also has a positive effect on lower emissions and better operating economy. An experimental assembly suitable for laboratory conditions was designed and constructed to investigate the thermal parameters of the coolants in the engine cooling system. It consists mainly of the heater, engine, water pump, expansion tank and connecting hoses.

The thermal properties of ethylene glycol-based coolants containing organic corrosion inhibitors G11, G12+, and G13 were investigated. The coolant G12+ (1:2 mixture of water and antifreeze) was evaluated as the most advantageous for the used cooler and Škoda Felicia 1.3 MPi engine. The coolant G12+ was heated and cooled in the shortest time in compared to other tested fluids; the G12+ achieved faster heating by 4′50′′ and 6′54′′, and cooling by 7′41′′ and 11′30′′ compared to G11 and G13, respectively. This type of coolant is suitable for sealing materials, material of individual components (mostly aluminum), which are used with the engine type and do not damage them by their operation.

ACKNOWLEDGMENT

The contribution was created within the project VEGA 1/0086/18 "The Research of Temperature Fields in the System of Shaped Heat Exchange Surfaces" funded by the Ministry of Education, Science, Research, and Sport of the Slovak Republic.

REFERENCES

EFEOVBOKHAN, V.E. & OHIOZUA, O.N. 2013. Comparison of the cooling effects of a locally formulated car radiator coolant with water and commercial coolant. In The International Journal of Engineering and Science, 2013, vol. 2, no. 1 , pp. 254-262, ISSN 2319-1813.

GOLLIN, M & BJORK, D. 1996. Comparative performance of ethylene glycol/water and propylene glycol/water coolants in automobile radiators. In SAE Technical Paper Series SP-1175, 1996, pp. 115–123. DOI:10.4271/960372, ISSN 0148-7191.

HUSSEIN, A. M., BAKAR. R. A., KADIRGAMA, K., SHARMA, K. V., 2014. Heat transfer enhancement using nanofluids in an automotive cooling system. In International Communications in Heat and Mass Transfer, 2014, vol. 53, pp. 195-202 DOI:10.1016/j.icheatmasstransfer.2014.01.003.

CHANNANKAIAH, Dr., ARUNPANDIYAN, D. 2016. A review of automotive radiator performance. In International Journal for Innovative Research in Science and Technology, 2016, vol. 2, no. 10, pp. 166-169, ISSN 2349-6010.

JUGER, J.J., CROOK, R.F. 1999. Heat transfer performance of propylene glycol versus ethylene glycol coolant solutions in laboratory testing. In SAE Technical Paper Series SP1456, 1999, pp. 23–33, ISSN 0148-7191.

KOLEDA, P., KOLEDA, P., GRÚBEL, S. 2016. Analysis of temperatures in the mould area during the process of engine cylinder heads casting. Acta Facultatis Technicae, XXI, 2016 (1), pp. 31-40. ISSN 1336-4472.

OLIET, C., OLIVA, A., CASTRO, J. a PÉREZ-SEGARRA, C.D. 2007. Parametric studies on automotive radiators. In Applied Thermal Engineering, 2007, vol. 27, no. 11-12, pp. 2033-2043. DOI:10.1016/j.applthermaleng.2006.12.006, ISSN 1359-4311.

PATIL, V.R., PATIL, S.S., KUMBHAR, V. a KOLHE, K. 2017. Review of problems of heat transfer in car radiator and suggested solutions. In International Journal of Scientific Development and Research, 2017, vol. 2, no. 1, pp. 94-98, ISSN 2455-2631.

ROSLAN, A., ARBANAH, M., TUKIMAN, N., IBRAHIM, N. N., JUANIL, A. R., 2017. The effects of ethylene glycol tu ultrapure water on its specific heat capacity and freezing point. In Journal of Applied Enviromental and Biological Sciences, pp. 54-60, ISSN 2090 4274.

SAINI, A., BISHT, K. S., MISHRA, S. 2014. Advance engine cooling system. In Journal of Advanced Technology & Engeneering Research (IJATER). 1st International Conference on Research in Science, Engineering & Management (IOCRSEM 2014), pp. 103-106, ISSN 2454 2377.

SELVAM, C., SOLAIMALAI RAJA, R., MOHAN LAL, D. a HARISH, S. 2017. Overall heat transfer coefficient improvement of an automobile radiator with graphene based suspensions. In International Journal of Heat and Mass Transfer. vol. 115, pp. 580-588. 2017. ISSN 0017-9310.

SHARIFF, K.B., ABDULLAHI, B. a ABUBAKAR, S.B. 2018. Modelling and simulations of car radiator: Effects of fins under the atmospheric condition of Kano, Nigeria. In Journal of Advanced Research in Fluid Mechanics and Thermal Sciences. 2018, vol. 48, no. 1, pp. 1-16, ISSN 2289-7879.

SUDHAKAR BABU, S., YASIN, S. 2019. Heat transfer Analysis of Automobile Radiator with Helical Tubes using CFD. In International Journal of Innovative Technology and Exploring Engineering (IJITEE) 2019. Vol. 8, pp. 999-1003. ISSN 2278-3075.

TURIZO-SANTOS, J., BARROS-BALLESTEROS, O., FONTALVO-LASCANO, A., VASQUEZ-PADILLA, R. a BULA-SILVERA, A. 2015. Experimental characterization of thermal hydraulic performance of louvered brazed plate fin heat exchangers. In Revista Facultad de Ingeniería Universidad de Antioquia, 2015, vol. 74, pp. 108- 116, ISSN 0120-6230.

YADAV, J. P., SINGH, B. R. 2011. Study on performance evaluation of automotive radiator. In Samriddhi: A Journal of Psysical Sciences, Engineering and Technology, 2011, vol. 2, Issue 2, pp. 47-56, ISSN 2229-7111.

Corresponding author:
Ing. Marek Lipnický, tel.: +421 45 5206 053, e-mail: xlipnicky@is.tuzvo.sk
doc. Ing. Zuzana Brodnianská, PhD., tel.: +421 45 5206 678, e-mail: zuzana.brodnianska@tuzvo.sk

PROPOSAL FOR MODIFICATION OF A SNOW PLOUGHSHARE BY HARD SURFACING TO INCREASE ITS SERVICE LIFE

NÁVRH ÚPRAVY SNEŽNEJ RADLICE NAVÁRANÍM TVRDOKOVU PRE ZVÝŠENIE JEJ ŽIVOTNOSTI

Monika Vargová[1], Miroslava Ťavodová[2]

Department of Manufacturing Technology and Quality Management, Faculty of Technology, Technical University in Zvolen, Študentská 26, 960 01 Zvolen, Slovakia
email: [1]xvargovam1@is.tuzvo.sk, [2]tavodova@is.tuzvo.sk

ABSTRACT: The article presents partial results from the research of increasing the service life of snow blades. Snow ploughshares work in a heterogeneous environment, and therefore comes into contact with various abrasive particles, such as minerals, rocks, etc. For this reason, they wear out quickly and are subsequently taken out of service. This causes technical and economic problems for forestry companies. In the experiment, several options were made to increase the life of snow ploughshares. One of the possibilities was to weld a material with different properties and structure than the original material of the snow ploughshare, on its exposed parts. Entrance laboratory tests were performed on the discarded blade, namely chemical analysis, hardness measurement and microscopic analysis. The weld deposit metal was chosen according to the chemical composition of the base material and the type of wear. After application of the weld deposit to the sample, laboratory tests were performed, namely hardness measurement and microscopic analysis. With the hardness of the weld deposit, we approached the hardness of the raking blade; on the basis of microscopic analysis we can state that there has been sufficient mixing of the weld deposit with base material, and therefore should not crack off in the work process. By a suitable choice of welding material, we can achieve an effective increase in the life of the snow ploughshare.

Key words: forest road, ploughshare, wear, hard surfacing

ABSTRAKT: V článku sú predstavené čiastkové výsledky z výskumu zvyšovania životnosti snežných radlíc. Snežné radlice pracujú v heterogénnom prostredí, a teda prichádzajú do styku s rôznymi abrazívnymi časticami, ako sú minerály, horniny a pod.. Z tohto dôvodu dochádza k ich rýchlemu opotrebeniu a následnému vyradeniu z prevádzky. Toto spôsobuje ako technické, tak aj ekonomické problémy spoločnostiam pôsobiacich v lesnom hospodárstve. V experimente bolo vykonaných niekoľko možností zvýšenia životnosti snežných radlíc. Jednou z možností bolo navarenie prídavného materiálu s inými vlastnosťami a štruktúrou, ako mal pôvodný materiál snežnej radlice na jej exponované časti. Na vyradenej radlici boli vykonané vstupné laboratórne skúšky, a to chemická analýza, meranie tvrdosti a mikroskopická analýza. Podľa chemického zloženia základného materiálu a typu opotrebenia bol zvolený návarový kov. Po aplikácií návarového kovu na vzorku boli vykonané laboratórne skúšky, a to meranie tvrdosti a mikroskopická analýza. Tvrdosťou návarového materiálu sme sa priblížili k tvrdosti zhrňovacieho noža; na základe mikroskopickej analýzy môžeme konštatovať, že došlo k dostatočnému premiešaniu návarového materiálu, a teda by sa nemal v procese práce odlupovať. Vhodnou voľbou návarového materiálu môžeme dosiahnuť efektívne zvýšenie životnosti snežnej radlice.

Kľúčové slová: lesná cesta, snežná radlica, opotrebenie, naváranie

INTRODUCTION

Forest roads are important in term of forest management. They are used for the transport of wood and people, ensure the protection of life and health of workers (better accessibility of rescue equipment) and increase their efficiency, facilitate the mechanization of forest work and also serve for the spatial division of forests (Smreček & Sedliak 2012; Hnilica *et al*. 2015). For this reason, it is necessary to ensure the road in a passable condition not only in summer, but also in winter. Snow ploughshares, cutters, but also bulldozers are used to remove snow. Snow ploughshares are exposed to unfavorable working conditions in the process of their work. They are subject to wear, especially abrasive wear, as they work in a heterogeneous environment. They come into contact with various mineral particles, rocks and sand. Furthermore, corrosive wear occurs throughout the raking period and the first contact the ploughshare comes into contact with the road, it is loaded by impact. Consecutive early decommissioning causes both technical and economic problems for companies operating in forestry. Therefore, it is necessary to focus on the wear of snow ploughshares and find suitable methods to increase their service life.

MATERIAL AND METHODS

A forest road is a purpose-built road that is part of a forest transport network. It is intended for the transport of wood, people, materials, for the passage the special vehicles (fire, medical service), but it can also be used for other purposes. It has a built-in earth body and at least a simple drainage (Smreček & Sedliak 2012). According to the valid Slovak standards from forestry sphere, the transport forest roads of 1st class (1L) are usually single-lane, enabling their spatial arrangement and technical equipment to operate all year round (assuming winter maintenance) with a relevant vehicle, by the considered design intensity of traffic. These roads have a roadway, complete drainage of the crown and the body of the forest road and must be equipped with shunt. The recommended lane width is 3.5 m (at least 3.0 m), the free width of the road is recommended 4.5 m (at least 4.0 m). The maximum permissible longitudinal slope is 10% (max. 12%) (Figure 1) (Smreček & Sedliak 2012; www.enviromagazin.sk).

Fig. 1 The 1st class forest transport road (1L) (www.ekomonitor.cz; www.pixnio.com)
a – forest road in summer, b – forest road in winter
Obr. 1 Lesná odvozná cesta prvej triedy (1L) (www.ekomonitor.cz; www.pixnio.com)
a – lesná cesta v lete, b – lesná cesta v zime

According to the valid Slovak standards from forestry sphere, maintenance of forest roads is regular or cyclical care for the preservation of the forest road in a condition that

meets its planned transport use. In order to ensure the safe passability of forest transport roads in the winter, is winter maintenance necessary, primarily snow removal and spreading of icy roads.

Snow ploughshares, snow cutters, guards, bulldozers, etc. are used to remove snow from roads. On forest roads, arrow ploughshares, which are mounted in front of trucks or tractors, have proved their worth in removing snow. A snow ploughshare is a device designed to be mounted on a vehicle. It is used for winter maintenance of roads and is used to remove snow from external surfaces, especially pavements, roads and rails (Hrůza 2014). The snow ploughshare (arrow or straight) can be located in front of the front axle, between the axles or behind the axles of the vehicle. Snow ploughshares are usually placed on the chassis of cars, which are used for other purposes, such as spreaders, etc. (Jeřábek 1996). The snow ploughshare works in a heterogeneous environment. During work, it comes into contact with the road, and therefore snow, stones, mineral particles, gravel, sand, etc. First, the raking blade comes into contact with the road, which is stressed by impact during the first contact with the road and further throughout the raking, by abrasion and corrosion. In addition to the raking blade, the rest of the ploughshare is also stressed, because the accumulated snow, together with the sand and gravel, exerts a force on the body of the blade from shirr to its buldoze to the side of the road. As a result, wear occurs due to abrasion and corrosion not only of the raking blade, but of the entire working part of the ploughshare (weldment).

Fig. 2 Arrow snow ploughshare (www.agra.sk)
Obr. 2 Šípová snežná radlica (www.agra.sk)

The blades are exposed to abrasive, impact and corrosive wear in the environment in which they work. The current standards state that abrasive wear is characterized by the separation of particles from the worn surface:

a) Grooving and cutting with hard particles – hard foreign particles cut or scratch the surface of the body. During abrasive wear, hard particles may also be present between the two friction surfaces. In this occurrence, the particles may be adhered to one of the surfaces or may be pushed into the softer surface and grooved or cut the other surface.
b) Grooving and cutting the hard and rough surface of the second body - unevenness of the surface of the harder body penetrates into the softer surface of the second body and carves scratches in it (Javaheri 2020).

During impact wear, the material is exposed to impact and high pressure, deformation or local disturbance may occur, possibly even breakage. Under the given conditions, the tools must have hard surfaces which are resistant to wear (www.esab.sk; Falat et al. 2019).

Exist a lot of methods for increasing the life of machine parts, tools or components. After a correct analysis of the working environment, we can identify the causes of short life and choose a suitable method to increase it. Methods of increasing service life include e.g. heat treatment, chemical-thermal treatment, hard surfacing, material change.

By hard surfacing, we can achieve resistance to a specific type of wear or specific properties, which depend on the type of weld deposit material. Hard surfacing is used for renovate tools to a usable condition, but also for produce new tools. The production of new tools by hard surfacing is more economically advantageous, because the tool can be made of a cheaper material and its surface properties are achieved by hard surfacing the weld deposit material. The weld deposit material must be selected according to the working conditions of the tool and must have properties suitable for use in the given conditions (Ťavodová *et al*. 2017). When choosing a weld deposit material, we must know what is the basic material to which it will be welded, what type of wear will be exposed to at work and what kind of surface is required after hard surfacing. The weld deposit material can be applied by any welding process (www.esab.sk). Weld deposit metals can be classified according to their chemical composition, according to the International Institute of Welding (IIW), but also according to their characteristic properties and wear resistance (Jesánek 2007). So far, there is no unified thorought on the most suitable type of structure in terms of abrasion resistance. The reason is the wide variety of working conditions and the diversity of the abrasion process. Some authors consider austenitic-carbide structure to be the most advantageous, while others consider the martensitic-carbide structure to be the most advantageous (Brziak *et al*. 2003). Weld deposit materials of the austenitic steel type are suitable for abrasive wear, which cooperates with impact wear. Weld deposit materials with austenitic base and hard carbide particles have a ductile matrix and therefore do not fracturing (Hrabě & Brožek 2006; Ťavodová 2018). Austenitic-carbide structure can be considered the most advantageous for abrasion conditions at high specific pressures and the presence of impact (Brziak *et al*. 2003). Austenitic-manganese weld deposit materials are also suitable for abrasive wear accompanied by impact. During impacts, the structure is strengthened, making the structure more resistant to abrasive wear. The structure which is resistant to abrasive wear can be achieved in advance by cold deformation of weld deposit (Kučera & Rusnák 2008). Weld deposit materials with a basic martensitic mass are characterized by high resistance to abrasive wear. This is caused to the high hardness of the martensitic structure and the fact that strain hardening occurs on the worn surface. Strain hardening is formed by the transformation of residual austenite and the precipitation of fine carbides, which is caused by deformation. By this process, the wear resistance increases (Adamka 1995). The martensitic-carbide structure is more suitable for low-voltage abrasion (Brziak *et al*. 2003).

RESULTS AND DISKUSSION

The ploughshare that was the subject of the experiment is a commonly used tool for road modification in winter. It is attached to the working machine with a front clamping plate or, in the case of more difficult terrain, with a three-point hitch. In Figure 3 is a part of an arrow ploughshare from which samples were taken for the experiment.

Fig. 3 Part of the discarded ploughshare
Obr. 3 Časť vyradenej radlice

Input tests and measurements performed on a discarded blade:
– chemical analysis of basic material and raking blade,
– hardness measurements,
– microscopic analysis of basic material, weld joint and raking blade.

Chemical elemental analysis of the samples was determined by the atomic emission method with spark discharge on ARL 4460 spectrometers. THERMO ARL and IR absorption. Based on the performed chemical analysis, we found that the basic material (BM) of the weldment used in the experiment was made of 11 484 steel. It is a fine-grained steel of the usual quality for low temperatures with guaranteed weldability. It is used in parts of equipment operating at temperatures up to -50 ° C made of sheet metal with a guaranteed value of notched toughness up to -50 °C. The characteristik stress is Re = 355 MPa and the failure strenght is Rm=470-610 MPa. In Table 1 is the chemical composition of the basic material.

Table 1 Cemical composition of basic material
Tabuľka 1 Chemické zloženie základného materiálu

Element[1]	C	Mn	Si	Cr	Ni	Cu	Al	Mo	P	S	Fe
wt.[2] [%]	0,2	1,4	0,3	0,041	0,055	0,16	0,02	<0,01	<0,005	<0,15	rest

[1]Prvok; [2]hm.

We further found that the raking blade used in the experiment was made of 13 240 steel. It is a manganese-silicon steel suitable for tempering. It is used on medium-stressed parts of machines and parts of road vehicles particularly resistant to wear, e.g. shafts, axles, connecting rods, levers, bolts. Value of the failure strenght is Rm=760 MPa. In Table 2 is the chemical composition of the raking blade.

Table 2 Chemical composition of raking blade
Tabuľka 2 Chemické zloženie zhrňovacieho noža

Element[1]	C	Mn	Si	Cr	Ni	Cu	Al	Mo	P	S	Fe
wt.[2] [%]	0,33	1,24	1,36	0,27	0,47	0,04	0,015	0,178	0,017	<0,15	rest

[1]Prvok; [2]hm.

Vickers HV 0.5, Rockwell HRC and Brinell HBW hardness measurements were performed on samples taken from the discarded ploughshare. Vickers hardness was performed according to the procedure given in ISO 6507-1: 2018 (ISO 6507-1: 2018), Rockwell

hardness in accordance with ISO 6508-1: 2016 (ISO 6508-1: 2016) and Brinell hardness in accordance with ISO 6506-1:2014 (ISO 6506-1: 2014). The average hardness of BM was 0.5 according to Vickers 168 HV, 156 HBW according to Brinell and Rockwell hardness could not be measured as it is a relatively soft material. The average hardness of the raking blade was 0.5 according to Vickers 538 HV, 50 HRC according to Rockwell and 170 HBW according to Brinell.

Table 3 Hardness of basic material and raking blade measured on discarded ploughshare
Tabuľka 3 Tvrdosť základného materiálu a zhrňovacieho noža merané na vyradenej radlici

Number of measuring[3] [-]	1	2	3	4	5	Average[4]
BASIC MATERIAL[1]						
Vickers hardness[5] [HV 0,5]	174	165	166	171	164	**168**
Rockwell hardness[6] [HRC]	–	–	–	–	–	**–**
Brinell hardness[7] [HBW]	159	159	155	155	150	**156**
RAKING BLADE[2]						
Vickers hardness[5] [HV 0,5]	537	550	543	545	517	**538**
Rockwell hardness[6] [HRC]	50	50	50	49	49	**50**
Brinell hardness[7] [HBW]	159	159	179	185	164	**170**

[1]Základný materiál; [2]zhrňovací nôž; [3]Číslo merania; [4] Priemer; [5]Tvrdosť podľa Vickersa; [6]Tvrdosť podľa Rocwella; [7] Tvrdosť podľa Brinella

Samples for metallography were taken to characterize the condition of the examined material (Figure 4). The process of cutting the sample must not thermally affect the surface of the observed area. Metallographic sample preparation was performed according to standard procedures. The samples were etched with 2% Nital etchant (2 ml HNO3, 98 ml etylalcohol) and Cor etchant (120 ml CH3COOH, 20 ml HCl, 3g picoric acid, 144 ml CH3OH). Cor etchant was used for etching welds and hard surfaces.

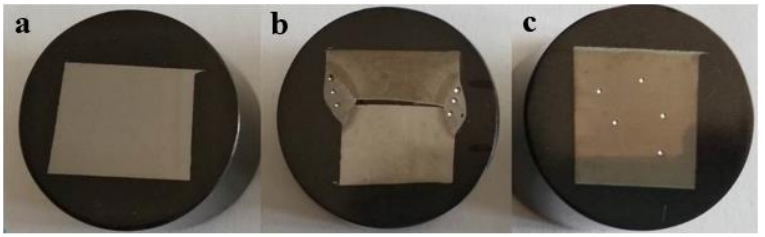

Fig. 4 Samples for input microscopic analysis
a – basic material; b – weld joint;c – raking blade
Obr. 4 Vzorky pre ctupnú mikroskopick analýzu
a – základný materiál; b – zvar; c – zhrňovací nôž

After etching the samples, an input analysis of the base material, weld and material of raking blade was performed. In Figure 5a we can see the microstructure of BM, which is characterized by a slight linearity. It is a ferritic-pearlitic steel with a higher proportion of ferrite. A hint of linearity indicates that it is rolled steel. In Figure 5b we can see the microstructure of the weld with a characteristic growth of structural components, which

were welded parts of the ploughshare – BM and raking blade. In Figure 5c we can see the microstructure of the material of the raking blade. It is a sorbitic structure that was formed after tempering.

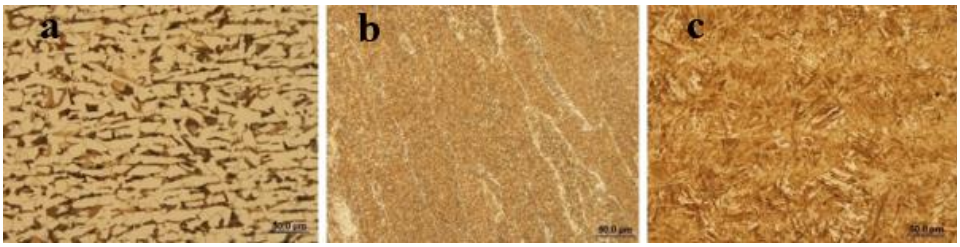

Fig. 5 Microstructure – light microscopy – input analysis of weldment
a – basic material; b – weld joint; c – raking blade
Obr. 5 Mikroštruktúra – svetelná mirkoskopia – vstupná analýza
a – základný materiál; b – zvar; c – zhrňovací nôž

In Figure 6 is a state of wear of the raking blade. In the lower part we can see uneven wear on the blade.

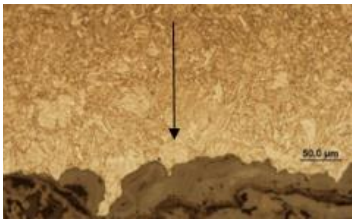

Fig. 6 Microstructure – light microscopy – wear condition of the raking blade
Obr. 6 Mikroštruktúra – svetelná mikroskopia – tvar opotrebenia zhrňovacieho noža

In Figure 7a we can see the mixed zone of the weld – the blade. The weld has a typical dendritic structure. In Figure 7b is weld joint – basic material. We can state that in both cases there was sufficient mixing of both materials with the weld, without the occurrence of defects.

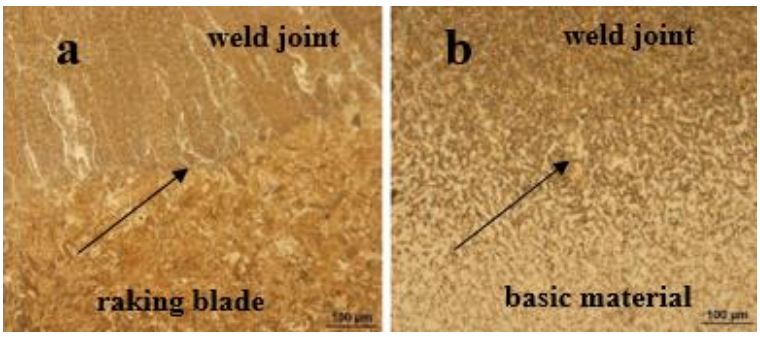

Fig. 7 Mixing zone – light microscopy
a – weld joint – raking blade; b – weld joint – basic materiál
Obr. 7 Zóna stavenia – svetelná mikroskopia
a – zvar – zhrňovací nôž, b – zvar – základný materiál

Based on input measurements and analyzes, we proposed a modification of the ploughshare by welding to increase its service life. In Figure 8a is a portion of a discarded ploughshare from which for hard-surfacing sample was taken.

On a sample from the ploughshare (Figure 8a) we welded the selected weld deposit material in one layer. We chose the weld deposit material according to the type of wear to which the ploughshare is exposed and according to data obtained from the literature (www.esab.sk). Chemical composition of the electrode OK 84.58 EN 14700: E Z Fe 6 is C – 0,7%; Si – 0,6%; Mn – 0,7%; Cr – 10,00%. The hardness of the weld deposit without preheating is 52 - 59 HRC. OK 84.58 is a hardfacing electrode depositing a semi-corrosion-resistant martensitic steel. Full hardness is obtained even in the first bead, irrespective of the cooling rate. Suitable for hardfacing parts exposed to abrasive and impact wear, such as farm equipment, forestry tools, loading machines and mixers. The weld deposit can be machined by grinding (www.esab.sk). Hard surfacing was performed by certified welders. An OK 84.58 electrode with a diameter of 3.2 mm was welded on the sample in one layer (Figure. 8a). The electrodes were dried in a ZEPACOMP oven 2 hours at 200 °C with preheating of the sample at 150 °C. The set welding voltage was $U = 21.5\ V$ and welding ampere $I = 140\ A$, welding time $t{=}222\ s$. Welding position PA (horizontal position from above). The welded length was $L = 760\ mm$. These data are necessary for a possible economic evaluation of OK 84.58 hard surfacing at real ploughshare dimensions.

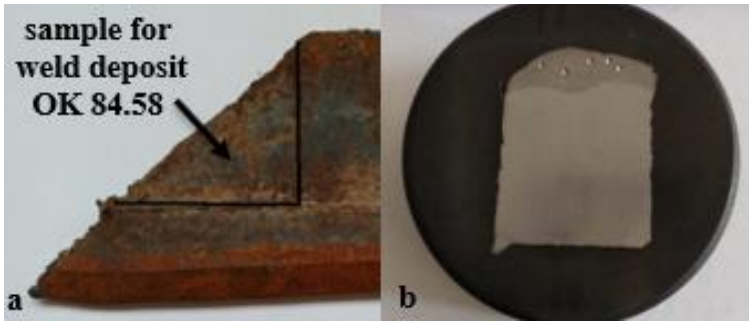

Fig. 8 Samples OK 84.58
a – for weld deposit ; b – for microscopic analysis
Obr. 8 Vzorky OK 84.58
a – pre návar; b – pre mikroskopickú analýzu

A sample for microscopic analysis was prepared by standard procedures. A 2% Nital etchant was used to etch the base material and a Cor etchant was used to etch the weld deposit (Figure 9b). In Figure 9a, b we can see the mixed zone of the weld deposit OK 84.58 – BM. We can allege that there has been sufficient mixing of BM and weld deposit. Cracks or other unacceptable defects are not visible that would reduce the coherence between the BM and the weld deposit. This confirms the correct selection of the hard surface material as well as the selection of the welding parameters.

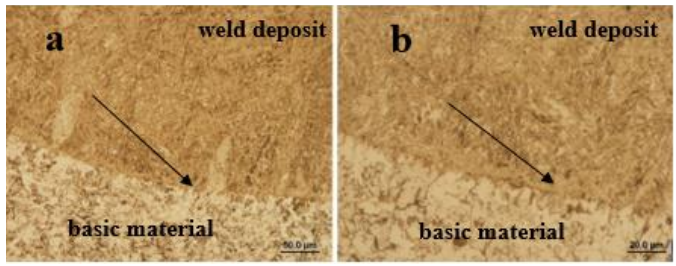

Fig. 9 Mixing zone – light microscopy – weld deposit OK 84.58 – basic material
Obr. 9 Zóna stavenia – svetelná mikroskopia – návar OK 84.58 – materiál zvarenca

In the performed EDX analysis of the weld deposit – BM interface (Figure 10) we can see the present diffuse mixing of the weld deposit and BM.

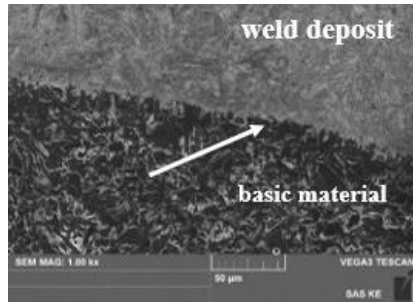

Fig. 10 Misxing zone – EDX – weld deposit OK 84.58
Obr. 10 Zóna stavenia – SEM – návar OK 84.58

The hardness of the OK 84.58 weld deposit was measured according to Vickers and according to Rocwell. The average value of the hardness of the weld deposit was 546 HV 0.5 and 50 HRC. The hardness of the OK 84.58 weld deposit stated in the electrode data sheet is 52 to 59 HRC. Hardness is an important mechanical property. It is expressed by the resistance of the material against deformation of its surface. This deformation is caused by the action of the body, which penetrates a certain force into the surface of the body. It is the martensitic structure that provides for the weld deposit with higher hardness, and therefore greater resistance to the penetration of the body into the surface of the material.

Table 4 Hardness of weld deposit OK 84.58
Tabuľka 4 Tvrdosť návaru OK 84.58

Number of measuring[1] [-]	**1**	**2**	**3**	**4**	**5**	**Average[2]**
Vickers hardness[3] [HV 0,5]	526	513	561	550	579	**546**
Rockwell hardness[4] [HRC]	49	49	49	51	51	**50**

[1]Číslo merania; [2]Priemer; [3]Tvdosť podľa Vickersa; [4]Tvrdosť podľa Rocwella

The hardness of the basic material and the raking blade can be compared with the surface hardness achieved after hard-surfacing of OK 84.58 electrode on the basis of graphs.

Graph 1 (Figure 11) characterizes the course of hardnesses measured from BM to the raking blade through the weld, where the probable strain hardening in the area behind the heat affected zone (HAZ) closer to the weld is interesting. As this is a blade that has been in operation for a long time, the strain hardening is probably caused by the action of forces from the environment in which the ploughshare worked. The strain hardening is higher at the raking blade-weld interface and approaches the measured hardness of the raking blade with hardness. The average hardness of the base material is 168 HV and a hardness of the raking blade is 538 HV 0.5. Graph 2 (Figure 12) characterizes the course of hardneses measured from BM to OK 84.58 weld deposit. We can see a slight decrease in hardness between distances of 4.5 mm to 12 mm, we can state that it is probably a HAZ. From a distance 13.5 mm and higher we can observe the hardness of the OK 84.58 weld deposit. The average hardness of this weld deposit is 546 HV 0.5. The hardness of the OK 84.58 weld deposit is higher than the hardness of the raking blade, and therefore, we can assume that the weld will have slightly better properties than the material of the original raking blade.

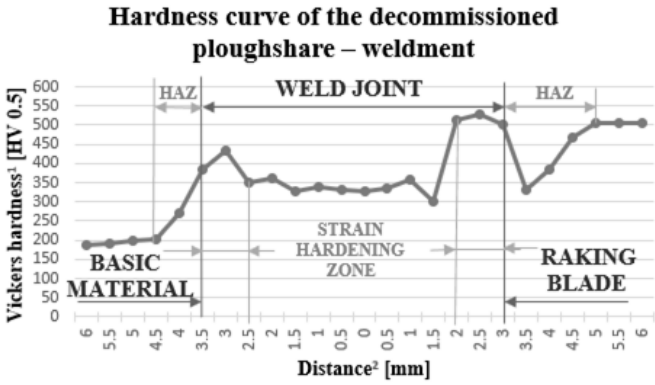

Fig. 11 Hardness curve of the decommissioned ploughshare
Obr. 11 Krivka tvrdostí vyradenej radlice – zvarenca
[1]Tvrdosť podľa Vickersa; [2]Vzdialenosť

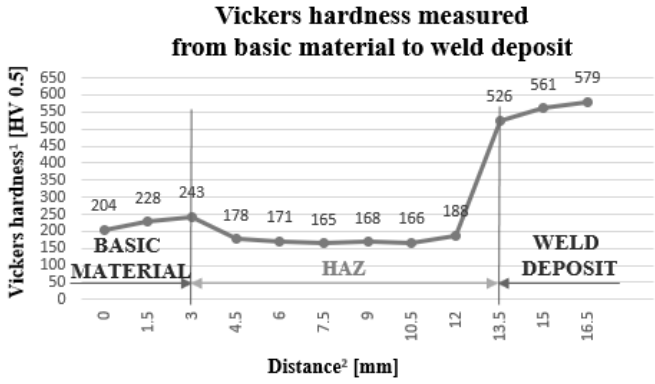

Fig. 12 Vickers hardness measured from basic material to weld deposit
Obr. 12 Tvrdosť podľa Vickera meraná od základného materiálu po návar
[1]Tvrdosť podľa Vickersa; [2]Vzdialenosť

From Figure 9 we can state that the weld deposit has a martensitic structure with content fine chromium carbides. Martensitic structure ensures hardness and chromium carbides should guarantee good abrasion resistance, and therefore there is a presumption of good resistance to abrasive wear (Ťavodová 2018). According to the author Adamka (1995), it is the martensitic structure that shows very good resistance to abrasive wear (Adamka 1995). Snow ploughshares are most exposed to this wear in the process of their work. Authors Brziak et al. (2003) state that the martensitic-carbide structure obtained by OK 84.58 weld deposit is more suitable for conditions of low-voltage abrasion accompanied by impact (Brziak et al. 2003). By weld deposit OK 84.58 (Figure 9) we achieve a similar structure as the structure of the original raking blade (Figure 5c). However, on the original raking blade, we can see the deformations that occurred to the action of the working environment.

CONCLUSION

Forest roads are important in terms of making the forest accessible for heavy machinery for timber transport. Therefore, it is necessary keep these roads passable both in summer and in winter. In winter, it is necessary to remove a layer of snow or ice from the road surface. Snow is removed from the road by snow ploughshares, which are attached to the vehicle at the front or at the arear. As the ploughshares are exposed to high wear during their work, especially abrasive, and their replacement is relatively economically demanding, it is necessary look for possibilities to increase their service life. By a suitable choice of the hard surface electrode, we can achieve an effective increase in the service life of the snow ploughshare, whether from a technical or economic point of view.

ACKNOWLEDGMENT

The article was supported by the APVV-16-0194 "Research on Impact of Innovation in Production Processes on the Life of Tooling and Components of Forest Mechanisms."

REFERENCES

ADAMKA J. 1995 Vplyv štruktúry na odolnosť návarov proti abrazívnemu opotrebovaniu. In *TECHNOLÓGIA*. Bratislava: STU, s. 396-399. ISBN 80-227-0782-1.

BRZIAK, P. kol. autorov. 2003. Materiály a ich správanie sa pri zváraní. VÚZ – Priemyselný inštitút, Bratislava. s. 216-235. ISBN 80-88734-10-X.

Enviromagazin, Professional scientific magazine about the environment http://www.enviromagazin.sk/enviro6_2/lesy10.html

ESAB. Příručka svařování. Opravy a údržba. http://products.esab.com/ESABImages/prirucka%206%20vydani%202011.pdf [accesed september 2020].

FALAT, L., DŽUPON, M., ŤAVODOVÁ, M., HNILICA, R., ĽUPTÁČIKOVÁ, V., ČIRIPOVÁ, L., HOMOLOVÁ, V. ĎURIŠINOVÁ, K. 2019. Microstructure and abrasive wear resistance of various alloy hardfacings for application on heavy-duty chipper tools in forestry shredding and mulching operations. In *Materials*, vol. 12, no. 13, pp. 2212. DOI:10.3390/ma12132212

HNILICA, R., MESSINGEROVÁ, V., STANOVSKÝ, M., SLUGEŇ, J., HNILICOVÁ, M., FERENČÍK, M. 2015. Možnosti mechanizácie prác pri zakladaní a výchove lesa. Monography. pp. 99, ISBN 978-80-228-2722-5.

HRŮZA, M. 2014. Návrh variabilního sněžného pluhu. Bakalárska práca. Brno: Vysoké učení technické v Brně, Fakulta strojního inženýrství, 2014. 45s.

ISO 6506-1:2014 Metallic materials – Brinell hardness test – Part 1: Test method.

ISO 6508-1:2016 Metallic materials – Rockwell hardness test – Part 1: Test method.

ISO 6507-1:2018 Metallic materials – Vickershardness test – Part1:Test method.

JAVAHERI, V., PORTER, D., KUOKKALA, V. 2018. Slurry erosion of steel – review of tests, mechanisms and materials. In *Wear*, vol. 408-409, pp. 248-273. DOI:10.1016/j.wear.2018.05.010

JEŘÁBEK, K. 1996. Stroje pro zemní práce: Silniční stroje. 1. vyd. Technická univerzita Ostrava. s. 464. ISBN 80-7078-389-3.

KUČERA M., RUSNÁK, J. Štúdium tribologockých vlastností materiálov nanesených na povrch vybranými technológiami navárania. Nitra: SPU. 2008. ISBN 978-80-552-0000-2.

SMREČEK, R., SEDLIAK, P. 2012. Lesná cestná sieť *a účelové* objekty – mapovanie *a* tvorba databázy. *Proceedings of Symposium GIS Ostrava 2012: Současné výzvy geoinformatiky.* Technical University of Ostrava, 2012

ŤAVODOVÁ, M., 2018. Výskum metód pre zvyšovanie životnosti nástrojov používaných v lesníckych technológiách. Habilitačná práca. Zvolen. Technická univerzita vo Zvolene. 2018. 158 s.

ŤAVODOVÁ, M., KALINCOVÁ, D., KOTUS M. 2017. Možnosti zvyšovania odolnosti voči opotrebeniu funkčných plôch mulčovacieho nástroja. In *CD Zborník prednášok z 45. medzinárodnej konferencie ZVÁRANIE 2017*: 08. - 10. november 2017: Tatranská Lomnica, Vysoké Tatry, Slovenská republika. pp. 116-123. ISBN 978-80-89296-21-7.

Technický týdeník. https://www.technickytydenik.cz/rubriky/archiv/porovnani-austenitickych-navaru-proti-abrazivnimu-opotrebeni_11116.html [accesed september 2020].

www page of AGRA s. r. o. [online] [cit. 2020-09-15] Available on: https://agra.sk/produkt/sipova-radlica-sr-t/

www page of ESAB Slovakia s. r. o., Bratislava [online] [cit. 2020-09-15] Available on: https://www.esab-slovakia.sk/sk/sk/products/filler-metals/repair-and-maintenance/hardfacing-alloys/ok-weartrode-55-hd.cfm

www page of PIXNIO.COM [online] [cit. 2020-09-14] Available on: https://pixnio.com/sk/media/cestne-lesna-cesta-zimne-strom-chladny

Corresponding author:
Monika Vargová, +421 455 206 861, xvargovam1@is.tuzvo.sk

ELEMENT COMPARISON BY MESHING AND COMPUTATION TIME FOR A FLOATING CALIPER BRAKE

POROVNANIE ELEMENTOV CEZ ČAS PRE SIEŤOVANIE A VÝPOČET PRE BRZDU S PLÁVAJÚCIM STRMEŇOM

Lukáš Hudec[1], Pavel Beňo[2]

Fakulta techniky, Technická univerzita vo Zvolene, T. G. Masaryka 24, 960 01 Zvolen,
e-mail: [1]xhudecl@is.tuzvo.sk, [2]pavel.beno@tuzvo.sk

Abstract: This paper focuses on performing an evaluation of elements c3d10m and c3d8i using Hypermesh and Abaqus CAE software in finite element analysis of brake caliper. In a workplace environment where these types of analyses are routine such as R&D centers for the automotive industry, there is high incentive put into minimizing the time required for these simulations with respect to accuracy. A simple brake-caliper assembly is assessed where the goal is to compare the deformation response to the hydraulic pressure to the brake fluid. The resulting displacements of reference points between the brake caliper and the piston is than used to calculate the change in volumes ΔV. The times being evaluated are the meshing time and the computational time. It also compares the values of the resulting displacements of reference points in both approaches and the ΔV occurring in the chamber between the piston and the brake caliper. The results tell us that the use of c3d10m elements is more advantageous. The c3d10m is considered less precise than c3d8i but in the case of our assembly the difference amounted to less than 1%. The gain in time we get was in some cases 242%.

Key words: brake caliper; deformation; element; fea; time

Abstrakt: Článok je zameraný na vykonanie analýzy prvkov c3d10m a c3d8i pomocou CAE softvéru Hypermesh a Abaqus v zostave brzdy pomocou MKP. V prostredí kde sú tieto typy analýz rutinné, ako sú výskumné a vývojové centrá pre automobilový priemysel, je vynaložené úsilie na minimalizáciu času potrebného na vykonanie simulácií s ohľadom na presnosť. V článku sa používa jednoduchá simulácia brzdovej zostavy, ktorej cieľom je vyhodnotiť deformáciu brzdy pri zaťažení hydraulickým tlakom spôsobeným brzdovou kvapalinou. Výsledná deformácia referenčných bodov medzi strmeňom brzdy a piestom sa použije na výpočet zmeny objemov ΔV. Hodnotené časy sú čas sieťovania a výpočtový čas. Porovnávajú sa tiež hodnoty výsledných posunov referenčných bodov oboch variantov a ΔV v komore medzi piestom a strmeňom brzdy. Výsledky nám hovoria, že použitie c3d10m prvkov je viac výhodnejšie. Element c3d10m je považovaný za menej presný ako c3d8i, ale v prípade našej zostavy rozdiel predstavoval menej ako 1%. Výnos v čase ktorý dostaneme bol v niektorých prípadoch až 242%.

Kľúčové slová: brzdový strmeň; deformácia; element; mkp; čas

INTRODUCTION

Among the first proposed computational methods for solving the discretization problem of two-dimensional stresses using a numerical solution were on the basis of simple elastic bars making up the discrete model (Hrennikoff 1941; Mchenry 1943). An important figure of the FEM was Richard Courant when he in 1943 first tried to solve the torsion problem by St. Venant. In 1960s. Ray William Clough applied the first computational FEM and coined the term finite element in his research. When he presented his findings in the 2nd ASCE Conference on Electronic Computation, it had little impact on the industry. The method could not be applied effectively at the time due to a lack of availability of sufficiently powerful computers (Clough 1960).

FEA has found a large host of applications inside the automotive industry since its inception. The main uses of FEA today in vehicle manufacturing are crash simulations, brake modelling, tire modelling. When simulating models using FEA analysis, we look for results with the greatest accuracy, smallest computing time and the smallest meshing time. In general, computing time increases with the use of a mesh with smaller elements. On the other hand, using a mesh with larger elements can cause stress values to be less accurate. A courser mesh can be beneficial if we try to get a simplified model for an approximate and quick calculation. The proper mesh aspect ratio alone does not guarantee accurate results. Adequate density of elements is needed for accurate stress values (Javidinejad 2012). In a static simulation of a plate model, it was found that adequate number of discretizations is about 10 divisions for an approximate error under 1% (Liu 2013). The error percentage is far less for deflections compared to von Mises stress. According to Finite Element Analysis theory, stresses are not predicted as accurately as displacement (Dutt 2015). The situation gets complicated when we use different types of elements, different orders of elements and solvers implemented in simulation software as these have a profound impact on the results. Automated meshing solutions are available, among the first written but never published was in 1958 by Mr. R. MacLean for the IBM 704 computer (Buell a Bush 1973). When meshing manually, factors such as the skill, experience and intuition in knowing where a finer mesh is required, are subjective to the person performing the simulation. Other factors like the complexity of the geometry, size of elements, desired quality parameters such as aspect ratio, skew, taper, internal angles are objective and can be quantified. The value we put on the FEA time can also play a big factor, for example when the analyst manually meshes the model for 5 minutes and the calculations takes 10 in contrast to a case where the meshing takes 10 minutes and the calculations 5 may be valued differently since the organizations usually value the analysts time higher compared to computational machine time. In this paper we consider only the raw time it takes to mesh the assembly and the wallclock time required for the computation.

Floating-caliper brake

The function of a disc brake is to generate the braking force on to the surface of the disc brake which rotates with the wheel. The brake has a U-shaped brake caliper that is attached to suspension system. The disc brake used in this paper is a variant of the disc brake called the floating caliper. The generated actuating force is generated from the hydraulic

pressure and transferred from the piston to the brake pads which clamp the disc from one side while a second pad attached to the caliper itself clamps the disc from the other side. When the hydraulic pressure is removed a piston seal located between the piston and the caliper retracts the piston back. The brake can in this manner automatically adjusts the brake-pad clearance.

Elements used

Quadrilaterals and hexahedra have a better convergence rate than triangles and tetrahedra. It is very convenient to mesh a complex shape with tetrahedra, and the second-order equivalents. However, a good mesh of hexahedral elements usually provides a solution of equivalent accuracy at a lower cost. The elements used are the c3d8i element and the c3d10m. The c3d8i is a brick type element where shear locking is removed, and volumetric locking is reduced. The c3d10m is a quadrilateral type element with improved application in contact relationships. (ABAQUS Analysis User's Manual)

MATERIAL AND METHODS

A CAD model of a floating-caliper brake is used. The housing part is a max model of a brake caliper. Part of the volume would have been removed as so it does not represent any actual housing currently in use. For the purposes of this paper it will be sufficient. The brake assembly is symmetrical so a half-model is used for modeling and simulation, the benefit of which is a faster meshing and computation time. For comparison two variants of the assembly are used, called ΔVg and ΔV_1. The assembly variant ΔV_1 consist of the housing (1) also known as caliper bracket, which holds the cylinder piston (2). The inner and outer backplates (3,7) connected to inner and outer pads (4,6) and the brake disc (5). The assembly variant ΔV_g represents a simplified alternative where the inner and outer pads (4,6) are replaced by a simplification in the form of an inner and outer domed steel spacer (8,9). In the simplified assembly variant ΔV_g we consider all components to be of the linear isotropic kind. The elastic properties in this case can be sufficiently described using Hooks law. In assembly variant ΔV_1 we consider that the material used for the inner and outer pads (4,6) is a compressible elastomeric foam.

The assembly geometry needs to be first simplified for the FEA in a way that maintains its mechanical properties. Chamfers and fillets of small sizes are removed even though perfect edges rarely exist in real-world, the square edges are easier to mesh. In addition, any functionally unnecessary geometry is removed. Fasteners are removed, and their mechanical function is replaced by equivalent contact constrains or boundary conditions. Inlet port is also removed from the assembly. Model simplification was performed in the preprocessor Altair Hypermesh.

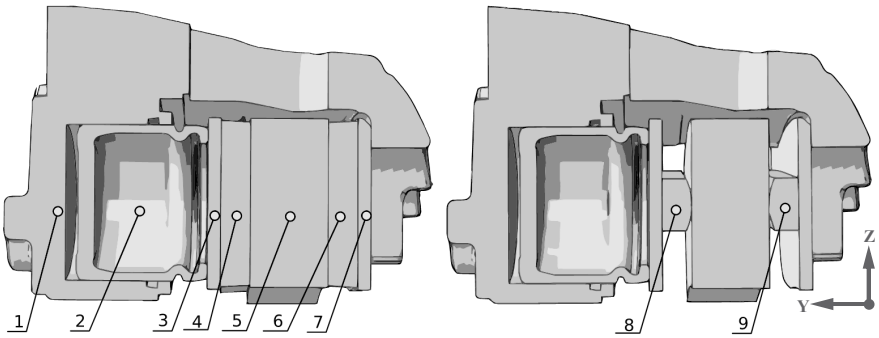

Fig. 1 Assembly of the floating-caliper brake after part simplification.
Obr. 1 Zostava brzdy s plávajúcim strmeňom po zjednodušení súčiastok.

Table. 1 Parts and material parameters.
Tabuľka. 1 Súčiastky a materiálové parametre.

Number	Part name	Material	E [GPa]	ρ [g/cm^3]	**ν**
1	Housing	GJS500	170	7.2	0.28
2	Piston	DD13	200	7.85	0.3
3	Backplate inner	S420MC	206.8	7.82	0.3
4	Pad inner	PADMAT	–	2.5	–
5	Disc	GG15HC	115	7.2	0.28
6	Pad outer	PADMAT	–	2.5	–
7	Backplate outer	S420MC	206.8	7.82	0.3
8	Domed steel spacer inner	STEEL	210	7.5	0.3
9	Domed steel spacer outer	STEEL	210	7.5	0.3

The material of the pads is a compressible elastomeric foam modeled using the '*HYPERFOAM' option. The material is defined by parameters μ_n, α_n, ν_n obtained from experimental test data as input. The parameters for pad inner are $\mu_1 = -283.43$, $\alpha_1 = 2$, $\mu_2 = 189.18$, $\alpha_2 = 4$, $\mu_3 = 94.46$, $\alpha_2 = -2$, $\nu_{1,2,3} = 0.12$. The parameters for pad outer are $\mu_1 = -421.52$, $\alpha_1 = 2$, $\mu_2 = 281.35$, $\alpha_2 = 4$, $\mu_3 = 140.48$, $\alpha_2 = -2$, $\nu_{1,2,3} = 0.12$.

where μ_n is shear modulus [GPa]
α_n is a constant specifying the shape of the stress strain curve
ν_n is Poisson's ratio

Defining boundary conditions and contacts

Since the assembly is symmetrical by the YZ plane the relevant boundary conditions are assigned thereby removing degrees of freedom for all the parts in the assembly. The displacement in the X direction is removed together with rotations R_Y and R_Z using the function "XSYMM". The disc will be completely fixed in its position. The rest of the boundary conditions will arise from the surface contacts between the parts. A contact pair

is defined by selecting the contact surfaces for each individual component after which we define the type of contact as small sliding, finite sliding or tied and assign the appropriate friction coefficient μ. Established contact pairs are housing/piston, piston/backplate inner, backplate inner/inner pad, pad inner/disc, disc/pad outer, pad outer/backplate outer, backplate outer/housing for the ΔV_1 variant. When simulating variant ΔVg the inner and outer pads are replaced by inner and outer domed steel spacers, all other contacts remain the same.

Pressure assignment

The assembly is loaded with a pressure of 100 and 160 bars, the pressure is distributed in the cylindrical space on the surfaces between the caliper and the plunger. Under real conditions, this load would be the force of the hydrostatic pressure of the brake fluid. The pressure shall be applied evenly and perpendicular to the the surfaces of the elements forming the space between the piston and the caliper. The pressure is defined using the "DSLOAD" function by defining the area name, load type and load pressure in MPa. Both variants were subjected to the same pressure.

```
*DSLOAD,OP=NEW
  surfpress_cylinder,    P,  1.5500E+01
  surfpress_piston, P,  1.5500E+01
```

Fig. 2 Defining pressure in Abaqus input file.
Obr. 2 Definovanie tlaku v Abaqus input súbore.

where *surfpress_cylinder/piston* is surface name
P is distributed pressure load type label
1.5500E+01 is reference load magnitude [MPa]

Reference point assignment

For the evaluation of the ΔV we will use reference points placed in as nodes in the setup at the locations in Fig. 3. After the simulation ends the displacement along the Y axis will be used for determining the ΔV. We are going to assume a cylindrical volume with the height being the average of the two reference values. The piston diameter used is 60 mm.

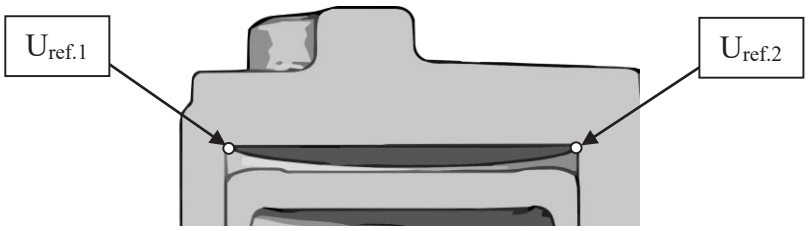

Fig. 3 Reference point location.
Obr. 3 Pozícia referenčných bodov.

RESULTS

The main findings of the FEA simulation are the values of stress and dislocation of the assembly. The displacement values are used to calculate ΔV in the space between the caliper and the piston. Although only deformations are needed for the ΔV the stress values will also be provided for informational purpose.

Meshing time

The time it took for the assembly to be meshed was significantly higher in the case of c3d8i than when meshing with c3d10m. This increase in time is mainly due to hexahedral elements being harder to fit into more complex geometry of the model, while maintaining the desired quality of the elements. Tetrahedral elements are better in this respect because the c3d10m naturally fits better into the sharp corners without deforming itself in a big manner. In the case of c3d8i, we would have to significantly reduce the size of the elements for equivalent accuracy. Element size criteria were 4 mm with an approximate layer thickness of 4 for the parts. The element quality criteria for quad elements are 140° for max angle allowed and 30° for minimal allowed angle. For tetra elements the angles are 146° and 17° respectively.

From Fig. 4 we can see that the biggest differences in times were observed in the backplates and piston. Both parts were geometrically more complex, and the percentage change was an increase of 96% in the piston case and 242% in backplates. In geometrically simpler parts the increases were smaller or even lower as was the case in the disc by 9%.

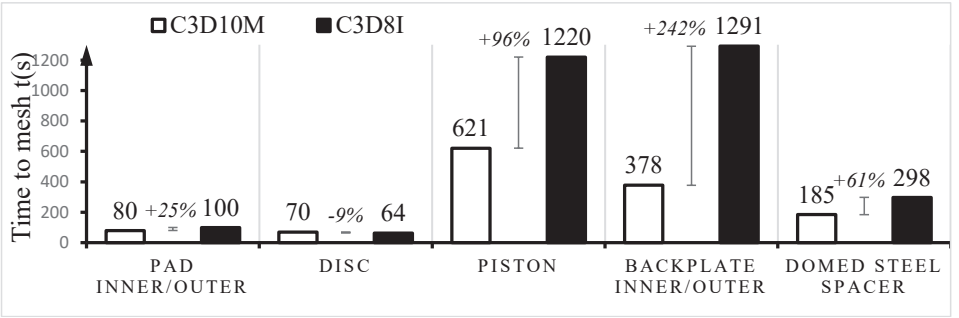

Fig. 4 Time required to mesh the models.
Obr. 4 Čas potrebný na sieťovanie modelov.

Computing time

All the variants were computed under the same conditions, on the same machine, with the same CPU cores delegated for the task. The values were taken from output file (.dat) as the „wallclock time“. The graph in figure Fig. 5 shows the times along the corresponding number of nodes and elements.

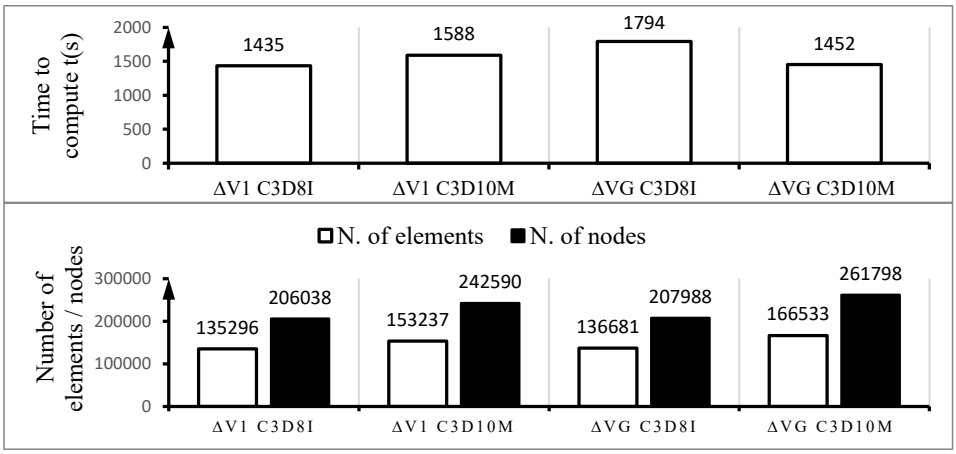

Fig. 5 Compute time compared to the number of elements.
Obr. 5 Výpočtový čas porovnaný ku množstvu elementov.

Effect on displacement and stress

The max. displacement values were 0.567 mm for ΔV_1 c3d10m with a max. For ΔVg c3d10m it was 0.364 mm. For ΔV_1 c3d8i it was 0.567 mm. For ΔV_g c3d8i it was 0.396 mm.

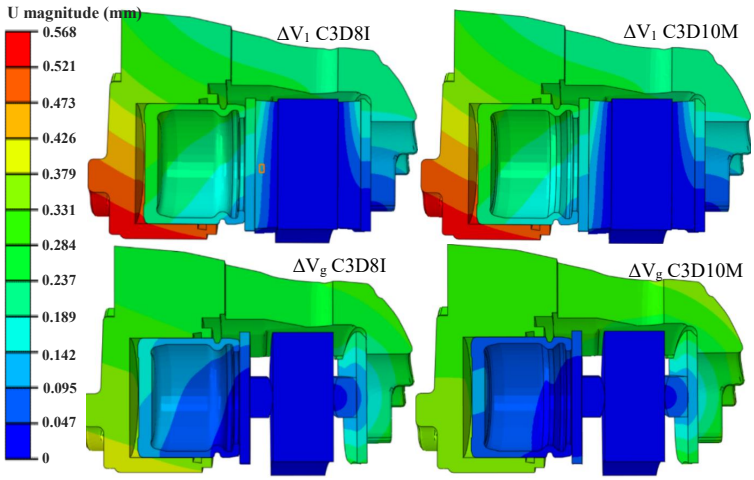

Fig. 6 Displacement distribution.
Obr. 6 Distribúcia posunutí.

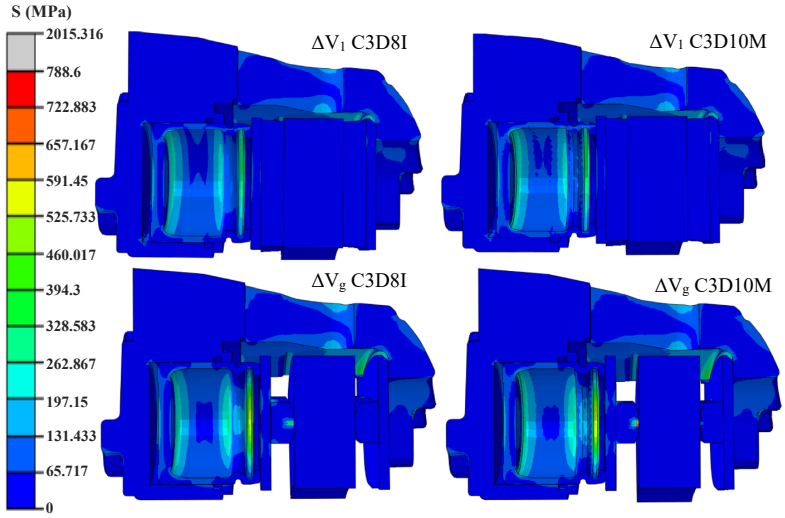

Fig. 7 Stress distribution.
Obr. 7 Distribúcia napätí.

In the ΔV_1 version the stress value is 788.502 MPa for c3d10m. For ΔV_1 c3d8i it is 788.198 MPa. In the ΔV_g variants stress concentration peaks were observed at the domed spacers, which were not taken into consideration.

Evaluation of reference points

From the results in Fig. 7 we can see that the change in elements had a small effect on the ΔV. The difference between Vg c3d10m and c3d8i was a 0.89% increase for the 160-bar test and 0.78% for the 100-bar test. For the V1 variant the difference between c3d10m and c3d8i was a 0.14% increase for 160-bar and 0.16% for 100-bar test.

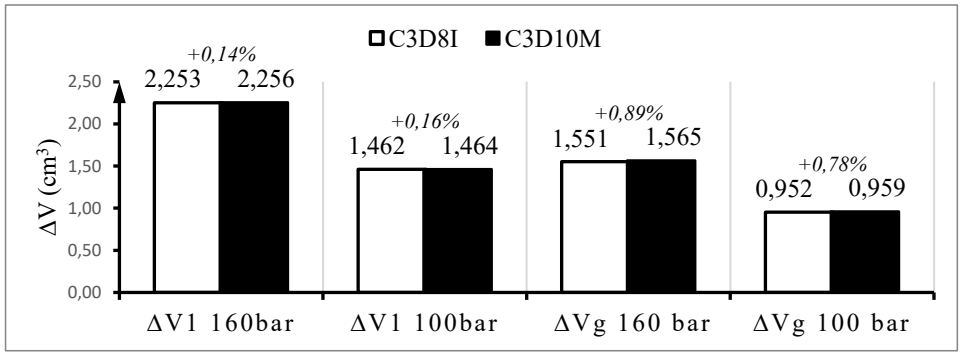

Fig. 8 ΔV values.
Obr. 8 ΔV hodnoty.

DISCUSSION

The evaluation matched with the consensus that tetrahedra elements are faster in respect to meshing time compared with hexahedral. It is much easier to mesh complex geometry with tetrahedra c3d4, and the second-order equivalent c3d10m. The general behavior of the elements used was in accordance with the expectations of the Abaqus documentation. The deformation and therefore ΔV values were largely unaffected by the changes in elements. We can therefore state that the use of tetrahedral elements would be an improvement compared to using hexahedral elements.

CONCLUSION

The time required for meshing with c3d8i elements increases for more geometrically complex components compared to the meshing time of the same component by c3d10m elements. With geometrically simpler components, this time is significantly lower.

Evaluating the calculation time, we could see that when measuring the variant ΔV1 using element type c3d10m, the program's calculation time increased compared to element type c3d8i, but it should be noted that the c3d10m mesh contained a larger number of elements. An exception occurred in ΔVg variant with c3d10m elements led to a decrease in calculation time even though the mesh was denser. Although it is clear that the use of denser mesh will increase computing time, there are many other factors such as boundary conditions, loads and the like, which have an effect on time and which we cannot always correctly predict.

For the evaluation of the reference points and ΔV, we can see that the replacement of the elements caused minimal differences in the displacement of the individual reference points and thus in the difference of ΔV.

In summary, although elements c3d8i are considered more precise the use of elements c3d10m for this assembly is sufficient considered only displacement values are needed.

ACKNOWLEDGMENT

Brake-caliper assembly and simulation software access provided by Continental Automotive Systems Slovakia s.r.o. Zvolen.

REFERENCES

BUELL, W. R. a B. A. BUSH, 1973. Mesh Generation-A Survey. *Journal of Engineering for Industry* . 1973, year. 95, n. 1, p. 332–338. ISSN 0022-0817. doi:10.1115/1.3438132

CLOUGH, R. W., 1960. The finite element method in plane stress analysis. 1960, p. 345–378.

DASSAULT SYSTÈMES, ABAQUS Analysis User's Manual, Version 6.6, sect. 22.1.1 Solid (continuum) elements., [online]. Cit. 2020-07-10, z https://classes.engineering.wustl.edu/2009/spring/mase5513/abaqus/docs/v6.6/

DUTT, A., 2015. Effect of Mesh Size on Finite Element Analysis of Beam. *International Journal of Mechanical Engineering*, roč. 2, č. 12, s. 8–10. ISSN 2348-8360. doi:10.14445/23488360/IJME-V2I12P102

HRENNIKOFF, A., 1941. Solution of Problems of Elasticity by the Framework Method. *Journal of Applied Mechanics* 1941., s. 169–175.
JAVIDINEJAD, A., 2012. FEA Practical Illustration of Mesh-Quality-Results Differences between Structured Mesh and Unstructured Mesh. *ISRN Mechanical Engineering*. roč. 2012, s. 7. ISSN 2090-5130. doi:10.5402/2012/168941
LIU, Yucheng, 2013. Effects of Mesh Density on Finite Element Analysis *SAE Technical Papers*. roč. 2013, . doi:10.4271/2013-01-1375
MCHENRY, D, 1943. A lattice analogy for the solution of stress problems. *Journal of the Institution of Civil Engineers*. roč. 21, n. 2, p. 59–82. ISSN 0368-2455 doi:10.1680/ijoti.1943.13967

Corresponding author:
Lukáš Hudec, e-mail: xhudecl@is.tuzvo.sk

REVIEW

DIGITAL TWIN IN MANUFACTURING: A SYSTEMATIC LITERATURE REVIEW

DIGITÁLNE DVOJČA V PRIEMYSELNEJ VÝROBE: SYSTEMATICKÝ LITERÁRNY PREHĽAD

Roman Bambura[1], Miroslav Dado[2], Erika Sujová[3]

[1] Department of Manufacturing Technology and Quality Management, Faculty of Technology, Technical University in Zvolen, Študentská 26, 960 01 Zvolen, Slovakia, [1]bambura.r@gmail.com [2]dado@tuzvo.sk, [3]erika.sujová@tuzvo.sk

ABSTRACT: Digital Twin (DT) is a key component for future of manufacturing. Key enabling Industry 4.0 technologies like Big Data, Cyber-Physical Systems, Internet of Things and Cloud Computing are necessary for future DT applications. DT is often referred to as a digital counterpart to the physical product, services, or production system. With expanding needs for digitalization in industries the concept of DT as virtual counterpart to the physical system grows on attention. The applications of DT can be unlimited and future development of this technology will show more possible applications. The aim of this paper is to provide literature review of DT applications in manufacturing that will be crucial for future improvements of production, and to analyse how other Industry 4.0 technologies can enhance development of DT. Our research was focused to the current definitions, applications, and trends in this area. This review was performed under pre-defined search criteria.

Key words: Industry 4.0, Digital Twin, Manufacturing

ABSTRAKT: Digitálne Dvojča (DD) je kľúčovým komponentom pre budúcnosť priemyselnej výroby. Kľúčové technológie Priemyslu 4.0, ako sú veľké dáta, kyber-fyzikálne systémy, internet vecí a cloud computing sú potrebné pre budúce aplikácie DD. DD sa často označuje ako digitálny náprotivok fyzického produktu, služieb alebo výrobného systému. S rastúcimi potrebami digitalizácie v priemysle narastá pozornosť koncepcie DD ako virtuálneho náprotivku fyzického systému. Aplikácie DD môžu byť neobmedzené a budúci vývoj tejto technológie ukáže viac možných aplikácií. Cieľom tohto príspevku je poskytnúť prehľad literatúry o aplikáciách DD v priemyselnej výrobe, ktoré sú rozhodujúce pre budúce zlepšenia výroby a analyzovať, ako môžu ďalšie technológie Industry 4.0 zlepšiť vývoj DD. Náš výskum bol zameraný na súčasné definície, aplikácie a trendy v tejto oblasti. Tento prehľad bola vykonaný podľa vopred definovaných vyhľadávacích kritérií.

Kľúčové slová: Priemysel 4.0, Digitálne Dvojča, Priemyselná výroba

INTRODUCTION

In the last few years, Industry 4.0 has been considered as one of the most prevalent topics in production engineering (Almada-Lobo, 2016). The trend and the current challenge for businesses is the Industry 4.0 concept aimed at digitizing all business processes

(Sujová et al., 2018). With the expansion of digital data driven manufacturing, many new Industry 4.0 technologies, such as Internet of Things (IoT), Big Data, Cloud computing, Cyber-physical systems (CPS), etc. have been employed into manufacturing processes. DT has provided a promising opportunity to implement Industry 4.0 technologies into production by integrating virtual and physical worlds in manufacturing (Qi et al., 2018, Tao et al., 2017).

In the recent years, the traditional manufacturing industry is challenged worldwide with the amazing growth and advancements in digital technologies that allow easy integration of interconnected intelligent components. Within the profound digitalization and rapid development of virtual technology and data acquisition technology in manufacturing industries, the concept of a virtual twin, digital equivalent to a physical system has increasingly gained on attention and DT technology gradually become one of the key research directions of intelligent manufacturing (Holler et al., 2016, Zheng et al., 2017, Negri et al., 2017). The vision of the DT refers to a comprehensive physical and functional description of a component, product or system, which includes more or less all information which could be useful in all - the current and subsequent - lifecycle phases and is commonly known as a key enabler for the digital transformation (Boschert, Rosen, 2016, Kritzinger et al., 2018). DT technology provides an effective resolution to integrate the physical world and the virtual world through ability to link enormous amounts of data to fast simulation also makes it possible to perform real-time optimization of products and production processes which allows the perform observation of the behaviour of the whole system and prediction of the system behaviour in different phases of production (Negri et al., 2019, Lohtander et al., 2018, Zhang el al., 2017, Luo et al., 2018).

The aim of this paper is to provide literature review of DT concept. Section 2 defines materials and methods used for literature review. PRISMA method was used as guideline to define methodology for this review. Section 3 presents results of this review including history and definitions of DT according to different authors and DT applications in different phases of production in industry is discussed.

MATERIAL AND METHODS

This review refers to the papers from eminent scientific databases, Web of Science (WoS), Science Direct, Scopus and Research Gate, which contains vast amount of distinguished publications, Elsevier, IEEE, Springer, etc. to provide a literature review for variety applications of DT for industrial purposes. The search was performed from January to June 2019 under specific criteria shown in Fig.1.

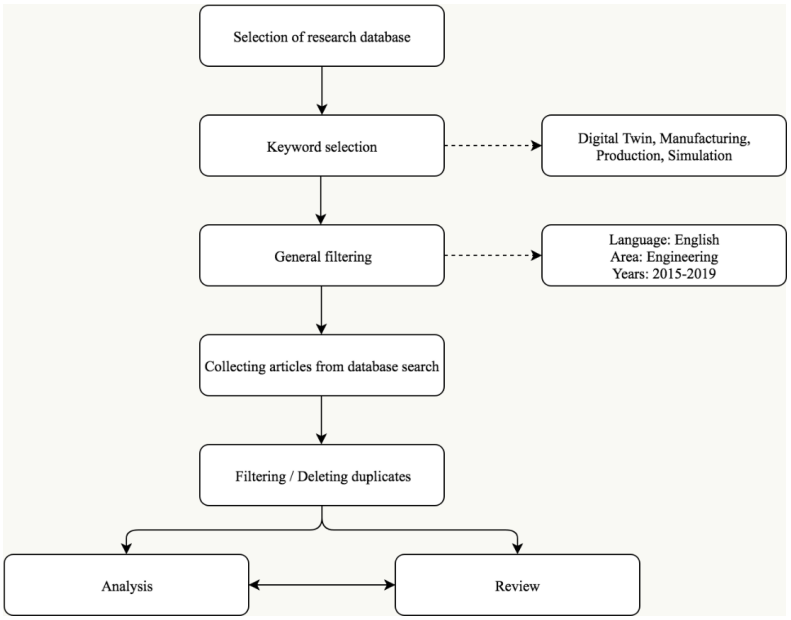

Figure 1 Research methodology
Obrázok 1 Metodológia výskumu

Database selection was performed under specific criteria to define and address research objectives. We focused on databases which provide us wide range of scientific publications and based on that the following databases were selected: WoS, Science Direct, Scopus and Research Gate. The initial search was performed in WoS database to define keywords for future research needs. After selection appropriate keywords we performed second search to collect articles based on criteria which will be described in next chapters.

Digital twin, Manufacturing, Production, and Simulation keywords were selected as appropriate to establish research needs.

Initial search was performed in WoS database to collect majority of articles. Other databases were used as secondary to cover and complete search. The initial search results in total of 112 publications.

Filters applied for search process are shown in Fig.1. English only articles and also research area related to engineering were chosen to focus on industrial applications of DT. To focus on articles published in recent years to analyse present and future possibilities of DT we chose articles which are published since 2014. This filtering results in total of 112 publications.

For better refinement of articles, duplicates and articles that did not fit needs of this paper were removed, which results in total of 31 articles for the final review. Figure 2 represents the PRISMA diagram showing selection of articles.

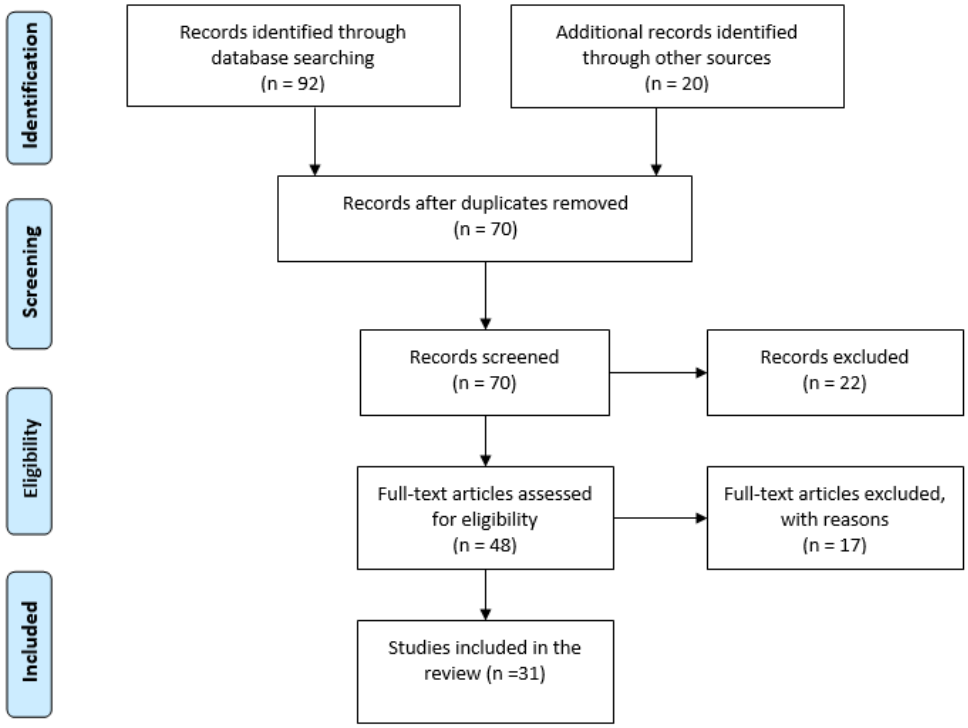

Figure 2 PRISMA diagram showing selection of articles
Obrázok 2 PRISMA diagram výberu článkov

RESULTS

Collecting and filtering of articles was done under PRISMA method criteria stated in section 2. Papers were analysed by their content. Review results are displayed in Table 1. Literature analysis was focused on DT implementation into different phases of lifecycle, implementation of other Industry 4.0 technologies to create, establish or define DT and to highlight application of DT in different fields.

Table 1. Summarization of literature review
Tabuľka 1 Súhrn prehľadovej literatúry

Year	Authors	Lifecycle phase	Big Data	IoT	CPS	Cloud
2017	Stark et al.	Preparation	✔	✔	✔	–
2018	Coronado et al.	Production	✔	✔	✔	–
2014	Lee at al.	Maintenance	✔	✔	✔	✔
2015	Lee at al.	Maintenance	✔	–	✔	–
2018	Senington et al.	Production	✔	–	–	–
2017	Vachálek et al.	Production	✔	✔	✔	–
2018	Ayani et al.	Maintenance	–	✔	✔	–
2018	Biesinger et al.	Multiphase	✔	✔	✔	✔
2018	Boschert et al.	Multiphase	✔	✔	✔	✔
2017	Cai et al.	Maintenance	–	✔	✔	–
2018	Damiani et al.	Preparation	–	–	–	–
2018	Haag, Anderl	Multiphase	✔	✔	✔	–
2016	Holler et al.	Multiphase	–	–	–	–
2018	Kritzinger et al.	Multiphase	–	–	–	–
2018	Liau et al.	Multiphase	✔	✔	✔	–
2018	Lohtander et al.	Preparation	–	–	–	–
2018	Luo et al.	Maintenance	✔	✔	✔	–
2017	Moreno et al.	Multiphase	–	✔	✔	–
2019	Negri et al.	Multiphase	–	✔	✔	✔
2017	Negri et al	Multiphase	✔	✔	✔	–
2018	Qi et al.	Maintenance	✔	✔	✔	–
2015	Rosen et al.	Production	✔	✔	✔	–
2017	Schleich et al.	Multiphase	–	–	–	–
2016	Schroeder et.al.	Multiphase	✔	✔	✔	–
2017	Söderberg et al.	Multiphase	✔	✔	✔	–
2017	Tao et al.	Preparation	✔	✔	✔	✔
2017a	Uhlemann et al.	Production	✔	✔	✔	✔
2017b	Uhlemann et al.	Production	✔	✔	✔	✔
2016	Weyer et al.	Production	✔	✔	✔	–
2017	Zhang et al.	Production	✔	✔	✔	–
2017	Zheng et al.	Multiphase	✔	✔	✔	–

DEFINITIONS OF DIGITAL TWIN

The first definition of DT was introduced in 2003 by Grieves at University of Michigan Executive Course on Product Lifecycle Management (PLM) as virtual, digital equivalent to a physical product (Grieves, 2014). In 2010 NASAs definition for DT comes from Modeling, Simulation, Information, Technology & Processing Roadmap study. Shafto et al. (2012) defined DT in the draft and in final release of this paper. According to Damieni et al. (2018) the distribution of publications over the years shows a growing trend of articles and it reveals a significant increase in 2017. With growing trends of articles, the definition of DT is changing. Table 2 contains various definitions of DT from 2003 to 2018.

Table 2 Digital twin definitions
Tabuľka 2 Definície digitálneho dvojčaťa

2003	Grieves	Virtual, digital equivalent to a physical product.
2012	Shafto et al.	An integrated multi-physics, multi-scale, probabilistic simulation of a vehicle or system that uses the best available physical models, sensor updates, fleet history, etc., to mirror the life of its flying twin.
2013	Reifsnider, Majumdar	Ultrahigh fidelity physical models and simulations of the materials and structures that control the life of a vehicle with on-board health management system, maintenance history and fleet data.
2014	Hochhalter et al.	Digital twin is a life management and certification paradigm whereby model and simulations consist of as-built vehicle state, as-experienced loads and environments, and other vehicle-specific history to enable high-fidelity modelling of individual aerospace vehicles throughout their service lives.
2015	Rosen et al.	Very realistic models of the current state of the process and their own behaviour in interaction with their environment in the real world.
2016	Schroeder et al.	The Digital twin being a virtual representation of the real product. It has product's information since the beginning of the life until the disposal of the product. The Digital Twin can be seen as a cyber representation in the context of the Cyber Physical Systems.
2017	Söderberg et al.	DT is referred as the concept of using digital copy of the physical system to perform real-time optimization.
2017	Grieves, Vickers	The Digital Twin is a set of virtual information constructs that fully describes a potential or actual physical manufactured product from the micro atomic level to the macro geometrical level. At its optimum, any information that could be obtained from inspecting a physical manufactured product can be obtained from its Digital Twin.
2017	Negri et al.	The DT is meant as virtual and computerized counterpart of a physical system that can be used to simulate it for various purposes, exploiting a real-time synchronization of the sensed data coming from the field; such a synchronization is possible thanks to the enabling technologies of Industry 4.0 and, as such, the DT is deeply linked with it.

Continued Table 2

2003	Grieves	Virtual, digital equivalent to a physical product.
2017	Zheng et al.	Application framework of DT consist of three parts, physical space, virtual space and information-processing layer. DT technology can realize full-physical system mapping, dynamic modelling and real-time optimization.
2018	Haag, Anderl	The digital twin is a comprehensive digital representation of an individual product. It includes the properties, condition and behaviour of the real-life object through models and data. The digital twin is a set of realistic models that can simulate its actual behaviour in the deployed environment. The digital twin is developed alongside its physical twin and remains its virtual counterpart across the entire product lifecycle.
2018	Boschert et al.	The Digital Twin refers to a description of a component, product, system or process by a set of well-aligned, descriptive and executable models

The results of Table 2 show that DT concept is recent. The application of DT evolved from mirroring the life of vehicles twin (Shafto et al., 2012) to the different solutions, sectors, and aspects of industry. Potential of DT increased with its popularity and various applications such as virtual representation of the real product is possible though DT, which represents virtual information constructs that fully describes a potential or actual physical manufactured product from the micro atomic level to the macro geometrical level (Grieves, Vickers, 2017) or a component, product, system or process by a set of well-aligned, descriptive and executable models defined by Boschert and Rosen (2016).

Definitions stated in Table 2 described scientific view on DT concept but there is also importance to define these definitions from software developer's perspective which are stated in Table 3.

Table 3 DT definition from software developers
Tabuľka 3 Definície digitálneho dvojčaťa softvérových vývojárov

Siemens	A digital twin is a virtual representation of a physical product or process, used to understand and predict the physical counterpart's performance characteristics.
PTC	A digital twin is a dynamic digital model of a product, process, or person, which analyses existing business system data combined with real-world data
PTC	A digital twin is a virtual representation of a physical product, asset, process, or operations used to understand and predict the physical counterpart's performance characteristics by leveraging real-time sensor and/or business system data related to the product or environment.
Ansys	DT of physical product or process can be used to monitor real-time prescriptive analytics and test predictive maintenance to optimize asset performance. The digital twin also provides data that can be used to improve the physical product design throughout the product lifecycle.

Continued Table 3

Siemens	A digital twin is a virtual representation of a physical product or process, used to understand and predict the physical counterpart's performance characteristics.
IBM	A digital twin is a virtual representation of a physical object or system across its lifecycle, using real-time data to enable understanding, learning and reasoning.
Microsoft	A virtual representation of a physical environment that brings in data from a variety of sources.
SEEBO	Digital Twin is a virtual representation that matches the physical attributes of a "real world" factory, production line, product or component in real time, through the use of sensors, cameras, and other data collection techniques.
GE Digital	Digital twins are software representations of assets and processes that are used to understand, predict, and optimize performance in order to achieve improved business outcomes. Digital twins consist of three components: a data model, a set of analytics or algorithms, and knowledge.
Oracle	A digital twin is a digital representation of a physical device, asset, or a system.
SAP	A digital twin is a virtual representation of a physical object or system – but it is much more than a high-tech lookalike. Digital twins use data, machine learning, and the Internet of Things (IoT) to help companies optimize, innovate, and deliver new services.

Table 2 and Table 3 analysis of DT definitions show that recent definition is similar with slight deviations. Definitions are in nature the same especially from software developer's perspective.

APPLICATION OF DIGITAL TWIN IN DIFFERENT PHASES OF LIFECYCLE

According to Boschert et al. (2018), DT evolves with the real system along the whole lifecycle and integrates the currently available and commonly required data and knowledge. Tao et al. (2017) sees application of DT with characteristics of ultra-high synchronization and fidelity on product design and preparation, manufacturing, and service. In other words, DT can be used to understand, in real-time, different aspects of what is happening on the shop-floor, and to update the real system with improvements that may be obtained in the digital model (Negri et al., 2019). With fully integrated DT with physical world, companies can gain information and real-time data about manufacturing processes in different phases of the products lifecycle which lead to the easily performed simulation, prediction, optimization and validation of manufacturing processes and products in their lifecycle. According to Westkamper et al. (2013) the methods and models of the DT can avoid approximately 70 percent of the planning errors, reduce about 30 percent of the planning time, reduce about 15 percent of the change costs and increase the planning maturity by roughly 12 percent.

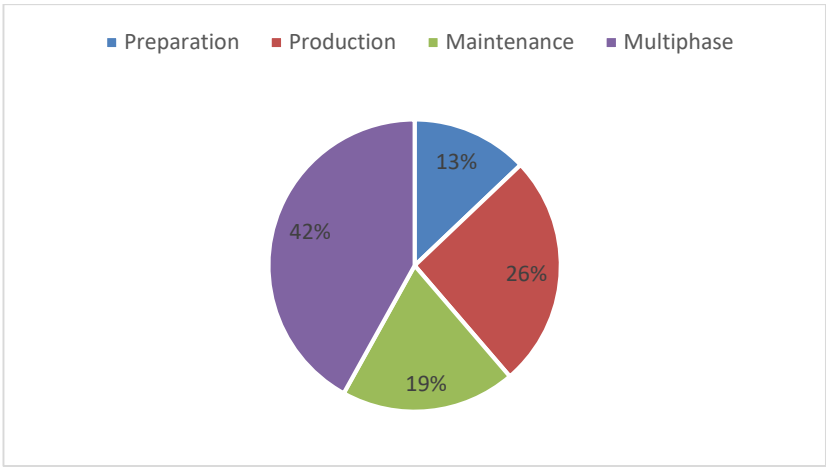

Figure 3 Digital Twin in different phases of lifecycle
Obrázok 3 Digitálne dvojča v rôznych fázach životného cyklu

DT was implemented into various phases of lifecycle by many scientists and practitioners. Aim of this chapter is to summarize and highlight possible applications of DT in three main phases of lifecycle, preparation phase, production phase and maintenance phase. However, DT can be used in multiple phases of lifecycle shown in Table 1 and Fig. 3 42 % of authors focused on DT concept, implemented DT across multiple phases of lifecycle. 26 % of authors implemented DT in production phase 19 % for maintenance phase and 13 % into preparation phase.

In preparation phase, the role of DT is to determine design, structures and specifications of a product or a system. Preparation phase affects subsequent production and maintenance phase. Correct preparation and design can highlight and explore advantages and disadvantages in planning and predict optimal manufacturing for production phase. Therefore, with the aid of the massive reference models, the designer can quickly complete the production line layout design, equipment configuration, and the virtual assembly of model but also to generate an authoritative digital design of the system at pre-production phase (Zhang et al., 2017). According to statistics done by Zhang et al. (2017), it takes average a day to satisfy customers individualized requirements, a week to enable the motion of whole production line, and a month to integrate the whole equipment including the products, equipment, and execution system, Moreno et al. (2016) shows that DT can be used to support the interactive design of optimal NC machining programs to optimize machining process.

The main role of DT in production phase is to optimize manufacturing processes, increase flexibility, productivity and production quality and reduce manufacturing expenses and energy consumptions. The possibility and benefits of DT in production phase are shown by Vachálek et al. (2017) where optimization of physical production line was possible through real time data collection and simulation of various parameters of production line through DT. Weyer et al. (2016) referred to a DT as next generation simulation tool with ability to perform synchronization of physical and virtual world. DT in production

phase is mainly used to connect virtual and physical manufacturing systems to analyse and control physical world through its virtual twin with ability to perform real time optimizations which elevate production flexibility and effectiveness. Uhlemann et al. (2017a, 2017b) shows that DT modelling combining real time data surpass traditional material and information flow mapping with manual data in production.

Maintenance phase also referred to as a usage phase or postproduction phase is mainly used to monitor health of a product or system. Based on analysis and diagnosis of production, maintenance strategies can be proposed through DT in advance to lower maintenance costs. Current maintenance strategies are performed especially with the use of data from real physical production, but with aid of DTs virtual data, these strategies can be enhanced, and failure prediction can be performed to lower failure rate and prevent unnecessary damages. Lee et al. (2014, 2015) developed DT models with integrated sensors and recorded historical data from production to explore machines conditions, failures and provided self-prediction strategies to the machines through simulation. Similar approach was chosen by Cai et al. (2017) to construct DT of machine with integrated data from sensors to provide engineers comprehensive data information fusion between physical and virtual world to perform diagnosis and through DT. Hochhalter et al. (2014) proved that DT and data collected from sensors can be used to accurate prediction of repair, inspection and replacement to overcome imperfection of classical methods. Luo et al. (2018) describes possibility to build DT with mapping ability from sensed data to drive analysis and simulation with descriptive model and algorithm model such an analysis can diagnose and predict failure.

However, digital data from production are generated from all phases of lifecycle, therefore many authors implemented DT in multiple phases of lifecycle. Boschert et al. (2018) explored DT ability to provide useful values across all lifecycle phases. DT will shorten preparation phase, reveal failures and bottlenecks in production through simulation of various scenarios in production and detect faults and suggest solutions and strategies to enhance maintenance phase. DT within multi phases of lifecycle was proposed by Soderberg et al. (2017) for quality inspection of final product. DT supported products design in preparation phase, inspection preparation, optimization of joining sequences and bottleneck and root cause analysis in production phase.

DIGITAL TWIN FUSION WITH INDUSTRY 4.0 TECHNOLOGIES

Technology such as Big Data, Cloud computing, Internet-of-Things (IoT) and Cyber Physical System (CPS) play important role in DT concept (Liau et al., 2018). Creation of DT requires huge quantity of data and information. The computing capacity is another crucial aspect for creating successful fully integrated DT. With a rise of CPS and IoT technologies which Big Data is closely linked with, these technologies will allow to collect and analyse production processes in more detailed picture through whole lifecycle. Using Ethernet/IP communication protocol, DT can be connected to the real world and cooperate to simulate virtual production lines (Moreno et al., 2016).

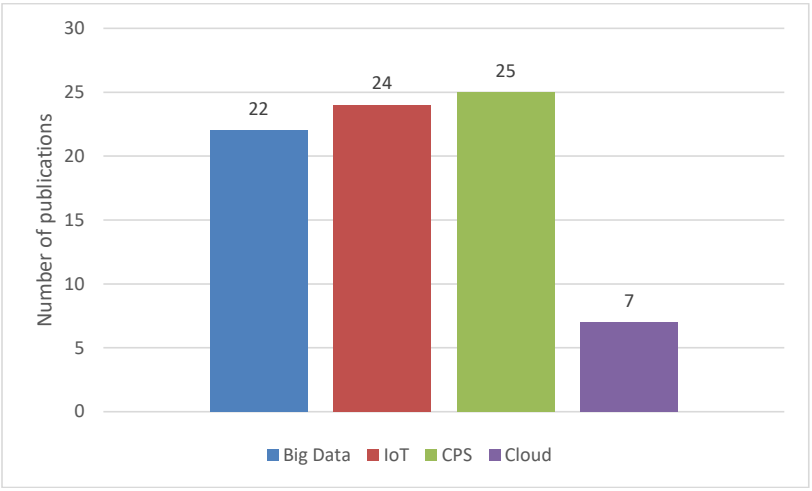

Figure 4 Industry 4.0 technologies linked to Digital Twin
Obrázok 4 Technológie Industry 4.0 prepojené s digitálnym dvojčaťom

Based on literature review, we can state that Big Data, IoT and CPS are deeply linked with DT and many authors used these Industry 4.0 technologies besides DT (see Fig. 4). Data collection and connection to the DT through Cloud computing is discussed by 7 authors, but with future research of DT concept we expect that cloud computing will be necessary part of DT.

CONCLUSION

This review demonstrated that DT often refers to a modelling of digital counter-part of physical system or connecting physical system to its digital counter-part. Wide range of application of DT shows that there is possibility to apply DT concepts in whole life-cycle including products, services, manufacturing processes, production system, layout planning, production planning, maintenance, etc. The benefits and applications of DT are almost unlimited in various aspects, but future development of DT can provide more case-studies to this subject, which will be beneficial for future application of DT in industries, where DT can reveal its protentional. The challenge is to connect physical and virtual systems in both directions to be able to communicate vice versa, which will allow collect more details about whole production process and provide crucial information for better decision making and optimization of processes and services. For such a vision Industry 4.0 technologies like CPS, IoT, Big Data and Cloud computing are necessary to be used. Several definitions of DT are available from different researchers, but official regulations and standards are non-existent, these regulations and standards can help define concept of DT for better understanding and development in the future.

REFERENCES

ALMADA-LOBO, F. 2016. The Industry 4.0 revolution and the future of manufacturing execution systems (MES). Journal of innovation management, 3(4), pp. 16-21.

ANDRADE-GUTIERREZ, E. S., CARRANZA-BERNAL, S. Y., HERNANDEZ-SANDOVAL, J., GONZALEZ-VILLARREAL, A. J., BERBER-SOLANO, T. P. 2018. Optimization in a flexible die-casting engine-head plant via discrete event simulation. The International Journal of Advanced Manufacturing Technology, 95(9-12), 4459-4468.

AYANI, M., GANEBÄCK, M., NG, A. H. 2018. Digital Twin: Applying emulation for machine reconditioning. In 51st CIRP Conference on Manufacturing Systems, Stockholm, May 16-18, 2018 (Vol. 72, pp. 243-248). Elsevier.

BIESINGER, F., MEIKE, D., KRAß, B., WEYRICH, M. 2018. A Case Study for a Digital Twin of Body-in-White Production Systems General Concept for Automated Updating of Planning Projects in the Digital Factory. In 2018 IEEE 23rd International Conference on Emerging Technologies and Factory Automation (ETFA) (Vol. 1, pp. 19-26). IEEE.

BOSCHERT, S., ROSEN, R. 2016. Digital twin—the simulation aspect. In Mechatronic Futures (pp. 59-74). Springer, Cham.

BOSCHERT, S., ROSEN, R., HEINRICH, C. 2018. Next generation digital Twin. In Proceedings of the 12th International Symposium on Tools and Methods of Competitive Engineering TMCE (pp. 209-218).

CAI, Y., STARLY, B., COHEN, P., LEE, Y. S. 2017. Sensor data and information fusion to construct digital-twins virtual machine tools for cyber-physical manufacturing. Procedia Manufacturing, 10, 1031-1042.

CORONADO, P. D. U., LYNN, R., LOUHICHI, W., PARTO, M., WESCOAT, E., KURFESS, T. 2018. Part data integration in the Shop Floor Digital Twin: Mobile and cloud technologies to enable a manufacturing execution system. Journal of Manufacturing Systems, 48, 25-33.

DAMIANI, L., DEMARTINI, M., GIRIBONE, P., MAGGIANI, M., REVETRIA, R., TONELLI, F. 2018. Simulation and Digital Twin Based Design of a Production Line: A Case Study.". In Proceedings of the International MultiConference of Engineers and Computer Scientists (Vol. 2).

Developing Applications with Oracle Internet of Things Cloud Service https://docs.oracle.com/en/cloud/paas/iot-cloud/iotgs/learn-oracle-iot-digital-twin.html [accessed February 2019].

Digital Twin – IBM Watson IoT. (n.d.). https://www.ibm.com/internet-of-things/trending/digital-twin [accessed February 2019].

Digital Twin | Siemens. (n.d.). https://www.plm.automation.siemens.com/global/en/our-story/glossary/digital-twin/24465 [accessed March 2019].

Digital Twin Technology – the new age of IoT technology. (n.d.). from https://www.seebo.com/digital-twin-technology/ [accessed March 2019].

Digital Twin Technology. (n.d.). https://www.ansys.com/products/systems/digital-twin [accessed March 2019].

Digital Twin. (n.d.). https://www.ge.com/digital/applications/digital-twin [accessed February 2019].

GRIEVES, M. 2014. Digital twin: Manufacturing excellence through virtual factory replication. White paper, 1-7.

GRIEVES, M., VICKERS, J. 2017. Digital twin: Mitigating unpredictable, undesirable emergent behavior in complex systems. In Transdisciplinary perspectives on complex systems (pp. 85-113). Springer, Cham.

GYULAI, D., PFEIFFER, A., KÁDÁR, B., MONOSTORI, L. 2016. Simulation-based production planning and execution control for reconfigurable assembly cells. Procedia CIRP, 57, 445-450.

HAAG, S., ANDERL, R. 2018. Digital twin–proof of concept. Manufacturing Letters, 15, 64-66

HOCHHALTER, J., LESER, W. P., NEWMAN, J. A., GUPTA, V. K., YAMAKOV, V., CORNELL, S. R., HEBER, G. 2014. Coupling Damage-Sensing Particles to the Digitial Twin Concept.

HOLLER, M., UEBERNICKEL, F., BRENNER, W. 2016. Digital Twin Concepts in Manufacturing Industries-A Literature Review and Avenues for further Research.

HOOF, B. V. 2018. Announcing Azure Digital Twins: Create digital replicas of spaces and infrastructure using cloud, AI and IoT. Retrieved March 15, 2019, from https://blogs.microsoft.com/iot/2018/09/24/announcing-azure-digital-twins-create-digital-replicas-of-spaces-and-infrastructure-using-cloud-ai-and-iot/

KRITZINGER, W., KARNER, M., TRAAR, G., HENJES, J., SIHN, W. 2018. Digital Twin in Manufacturing: A categorical literature review and classification. IFAC-PapersOnLine, 51(11), 1016-1022.

LEE, J., BAGHERI, B., & KAO, H. A. 2015. A cyber-physical systems architecture for industry 4.0-based manufacturing systems. Manufacturing letters, 3, 18-23.

LEE, J., KAO, H. A., & YANG, S. 2014. Service innovation and smart analytics for industry 4.0 and big data environment. Procedia Cirp, 16(1), 3-8.

LIAU, Y., LEE, H., RYU, K. 2018. Digital Twin concept for smart injection molding. In IOP Conference Series: Materials Science and Engineering (Vol. 324, No. 1, p. 012077). IOP Publishing.

LOHTANDER, M., AHONEN, N., LANZ, M., RATAVA, J., KAAKKUNEN, J. 2018. Micro Manufacturing Unit and the Corresponding 3D-Model for the Digital Twin. Procedia Manufacturing, 25, 55-61.

LUO, W., HU, T., ZHANG, C., WEI, Y. 2018. Digital twin for CNC machine tool: modeling and using strategy. Journal of Ambient Intelligence and Humanized Computing, 1-12.

MORENO, A., VELEZ, G., ARDANZA, A., BARANDIARAN, I., DE INFANTE, Á. R., CHOPITEA, R. 2017. Virtualisation process of a sheet metal punching machine within the Industry 4.0 vision. International Journal on Interactive Design and Manufacturing (IJIDeM), 11(2), 365-373.

NEGRI, E., FUMAGALLI, L., CIMINO, C., MACCHI, M. 2019. FMU-supported simulation for CPS Digital Twin. Procedia Manufacturing, 28, 201-206.

NEGRI, E., FUMAGALLI, L., MACCHI, M. 2017. A review of the roles of digital twin in cps-based production systems. Procedia Manufacturing, 11, 939-948.

QI, Q., TAO, F., ZUO, Y., ZHAO, D. 2018. Digital Twin Service Towards Smart Manufacturing. Procedia CIRP, 72(1), 237-242.

REIFSNIDER, K., MAJUMDAR, P. 2013. Multiphysics stimulated simulation digital twin methods for fleet management. In 54th AIAA/ASME/ASCE/AHS/ASC Structures, Structural Dynamics, and Materials Conference (p. 1578).

ROSEN, R., VON WICHERT, G., LO, G., BETTENHAUSEN, K. D. 2015. About the importance of autonomy and digital twins for the future of manufacturing. IFAC-PapersOnLine, 48(3), 567-572.

SAP Digital Twin Software & Technology. (n.d.). https://www.sap.com/products/digital-supply-chain/digital-twin.html [accessed March 2019].

SCHROEDER, G. N., STEINMETZ, C., PEREIRA, C. E., ESPINDOLA, D. B. 2016. Digital twin data modeling with automation ml and a communication methodology for data exchange. IFAC-PapersOnLine, 49(30), 12-17.

SENINGTON, R., BAUMEISTER, F., NG, A., OSCARSSON, J. 2018. A linked data approach for the connection of manufacturing processes with production simulation models. Procedia CIRP, 70, 440-445.

SHAFTO, M., CONROY, M., DOYLE, R., GLAESSGEN, E., KEMP, C., LEMOIGNE, J., WANG, L. 2012. Modeling, simulation, information technology & processing roadmap. National Aeronautics and Space Administration.

SÖDERBERG, R., WÄRMEFJORD, K., CARLSON, J. S., LINDKVIST, L. 2017. Toward a Digital Twin for real-time geometry assurance in individualized production. CIRP Annals, 66(1), 137-140.
STARK, R., KIND, S., NEUMEYER, S. 2017. Innovations in digital modelling for next generation manufacturing system design. CIRP Annals, 66(1), 169-172.
SUJOVÁ, E. ČIERNA, H., ŻABIŃSKA, I. 2019. Application of Digitization Procedures of Production in Practice. Management Systems in Production Engineering. 27. 23-28. 10.1515/mspe-2019-0004.
SUJOVÁ, E., STŘIHAVKOVÁ, E., ČIERNA, H. 2018. An Analysis of the Assembly Line Modernization by Using Simulation Software. Manufacturing Technology. 18. 839-845. 10.21062/ujep/187.2018/a/1213-2489/MT/18/5/839.
TAO, F., CHENG, J., QI, Q., ZHANG, M., ZHANG, H., SUI, F. 2018. Digital twin-driven product design, manufacturing, and service with big data. The International Journal of Advanced Manufacturing Technology, 94(9-12), 3563-3576.
UHLEMANN, T. H. J., LEHMANN, C., STEINHILPER, R. 2017a. The digital twin: Realizing the cyber-physical production system for industry 4.0. Procedia Cirp, 61, 335-340.
UHLEMANN, T. H. J., SCHOCK, C., LEHMANN, C., FREIBERGER, S., STEINHILPER, R. 2017b. The digital twin: Demonstrating the potential of real time data acquisition in production systems. Procedia Manufacturing, 9, 113-120.
VACHÁLEK, J., BARTALSKÝ, L., ROVNÝ, O., ŠIŠMIŠOVÁ, D., MORHÁČ, M., LOKŠÍK, M. 2017. The digital twin of an industrial production line within the industry 4.0 concept. In 2017 21st international conference on process control (PC) (pp. 258-262). IEEE.
WESTKÄMPER, E. 2013. Zukunftsperspektiven der digitalen Produktion. In Digitale Produktion (pp. 309-327). Springer, Berlin, Heidelberg.
WEYER, S., MEYER, T., OHMER, M., GORECKY, D., ZÜHLKE, D. 2016. Future modeling and simulation of CPS-based factories: an example from the automotive industry. IFAC-PapersOnLine, 49(31), 97-102.
YANG, S., ARNDT, T., LANZA, G. 2016. A flexible simulation support for production planning and control in small and medium enterprises. Procedia CIRP, 56, 389-394.
ZHANG, H., LIU, Q., CHEN, X., ZHANG, D., LENG, J. 2017. A digital twin-based approach for designing and multi-objective optimization of hollow glass production line. IEEE Access, 5, 26901-26911.
ZHENG, Y., YANG, S., CHENG, H. 2018. An application framework of digital twin and its case study. Journal of Ambient Intelligence and Humanized Computing, 1-13.

Corresponding author:
Roman Bambura, e-mail: bambura.r@gmail.com